



Université du Québec
à Rimouski

IMPACT DE DIFFÉRENTS RÉGIMES D'ÉCLAIRCIE SUR LES PROPRIÉTÉS DU BOIS ET LA
SÉQUESTRATION DU CARBONE DANS LES PLANTATIONS D'ÉPINETTE BLANCHE (*PICEA GLAUCA*
(MOENCH) VOSS)

MÉMOIRE PRÉSENTÉ

DANS LE CADRE DU PROGRAMME DE MAÎTRISE EN BIOLOGIE
EN VUE DE L'OBTENTION DU GRADE DE MAÎTRE ÈS SCIENCES

PAR

DIPAK MAHATARA

JUIN 2024



Université du Québec
à Rimouski

IMPACT OF DIFFERENT THINNING REGIMES ON WOOD PROPERTIES AND CARBON
SEQUESTRATION IN WHITE SPRUCE (*PICEA GLAUCA* (MOENCH) VOSS) PLANTATIONS
(DISSERTATION FORMAT: INTEGRATED ARTICLE)

DISSERTATION PRESENTED
IN PARTIAL FULFILLMENT OF THE REQUIREMENTS FOR THE MASTER'S PROGRAM IN BIOLOGY
TOWARDS THE DEGREE OF MASTER'S IN BIOLOGY

BY
DIPAK MAHATARA

JUNE 2024



BIBLIOTHÈQUE

UNIVERSITÉ DU QUÉBEC À RIMOUSKI

Mise en garde

La bibliothèque de l'Université du Québec à Rimouski (UQAR) a obtenu l'autorisation de l'auteur de ce document afin de diffuser, dans un but non lucratif, une copie de son œuvre dans un site d'archives numériques, gratuit et accessible à tous. L'auteur conserve néanmoins ses droits de propriété intellectuelle, dont son droit d'auteur, sur cette œuvre.

Warning

The library of the Université du Québec à Rimouski (UQAR) obtained permission from the author to use a copy of this document for nonprofit purposes to put it in the open archives Depositum, which is free and accessible to all. The author retains ownership of the copyright on this document.

ACKNOWLEDGEMENTS

I would like to express my sincere gratitude to my Director Professor Dr. Robert Schneider, for consistently fostering an environment that is both supportive and inspiring, filled with guidance, and care. Having both a family and a conducive working environment is a rare opportunity that not every graduate student is fortunate enough to have. I am also very grateful to my co-director Dr. Julie Barrette for her step-by-step feedback, contribution, and encouragement. Additionally, many thanks also go to my thesis advisory committee members, Dr. Pierre Francus, Prof. Dr. Dominique Arseneault, and Prof. Dr. Rosilei Aparecida-Garcia for the thorough review of the materials from the proposal to the final report and manuscript, along with their valuable suggestions for improvement. I have acquired precious experiences and will forever appreciate the independence I have gained through this journey.

I gratefully acknowledge the Ministère des Ressources naturelles et des Forêts, Québec (Formerly Ministère des Forêts, de la Faune et des Parcs) and the Natural Sciences and Engineering Research Council of Canada for the financial support, which made this study achievable.

I heartily thank Dr. Filipe Campelo, Laurent Houle, Dr. Alain Caron, and Dr. Boris Dufour for their technical guidance during the development of the research methodology and data analysis. My special thanks to Université Laval and Institut National de la Recherche Scientifique, Québec for their support during sample storage and processing. I heartily thank Dr. Murray Hay for proofreading and editing the first manuscript. I am thankful to Plourde Édith, management clerk of the biology program at Rimouski Campus, for her support in easing academic and administrative things at UQAR. Many thanks to Anne-Sophie Rioux, Yoana Leclerc, Charlotte Veillette, Jeremie Martel-Côté, and all my colleagues from the Chaire de Recherche sur la Forêt Habitée, for their help during field data collection and laboratory work.

Most importantly, I owe an enormous debt and appreciation to my family for their unwavering support and enduring love, which enabled me to complete my studies abroad. In the end, I am grateful to my beloved wife, Asmita Gautam, who has consistently been my source of strength.

PREFACE

This master's thesis is structured into four distinct chapters. In **Chapter I**, the context of the study, literature review, and objectives are presented. **Chapter II** focuses on the algorithm used to extract ring density profiles from X-ray medical computed tomography (CT) images. This chapter is formatted as a manuscript entitled "*CTRing: An R package to extract wood density profiles from computed tomography images of discs and logs*", which has been submitted for publication in *Dendrochronologia*. **Chapter III** presents a two-stage modeling approach to formulate a ring-density model, which is then applied to assess the CO₂ sequestration potential of various thinning regimes. This chapter is also ready for submission to a peer-reviewed journal. Finally, in **Chapter IV**, we summarize the primary contributions and conclusions of this study while emphasizing the need for future research endeavors. As this dissertation is presented as a compilation of articles, it's to be expected that there will be a certain degree of repetition between the chapters.

This thesis was supervised by Professor Dr. Robert Schneider, Chaire de recherche sur la forêt habitée at the Département de biologie, chimie et géographie, Université du Québec à Rimouski, Rimouski, Québec and co-supervised by Julie Barrette, Direction de la recherche forestière, Ministère des Ressources naturelles et des Forêts, Québec. Remaining co-authors contributed either during the project's development, throughout the study, or during the manuscript preparation stages.

TABLE OF CONTENTS

| | |
|------------------------------|-------------|
| ACKNOWLEDGEMENTS..... | iv |
| PREFACE | v |
| LIST OF FIGURES..... | viii |
| LIST OF TABLES..... | x |
| RÉSUMÉ..... | xi |
| ABSTRACT..... | xii |

| | |
|---|----------|
| CHAPTER I: GENERAL INTRODUCTION..... | 1 |
| 1.1. Context | 1 |
| 1.2. State of knowledge | 2 |
| 1.2.1. Wood density and its significance..... | 2 |
| 1.2.2. Variations in wood density..... | 3 |
| 1.2.3. Advances in wood density measurements | 7 |
| 1.2.4. White spruce (<i>Picea glauca</i> (Moench) Voss)..... | 7 |
| 1.2.5. Thinning and its effect on wood density..... | 9 |
| 1.2.6. Impact of thinning on carbon sequestration | 11 |
| 1.3. Objectives and hypothesis..... | 12 |

| | |
|---|-----------|
| CHAPTER II: CTRing: An R package to extract wood density profiles from computed tomography images of discs and logs..... | 14 |
| 2.1 Abstract..... | 15 |
| 2.2 Background..... | 16 |
| 2.3 Materials and methods..... | 19 |
| 2.3.1 Computerized tomography (CT) | 19 |
| 2.3.2 Method overview | 20 |
| 2.3.3 CT scan data | 28 |
| 2.3.4 Validation of pith location | 28 |
| 2.4 Results..... | 29 |
| 2.5 Discussion | 30 |
| 2.6 Acknowledgments | 33 |
| 2.7 Author contributions | 33 |

| | | |
|---|---|-----------|
| 2.8 | References | 33 |
| | | |
| CHAPTER III: Influence of commercial thinning on wood density and carbon sequestration in white spruce (<i>Picea glauca</i> (Moench) Voss) plantations | | 41 |
| 3.1 | Abstract..... | 42 |
| 3.2 | Introduction | 43 |
| 3.3 | Materials and methods..... | 47 |
| 3.3.1 | Sampling Design | 47 |
| 3.3.2 | Data Collection | 48 |
| 3.3.3 | Wood density measurements | 49 |
| 3.3.4 | Predicting post-thinning ring density profiles | 50 |
| 3.3.5 | Assessing post-thinning CO ₂ sequestration..... | 53 |
| 3.4 | Results..... | 56 |
| 3.4.1 | Model fitting..... | 58 |
| 3.4.2 | Tree volume and CO ₂ sequestration..... | 61 |
| 3.5 | Discussion | 67 |
| 3.5.1 | Variations in ring density..... | 68 |
| 3.5.2 | Post-thinning CO ₂ sequestration | 70 |
| 3.6 | Conclusions..... | 74 |
| 3.7 | References | 75 |
| 3.8 | Annex I: Supplementary information for RD model development..... | 90 |
| 3.9 | Annex II: Supplementary information for Height-DBH (HD) relationships | 93 |
| | | |
| CHAPTER IV: CONCLUSIONS AND FUTURE WORKS..... | | 96 |
| 4.1 | Conclusions..... | 96 |
| 4.2 | Perspectives and future research | 99 |
| 4.3 | References for chapter I and chapter IV | 101 |

LIST OF FIGURES

| | |
|---|----|
| Figure 1-1: Microscopic image of Earlywood Latewood structure (Source: USDA wood handbook)..... | 4 |
| Figure 1-2: White spruce distribution. Map from USGS: 1971 USDA (Thompson et al., 1999)..... | 9 |
| Figure 2-1: An X-ray computed tomography image of the cross section of a white spruce log in which the densities at different positions in the object are shown in a greyscale format. The darker zones indicate earlywood, and the lighter ones indicate latewood. | 20 |
| Figure 2-2: Calibration curve relating density to 8-bit grey values of known materials..... | 22 |
| Figure 2-3: (a) Initial estimate of the pith location and segmentation of the image from pith location; (b) the location of two ring-edge points from adjacent segments; (c) estimation of the new pith based on the principal that the perpendicular bisector of any arc of a circle passes through the centre of the circle; (d) number of bisectors along which the pith should be located; and (e) positions for the pith estimated as the intersection of two bisectors (blue points are considered as outliers, and red points are used to estimate pith location; the intersection of the green dotted lines indicates the estimated pith location.) | 23 |
| Figure 2-4: Profile path on the raster image, highlighting (a) the pixels through which the profile passes and (b) the plot of the profile from pith to the bark of the selected path. | 25 |
| Figure 2-5: Earlywood-latewood transition (a) established by polynomial method, (b) established by mid-point method when there are a low number of points within the ring, or when the minimum and maximum values fall outside the expected range, or when the inflection point is close to the minimum or maximum density of the ring and (c) established by mid-point method when the polynomial is concave-convex form. The black line is the fitted 3rd degree polynomial function; the red and blue solid lines indicate the minimum and the maximum density points, respectively and the black dashed line indicates the earlywood-latewood transition. | 27 |
| Figure 2-6: (a) Distances between the automatically and manually detected locations of pith in the x- and y-direction in terms of error (we considered all manually detected pith locations as 0, 0); (b) histograms showing the Euclidean distance between manually and automatically determined pith locations. The | |

blue dashed line denotes the mean value (0.72 mm). (c) Boxplots presenting the Euclidean distances between manually and automatically determined pith locations for different disc heights..... 29

Figure 3-1: Layout of the experimental unit (EU) with three sub-units; no gap, small gap, and large gap 49

Figure 3-2: Model predictions for relative density for different disc heights, dominance classes, thinning types, and ring widths. Plots A, C and E denote the observed spline-smoothed relative density of the annual rings plotted against disc heights, social classes, and thinning types respectively, whereas plots B, D, F and G denote the predicted relative density with years after thinning from final model (Eq. 2) for different disc heights, social classes thinning types and ring widths respectively. To plot the predicted curves, all the remaining tree-level and disc level variables were set to their respective mean values. The blue vertical dotted line in the plots of left panel represents the year of thinning (i.e., 2008). 57

Figure 3-3: Model residuals of the final model plotted against the fitted values of ring density. The gray levels represent the percentiles of the residuals. 61

Figure 3-4: Figures in the upper panel denote the annual volume increment for four thinning treatments at (A) growth period 1 (2008-2014) and (B) growth period 2 (2014-2021). Error bars are the standard error of the mean. Figures in the lower panel represent the annual volume increment during (C) growth period 1 and (D) growth period 2, as a function of stand density index (Pretzsch & Biber, 2005) calculated just before the start of the respective growth periods..... 64

Figure 3-5: Figures in the upper panel denote the annual CO₂ sequestration for four thinning treatments at (A) growth period 1 (2008-2014) and (B) growth period 2 (2014-2021). Error bars are the standard error of the mean. Figures in the lower panel represent the annual CO₂ sequestration during (C) growth period 1 and (D) growth period 2, as a function of stand density index (Pretzsch & Biber, 2005) calculated just before the start of the respective growth periods..... 66

Figure 3-6: TotalCO₂ sequestration per hectare of 13-year study period computed utilizing intra-tree density variation, average wood density at breast height and a published wood density of 412 kg/m³ for four thinning types. The numerical values presented above the bars represent the percentage difference between the total CO₂ sequestration obtained using respective wood density and that derived from intra-tree density variations. (The WD and BH in the figure represent wood density and breast height respectively).....67

LIST OF TABLES

| | |
|--|----|
| Table 2-1: Earlywood-latewood transition types of the annual rings in percentage for the 60-disc samples representing different heights. | 27 |
| Table 3-1: Tree and ring level characteristics of sampled trees before and after thinning treatment | 50 |
| Table 3-2: Descriptive statistics for parameters α_0 , α_1 and α_2 obtained by fitting Eq. 1 to 678 individual discs..... | 52 |
| Table 3-3: Definitions of the abbreviations for the candidate variables used to develop final ring density model | 52 |
| Table 3-4: Fit indices and error statistics calculated from the disc level model (Eq. 1) and final model (Eq. 2) | 58 |
| Table 3-5: Parameter estimates, standard errors (SE), t-values and standard deviation of the random effects estimates for the final model of ring density given by Eq. 2..... | 59 |
| Table 3-6: Average tree characteristics (standard deviation in parenthesis) of three inventory periods for each thinning treatment and their respective total volume, carbon sequestration and increment rates during the 13 years study period. | 62 |
| Table 3-7: F-values (P-values in parentheses) for the analysis of variance of stand level variables (volume increment and CO ₂ sequestration) with silvicultural treatments (control, thinned from below, thinned by CTR), growth periods (period 1 and period 2) and site..... | 63 |
| Table 3-8: F-values (P-values in parentheses) for the analysis of variance of stand level variables (volume increment and CO ₂ sequestration) with stand density index (SDI) just before the start of the respective growth periods, growth periods (period 1 and period 2) and site. | 63 |

RÉSUMÉ

Une bonne gestion des forêts peut contribuer à l'atténuation des changements climatiques. L'éclaircie commerciale, couramment inclus dans les scénarios sylvicoles des plantations, influence la croissance des arbres et les propriétés du bois et, par conséquent, peut modifier les taux de séquestration du carbone. Il n'est toutefois pas clair si la séquestration du carbone augmente ou diminue suite à une éclaircie. La séquestration du carbone varie avec plusieurs facteurs comme le moment et l'intensité du traitement d'éclaircie, l'espèce d'arbre et, surtout, la densité du bois. La présente étude a examiné les variations de la densité du bois annuelle entre les arbres et à l'intérieur des arbres afin d'estimer les taux de séquestration du dioxyde de carbone (CO₂) selon quatre types de traitements (contrôle, éclaircie par le bas, dégagement de 50 arbres élités à l'hectare (50 AÉ), et dégagement de 100 arbres élités à l'hectare (100 AÉ)) effectués dans des plantations d'épinettes blanches (*Picea glauca* (Moench) Voss) de l'Est du Québec. Les plantations datant de 1990 ont été éclaircies en 2008. En 2021, nous avons récolté des rondelles de bois de 140 arbres abattus lors de la deuxième éclaircie. Les variations inter-annuelles de la densité moyenne du bois ont été obtenues à partir d'un tomodensitomètre à rayons-X, et celles-ci ont servi à étalonner un modèle statistique qui prédit la densité moyenne d'un cerne après éclaircie. Les données d'inventaire provenant des placettes-échantillons mesurées en 2008, 2014 et 2021, combinées aux prédictions annuelles de densité du bois, ont permis de quantifier la quantité de carbone séquestrée à l'échelle de la placette. Les résultats montrent que : (1) la densité du bois annuelle est plus élevée près de la moelle, suivi d'une diminution rapide, et d'une augmentation légère vers l'écorce ; (2) l'éclaircie commerciale n'influence pas la variation radiale de la densité moyenne du cerne dans un arbre, ce qui a simplifié la comparaison entre les traitements après l'éclaircie ; (3) les placettes-échantillons éclaircies ont montré des taux de séquestration de CO₂ plus faibles que les placettes témoin, avec des valeurs moyennes de 5.17, 5.35, 4.75 et 5.84 tonnes/ha/an pour 100 AÉ, 50 AÉ, l'éclaircie par le bas et le témoin, respectivement. Ceci implique que la croissance des arbres résiduels n'était pas suffisante pour compenser la perte des arbres coupées, même 13 ans après éclaircie. Ces résultats montrent qu'il est tout aussi important de tenir compte des mesures de densité du bois que de croissance pour évaluer le stockage de carbone. Toutefois, une période de suivi plus longue est nécessaire afin de mieux comprendre les différents profils de croissance entre les divers traitements d'éclaircie et de dégagement.

Mots-clés: séquestration du CO₂, modélisation de la densité du bois, dégagement d'arbres élités, éclaircie commerciale, épinette blanche

ABSTRACT

Effective forest management can play a crucial nature-based solution for climate change mitigation. Commercial thinning, often included in silvicultural scenarios applied to plantations, influences tree growth and wood properties, and consequently can modify the carbon sequestration rate. The consensus on whether thinning increases or decreases carbon storage is unclear. Carbon sequestration is influenced by factors such as thinning timing and intensity, tree species, and, notably, wood density. The present study considered the inter and intra-tree density variations to estimate carbon dioxide (CO₂) sequestration rates under four treatments (control, thinning from below, early crop tree release (CTR) of 50/ha, and CTR of 100/ha) conducted in white spruce (*Picea glauca* (Moench) Voss) plantations in eastern Quebec. The plantations dating from 1990 were thinned in 2008. Firstly, the disc samples collected in 2021 from 140 trees across the 4 thinning intensities were used to construct a model that predicts ring density (RD) after thinning. Secondly, the plot inventory data from 2008, 2014, and 2021, combined with RD model were used to estimate individual tree carbon sequestration, which was then summed up to the plot level. The findings show: (1) RD displayed higher values near the pith, followed by a rapid decline, after which RD slightly increased towards the bark; (2) thinned and control treatments showed similar average RD chronologies throughout the study period, constraining the generalization of RD trends post-thinning; (3) thinned plots exhibited lower CO₂ sequestration rates than control plots, with the estimates of 5.17, 5.35, 4.75, and 5.84 tons/ha/year for 100 CTR, 50 CTR, thinning from below, and control respectively. The growth of residual trees did not sufficiently compensate for the stock loss during thinning, even after 13 years. This study shows the importance of considering inter and intra-tree density variations for accurate carbon estimation. However, a more extended follow-up period is necessary to discern the direction of changes in growth.

Keywords: Thinning, CO₂ sequestration, ring density modeling, crop tree release, intra-tree density variation, white spruce

CHAPTER I

GENERAL INTRODUCTION

1.1. Context

Forest ecosystems cover around 30% of Earth's land (4.06 billion hectares) and represent a major carbon sink, with current carbon stock estimated to be 861 ± 66 Pg C (Pan et al., 2011). A substantial portion of the Earth's carbon dioxide flux is attributed to terrestrial gross ecosystem productivity (GEP), of which 47% is attributed to forest biomes (Beer et al., 2010). Forests are no longer seen solely as a source of timber or land for development but as a critical tool for mitigating climate change. This recognition has led to a more holistic approach to forest management that balances the multiple benefits of forests, including their capacity to sequester and store carbon, with other land-use needs (D'Amato et al., 2011).

Stand density management is one of the most important and widely used silvicultural tools that directly influences tree growth, wood quality, and carbon content. The impact of silvicultural treatments on wood quality and carbon content has been a subject of concern to forest managers for decades. Although the prime objective of forest managers is to produce a higher quantity of large-sized trees by using proper silvicultural treatments, there is also a growing recognition of the need to maintain wood quality as it is directly related to carbon content of a tree (Zhang et al., 2009). Among different wood properties, wood density has been widely studied, especially in its relationship with other wood properties, commercial thinning, and radial growth. Wood density varies significantly due to genetic origins, site conditions, climate, and forest management practices. This also highlights the need to better understand how this variation is influenced by tree species, forest management, and growth conditions. This knowledge is vital for optimizing carbon storage within forest ecosystems and advancing forest management practices, aligning with the broader global objective of climate change mitigation.

1.2. State of knowledge

1.2.1. Wood density and its significance

Wood density refers to the mass of wood per unit volume, commonly measured in kilograms per cubic meter (kg/m^3) or grams per cubic centimeter (g/cm^3). It is a fundamental characteristic of wood, representing its compactness, and plays a significant role in determining its mechanical, physical, and chemical properties (Smith & Hawley, 1993). In practice, wood density is defined as the ratio of either oven dry weight and volume, green weight and volume, or weight and volume at specific moisture content (Haygreen & Bowyer, 1996).

In terms of mechanical properties, wood density is well linked to wood strength. The denser the wood, the higher its strength (modulus of rupture) and stiffness (modulus of elasticity) tend to be, making it a valuable factor in determining the wood's overall structural integrity and load-bearing capacity (Chudnoff, 1984). Additionally, when estimating aboveground biomass at large scales or across diverse forest types, accounting for variations in wood density becomes essential. Different tree species have distinct wood densities, and ignoring this variability can lead to substantial inaccuracies in biomass estimations (Laurance et al., 2007). Models that incorporate wood density variations for specific tree species or forest types have been shown to enhance the accuracy of aboveground biomass estimates (Chave et al., 2014).

Furthermore, wood density holds increasing importance in dendroclimatology, especially in recent years, due to its potential to enhance climate-growth relationship studies and improve our understanding of past climatic variability. By analyzing variations in wood density within tree rings, researchers can discern changes in growth rates and physiological adaptations, aiding in the reconstruction of past climates and ecological shifts (Wimmer, 2002).

1.2.2. Variations in wood density

1.2.2.1 Intra-tree variation

Intra-ring variations in wood density represent a fundamental aspect of dendrochronology, providing detailed insights into the seasonal dynamics of wood formation within a single growth ring. Tree rings, a reflection of annual growth cycles, consist of earlywood and latewood, each exhibiting distinctive characteristics. Earlywood, formed during the early phase of the growing season, is characterized by larger radial diameter, thinner and less dense cells with a larger lumen (Figure 1-1), facilitating efficient water conduction and storage (Zobel & Buijtenen, 1989). Conversely, latewood, which develops later in the growing season, features higher cell density and thicker cell walls with a small lumen, resulting in a denser structure that offers mechanical support to the tree (John, 1980; Fonti et al., 2010). The earlywood to latewood ratio is significant in understanding wood characteristics. A higher ratio typically indicates faster growth and may result in wood with different properties, such as lower density and strength.

Numerous studies have highlighted notable shifts in wood density between earlywood and latewood. Larson (1969) extensively explored the rationale behind this density shift, suggesting that cell diameter is influenced by auxin, a plant hormone produced in apical meristems. With apical activity, auxin production decreases at the base of the tree due to the distancing of the live crown, resulting in smaller cell diameter, enhanced cell wall thickness, and consequently, higher wood density.

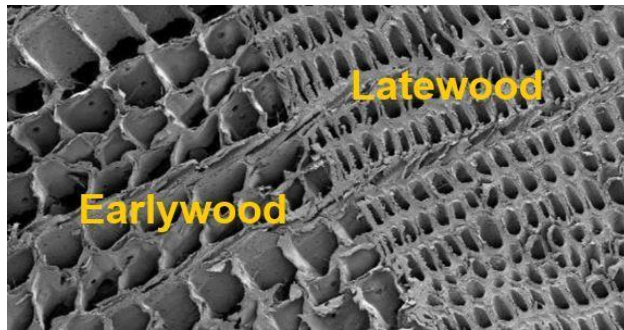


Figure 1-1: Microscopic image of Earlywood Latewood structure (Source: USDA wood handbook)

In addition to intra-ring variation, radial density variation is a fundamental characteristic of wood and is influenced by a multitude of factors related to tree growth, wood anatomy, and physiological processes (Zobel & Buijtenen, 1989). In many studies, the cambial age has been used to define radial density patterns of conifers (Ivković et al., 2013; Auty et al., 2014; Xiang et al., 2014; Franceschini et al., 2018; Vaughan et al., 2021). In fact, cambial age serves as a valuable indicator of the transition from vigorous growth to reduced growth over a tree's lifespan and represents the variation in anatomical structure between juvenile wood (JW) and mature wood (MW). JW, also known as inner wood, represents the initial phase of wood formation in a tree, typically originating closer to the pith or central core. MW constitutes the later, more advanced growth stages of the tree, typically located toward the bark. For conifers, JW usually displays larger earlywood to latewood ratio than MW, which could be a major factor controlling the ring density variation (Koubaa et al., 2005).

The radial density variation in conifers typically exhibits one of three patterns: a gradual increase in average ring density from JW to MW (type I), high initial density near the pith with a rapid decrease followed by a gradual increase (type II), or a consistent decrease in density from pith to bark (type III; John, 1980; Schimleck et al., 2022). Radial variations in wood density are closely linked to a species' successional status and corresponding growth strategies. In pioneer and early successional species, wood density increases from pith to bark, while an opposite pattern is observed for late-successional

species like conifers (McCulloh et al., 2011). Early-successional species initially grow rapidly, producing wood with low density, and later transition to producing denser wood. Interestingly, the type II and III patterns occur because of higher earlywood density near the pith, which is a clear adaptive strategy of conifers to respond to complex loading patterns (Telewski, 1989; Van Gelder et al., 2006). Moreover, the denser earlywood near the pith in conifers is evolutionarily advantageous, facilitating improved stability and resilience in response to dynamic mechanical stresses encountered during early growth phases.

Furthermore, understanding how wood density varies within a tree, from its base to its crown, is crucial for assessing wood quality. The variations of wood density along the vertical axis are less studied in comparison to radial patterns because of the complication of acquiring the samples. In general, wood density has been reported to decrease from the bottom to the top of the tree. However, these variations in wood density along the stem are also known to vary among different tree species. For instance, the wood density of black spruce was reported to increase from base to top (Alteyrac et al., 2005), as was the case with Norway spruce wood density (Longuetaud et al., 2017). In contrast, the wood density of hybrid larch was found to decrease from the base of the stem upwards (Levoy et al., 2021). This can be explained by the variation in the proportion of juvenile to mature wood, as it changes from the base to the top of the tree (Zobel & Van Buijtenen, 2012). In fact, studies on radial and vertical variations are important to develop sampling strategies, as most of the studies consider wood properties from breast height.

1.2.2.2 Inter-tree variation

The variability in wood density between trees within a forest stand can be substantial, influenced by a complex interplay of genetic, environmental, and management factors. Genetic diversity plays a pivotal role, contributing to distinct wood density patterns among individual trees even within the same species (Zobel & Buijtenen, 1989). Environmental factors, including soil quality, light availability, and water

accessibility, further shape these variations. Competition for limited resources among neighboring trees, driven by environmental conditions, leads to variations in growth rates and ultimately in wood density (Zubizarreta Gerendiain et al., 2007). Moreover, the variations become more evident at the site level, reflecting the distinct interplay of local environmental conditions on wood density (Schneider et al., 2008). Auslander et al. (2003) and Rossi et al. (2006) demonstrated contrasting cambial activities on the same species grown on north- and south-facing slopes, underlining the role of temperature variation. Likewise, Vaganov et al. (2006) emphasized the close correlation between wood density trends and local climate and soil conditions, underscoring the necessity to account for site variations in density studies.

Furthermore, trees respond dynamically to climatic variables such as temperature, precipitation, and sunlight, influencing growth rates, ring formation, and ultimately, the quality of wood. In general, increased temperatures, particularly during the growing season, often result in lower wood density (Wang et al., 2002). However, (Briffa et al., 1992) revealed a close association between ring density and summer temperature, emphasizing the sensitivity of wood density to seasonal climatic variations. Conversely, higher precipitation levels tend to be associated with higher wood density due to enhanced cell wall formation (Kozłowski & Pallardy, 2002). Summer precipitation, particularly June precipitation has been reported to be positively related to density (Conkey, 1988; Wimmer & Grabner, 1997). The relationship between climate and wood density is not uniform across species. For instance, studies on *Pinus sylvestris* by Rehfeldt et al. (2002) have revealed that warmer temperatures during the growing season contribute to higher wood density. In contrast, some tropical species demonstrate an inverse relationship, with higher temperatures associated with lower wood density due to faster growth rates (Worbes et al., 2003). Understanding these intricate interactions of climatic variables with the growth of tree species is crucial for predicting how changing climate patterns may affect wood density and, consequently, the quality of timber resources and forest ecosystems.

1.2.3. Advances in wood density measurements

Advances in the field of wood density measurement encompass a spectrum of traditional and modern techniques aimed at accurately and non-destructively assessing wood properties. Traditional methods involve direct measurement by weighing a wood sample and then determining its volume, either through water displacement or geometric measurements. These methods, while effective, can be laborious and destructive.

X-ray densitometry, that can be applied to samples obtained without felling the tree, has been widely used to study the internal wood properties (Bergsten et al., 2001; GÜLLER, 2010; Jacquin et al., 2017; Campelo et al., 2019; Kharrat et al., 2019). It uses X-rays to measure wood density by analyzing the attenuation of X-rays as they pass through the wood sample. Moreover, numerous studies have utilized images of cross-sections of logs generated from X-ray computer tomography (CT) scanning to determine internal wood properties (Espinoza et al., 2005; Freyburger et al., 2009; Osborne et al., 2016; Fabijańska et al., 2017; Jacquin et al., 2019; Q. Wang et al., 2019). More recently, ultrasonic methods and optical scanning of wood cross-section are also used to study the wood properties non-destructively (Perlin et al., 2018; Habite et al., 2020). Both techniques have shown promising results in accurately determining wood properties. Additionally, nuclear magnetic resonance (NMR) has emerged as a powerful non-destructive tool, measuring the relaxation times of protons in wood to estimate its density and offering insights into internal wood structure (Maunu, 2002; Dvinskikh et al., 2011).

Advances in technology have also facilitated the use of machine learning and image processing techniques in wood density measurement. Algorithms can analyze images of wood samples and estimate density, providing a faster and more efficient method for large-scale assessment.

1.2.4. White spruce (*Picea glauca* (Moench) Voss)

White spruce (*Picea glauca* (Moench) Voss) is a conifer tree species native to the northern temperate and boreal forests of North America and extends from Alaska and western Canada through the interior of Canada to the northeastern and north-central parts of the United States (Eyre, 1980; Figure 1-2). The species tolerates a wide range of temperatures but favors colder climates, with annual precipitation typically ranging from 750 to 1500 mm (Martin-DeMoor et al., 2010). White spruce can adapt to various well-drained soils, including sandy, loamy, and clayey types and tends to prefer slightly acidic to neutral soils, with optimum pH likely between 4.7 and 7.0 (Nienstaedt & Zasada, 1990). White spruce is adaptable to varying altitudes, from sea level to high elevations (up to 2000 m), depending on the region and local conditions (Hoffman, 1987). White spruce grows in pure and mixed stands associated with other species such as black spruce (*Picea mariana* (Mill.)), balsam fir (*Abies balsamea* (L.) Mill.) and white birch (*Betula papyrifera* Marshall) (Eyre, 1980). While it is shade-tolerant in its early stages, it grows more vigorously in full sunlight as it matures.

It is an ecologically and economically important tree species that has been managed intensively, and one of the main species that is used for plantations (D'Amato et al., 2011). Previous studies have found a positive response of white spruce to intensive silvicultural management (Pelletier & Pitt, 2008; Ott, 2010; Olson et al., 2014; Dupont-Leduc et al., 2020). These studies showed that productivity and growth are sensitive to tree spacing. While different wood properties of white spruce have been studied extensively (Zhou & Smith, 1991; Hernandez et al., 2001; Hasegawa et al., 2020), including genetic effects on wood quality traits (Park et al., 2012), acoustic velocity (Bérubé-Deschênes et al., 2016) and modulus of elasticity (Kuprevicius et al., 2013), very few have made the attempt to study the growth characteristics and carbon content of white spruce after commercial thinning (Omari et al., 2016; Mvolo et al., 2021). Hence, a study of wood density is crucial for enhancing our understanding of the species and integrating it effectively into forest growth, management, and utilization.



Figure 1-2: White spruce distribution. Map from USGS: 1971 USDA (Thompson et al., 1999)

1.2.5. Thinning and its effect on wood density

Thinning typically involves removing weaker, diseased, or less desirable trees to enhance the growth and vigor of the remaining ones by providing more access to water, nutrients, solar radiation, and increased spacing between individual trees (Wimmer & Downes, 2003). In the past, the most common objective of thinning was timber production. In recent years, however, carbon sequestration and forest conservation have also become important management goals. More recently, Moreau et al. (2022) suggested thinning as an effective measure to reduce climatic vulnerability, offering a strategic opportunity for the implementation of long-term adaptive management strategies.

In general, it has been suggested that the radial growth and the percentage of earlywood of conifer species increase with spacing (Zhang, 1995; Tasissa & Burkhart, 1997; Mäkinen et al., 2002). The wider or proper spacing is attributed to lower competition among the remaining trees and higher availability of water, nutrients, and solar radiation. These factors potentially alter tracheid growth and thus affect

wood density. Moreover, dominant and codominant trees show a higher response to the thinning compared to trees of suppressed and intermediate classes because of their improved growth conditions (Pukkala et al., 1998; Peltola et al., 2002). One of the studies from Larson (1963) showed that crown characteristics also influence the ring width of trees, suggesting ring growth is influenced by the foliage and branches present in proximity to the point of measurement. Furthermore, the timing of thinning operations is critical as the optimal wood properties and growth are often associated with moderate thinning carried out at specific stages of stand development (Río et al., 2008). Early thinning in a stand's life cycle can influence wood properties differently compared to thinning in more mature stages. In early thinning, when trees are younger, removing certain individuals enables the remaining trees to allocate resources more efficiently. On the one hand, this promotes faster growth, and on the other delays the production of mature wood compared to non-thinned or practice-oriented thinned stands, as evidenced in loblolly pine trees (Dobner et al., 2018). Furthermore, according to stand dynamics theory, tree growth rates exhibit a faster recovery from thinning compared to late thinning (Oliver et al., 1996; Varmola & Salminen, 2004), leading to alterations in wood properties. So, the magnitude of thinning impacts on wood properties depends on the intensity of thinning and its type, tree species and status in the stand, tree age, and environmental conditions (Tasissa & Burkhart, 1997; Vaganov et al., 2006; Downes & Drew, 2008).

The accelerated growth after thinning generally reduces wood density (Pape, 1999b), which might be because of the increased production of earlywood relative to latewood. A study by Cown (1973) reported that a notable change in wood density can be observed if the stands are released suddenly from high competition through intense thinning. In such circumstances, wood density may drop for some years following thinning. However, a clear relationship between wood density and ring width has not been found yet, as all positive, negative, and weak relations have been observed in different studies. For example, a slight reduction in wood density was observed after thinning in Norway spruce (*Picea abies*

L.) (Herman et al., 1998; Jaakkola et al., 2005), jack pine (*Pinus banksiana*, Lamb.) (Schneider et al., 2008), balsam fir (Koga & Zhang, 2002), and Scots pine (*Pinus sylvestris*, L.) (Mörling, 2002). Conversely, an increase in wood density was observed after thinning in loblolly pine (*Pinus taeda* L.) (Megraw, 1985) and red pine (*Pinus resinosa* Sol., Paul, 1958). This might be the result of prolonged latewood production due to increased soil moisture (Zobel & Van Buijtenen, 2012). Also, very little or no changes in wood density after thinning were observed for Scots pine (Peltola et al., 2009). This suggests that the relationship between thinning, wood density, and growth is complex and can be influenced by tree species and environmental conditions.

1.2.6. Impact of thinning on carbon sequestration

Concerns regarding the increasing levels of carbon dioxide (CO₂) in the atmosphere have pushed researchers and practitioners to develop forest management strategies that aim to optimize carbon storage. Despite extensive research to optimize growth through thinning in various forests, limited research has directly assessed the long-term carbon effects of thinning or selection cutting in forests (Finkral & Evans, 2008; Davis et al., 2009). Numerous studies on short-term impacts reveals several potential effects of thinning on carbon storage in managed forests. Thinning reduces mortality, accelerates the diameter growth and shortens the rotation age for sawlog production (Zarnovican & Laberge, 1996). It is true that thinning increases the number of large high-quality logs (Zobel & Buijtenen, 1989), but it does not necessarily lead to an increase in total wood volume of a stand. Therefore, it is important to understand the impact of different thinning regimes from both qualitative and quantitative perspectives of wood production.

The carbon content of a tree is generally calculated using a volume equation, including a conversion factor for carbon concentration in dry biomass (%C) and basic wood density (Houghton et al., 1990). Carbon content and wood density are positively correlated as thicker vessel walls have higher cellulose

and lignin in comparison to narrower walls (Martin & Thomas, 2011). A common understanding is that the carbon sequestration rate increases after thinning because of the acceleration in the growth rate of the trees. However, various studies showed that thinning from above (removal of the largest trees) significantly alters the stand density and hence decreases aboveground carbon storage both immediately and over the long-term (Harmon et al., 2009; Chatterjee et al., 2009; D'Amato et al., 2011). Likewise, some studies have shown that unthinned or lightly thinned stands present higher carbon storage in comparison to moderate and heavily thinned stands (Powers et al., 2011; Keyser & Zarnoch, 2012). Again, a study by D'Amato et al. (2011) found that thinning from above and below store equal amounts of carbon over the long-run. Certainly, these inconsistent results can be explained in part by the variations in wood density. This underlines the importance of including both the tree growth patterns and wood density for the realistic projections of carbon sequestration (Weber et al., 2018).

1.3. Objectives and hypothesis

Objectives:

The general objective of this study was to evaluate the impact of different commercial thinning regimes on the growth-ring characteristics and CO₂ sequestration in white spruce plantations.

Specific objectives:

1. To build a relationship between thinning type and ring density along the bole of a tree.
2. To estimate the amount of sequestered carbon per thinning type by utilizing the intra-tree density variations.
3. Compare the estimated carbon sequestration obtained in objective 2 with the one estimated by using published wood density.

Hypothesis:

1. We assumed that there would be different ring densities for the same ring width after commercial thinning due to the change in EW to LW proportion. We also hypothesized that the ring density decreases with thinning throughout the tree.
2. We assumed that the average wood density at breast height overestimates a tree's CO₂ sequestration. We further hypothesized that for a more precise estimation of carbon in a forest stand, it is essential to account for the effects of age and treatments on wood density.
3. There would be a significant difference in CO₂ sequestration for different thinning regimes, primarily due to differences in ring density after thinning. Thus, we assumed that there would be a different CO₂ sequestration rate per thinning depending on the post-thinning ring density and initial stand density.

CHAPTER II

CTRing: An R package to extract wood density profiles from computed tomography images of discs and logs

Dipak Mahatara^{*,1}, Filipe Campelo², Laurent Houle¹, Alain Caron¹, Julie Barrette³, Pierre Francus^{4, 5} and Robert Schneider¹

1. Département de Biologie, Chimie et Géographie, Université du Québec à Rimouski (UQAR), 300 Allée des Ursulines, Rimouski, QC G5L 3A1, Canada.
2. CFE – Centre for Functional Ecology – Science for People & the Planet, Department of Life Sciences, University of Coimbra, Calçada Martim de Freitas, 3000-456, Coimbra, Portugal
3. Direction de la recherche forestière, Ministère des Ressources naturelles et des Forêts, 2700 rue Einstein, Québec, QC G1P 3W8, Canada
4. INRS – Institut National de la Recherche Scientifique, Centre Eau Terre Environnement, G1K 9A9, Québec, QC, Canada
5. GEOTOP - Research Centre in Earth System Dynamics, H3C 3P8, Montréal, QC, Canada

*Corresponding author: dipak.mahatara@uqar.ca

Copy of the manuscript

Submitted to the Dendrochronologia journal

2.1 Abstract

Accurately determining the position of pith and accessing tree-ring density profiles, including intra-ring variations, is important for both the forest industry and dendroclimatology. Although several available methods exist for acquiring this information, such as X-ray computed tomography (CT), micro-CT, and X-ray films, the availability of open-source programs for extracting data remains limited. The CTRing package in the R environment integrates a series of functions to precisely detect the pith and tree-ring boundaries and generate tree-ring density profiles using CT images of tree cross-sections. Before processing, grey values are transformed into density using a calibration function. Pith position is then detected by combining an adapted Hough Transform method and a one-dimensional edge detector. Tree-ring profiles along the pith-to-bark path of interest are inspected visually, and tree-ring boundaries can be easily added or removed manually via a graphical user interface. After correcting for tree-ring boundaries, the inflection points of a 3rd-degree polynomial obtained from density profiles are used to delimit the earlywood–latewood transition. We tested this package using 60 CT-scanned images of white spruce (*Picea glauca* (Moench) Voss) discs collected at various tree heights (0%, 25%, 50%, and 75% of the total tree height as well as at 1.3 m). The pith detection function had an average mean error of 0.72 mm with 95% of the automatically detected pith locations that differed by less than 2 mm from their manually located positions. Error decreased toward the apex of the tree. The functions of the CTRing package are flexible and can be easily implemented or adapted. The package could also be used with simple images of discs to obtain ring-width time series; however, this use must be evaluated further. Future work with this package involves assessing the use of low-quality images and ring-porous species.

Key-words: Automatic detection, computed tomography, EW–LW transition, pith, tree-ring profile

2.2 Background

Tree rings are commonly used to understand tree growth dynamics and their response to climate. These growth rings hold information related to the surrounding biotic and abiotic conditions. Cell formation in the rings is first determined by the genetic features of the species and the age of the cambial cells (Harold, 1990; Vaganov et al., 2006; Rathgeber et al., 2016). The number of cells produced in the apical and secondary meristems of a tree is nevertheless regulated by a series of complex interactions between biotic and abiotic factors, including competition, geographic location (e.g., solar radiation, growing season length), wind speed, soil nutrition, soil moisture, and climate (Bradley, 1985; Fritts, 2012; Ford et al., 2017; Abedi, 2021; Wu et al., 2022). Temperature and precipitation often limit cell formation and, hence, tree growth (Kozłowski & Pallardy, 1997; Żywiec et al., 2017; Gauli et al., 2022). Thus, tree-ring growth patterns can provide important information about past climatic conditions and indicate whether the trees have experienced favorable or unfavorable conditions over their lifetime (Fritts, 2012; Koprowski, 2013; De Micco et al., 2016; Visser, 2021).

Over the last few decades, interest has shifted from ring width to ring density profiles for several reasons. Wood density is important for the forest industry and is frequently linked to other wood properties such as the modulus of elasticity and the modulus of rupture (Zobel & Van Buijtenen, 2012; Schneider et al., 2008; Baar et al., 2015; Morel et al., 2018). Wood density, especially when scaled to the entire tree, plays a crucial role in assessing tree and stand biomass and effectively evaluating forest carbon sequestration (Baker et al., 2004; Babst et al., 2014; Pothong et al., 2022). Use of ring density has also increased in dendrochronology primarily because this trait appears more closely correlated with climatic variables than ring width alone. Density-based dendroclimatology relies heavily on the density of latewood (LW), which is formed at the end of the growing season. LW contains a more pronounced climate signal than earlywood (EW, formed at the beginning of the growing season) as it is particularly

sensitive to summer climate factors, including temperature and precipitation (Bouriaud et al., 2005; Li et al., 2018; Deng et al., 2022).

Various approaches have been explored in the literature to measure wood density at the ring or intra-tree ring levels. These methods include the use of beta rays (Phillips, 1960), gamma rays (Woods & Lawhon, 1974), X-rays (Polge, 1966), high-frequency densiometry (Boden et al., 2012), optical method (Dolgova, 2016) and, neutron imaging (Mannes et al., 2007). X-ray-based methods stand out as the most widely employed technique for measuring wood density. Often, radiograph films are employed, providing a 2D representation of a 3D object and thereby forfeiting depth information. This approach relies on samples with a defined thickness, and to minimize biases, sample preparation is important. Hounsfield (1973) addressed this issue through tomography: capturing projections from varied angles with a subsequent 3D reconstruction of an object. Since then, X-ray tomography has revolutionized wood imaging, especially for dendrochronological studies or for the assessment of internal features of tree logs.

The automatic measuring of tree rings is important for obtaining high sample throughputs. The first step is to identify the location of the pith. Although this is the first step in generating radial profiles (Norell, 2009), pith position provides information related to the inner structure of logs, helps detect longitudinal gradients as well as knots and cracks in the wood and allows determining growth-ring eccentricity (Saint-André & Leban, 2001). Numerous techniques have been proposed to facilitate the automated or semi-automated detection of pith position from various image sources, including X-ray tomography, ultrasonic tomography (UT), inexpensive cameras and surface laser scans of tree cross sections. Among these approaches, the Hough Transform (HT) method is commonly applied (Bhandarkar et al., 1999; Andreu & Rinhofer, 2001; Longuetaud et al., 2004; Norell & Borgefors, 2008; Boukadida et al., 2012). In the HT-based method, growth rings are conceptualized as concentric circles centred around the pith.

Some studies have also used the biological or morphological properties of trees to locate the pith ([Jaeger et al., 1999](#); [Flood et al., 2003](#)). [Wei et al. \(2011\)](#) and [Beaulieu & Dutilleul \(2019\)](#) provide comprehensive reviews of different pith detection approaches. HT-based methods work very well for small-sized and fast-growing tree species, as they have relatively regular, circular, and wide annual rings. However, HT-based methods can produce inaccurate pith locations when the annual rings contain irregularities, defects, and decay.

After the pith's location is identified, the following step involves identifying tree-ring edges within the pith-to-bark profile. Most studies have adopted an edge detection approach, in which annual rings are tracked by locating the sharp transition and abrupt changes in the pixel intensity of the image ([Cerdeira et al., 2007](#); [Kalle et al., 2009](#); [Entacher et al., 2007](#); [Sundari & Kumar, 2014](#)). These discontinuities in pixel intensity result from the density change between the dark-coloured LW and the light-coloured EW. Many commercial and freely available tools (e.g., ImageJ, WinDENDRO™, Coorecorder, LignoVision™) can detect and measure tree rings.

Several research groups have developed R packages and algorithms for tree-ring analyses. [Hietz \(2011\)](#) linked the commercial image analysis program SigmaScan with Excel and R code to analyse tree rings. [Lara et al. \(2015\)](#) delineated rings through variations in greyscale values using the measuRing R package through a visual interface. Moreover, [Campelo et al. \(2019\)](#) developed the xRing package, designed specifically for analysing micro-densitometry data, to automatically detect tree-ring boundaries, and this package also provided a graphical user interface (GUI) for manual correction. More recently, [Poláček et al. \(2023\)](#) applied deep learning to detect and measure tree rings automatically, and [Martinez-Garcia et al. \(2021\)](#) developed a new algorithm to visualize the 3D structure of tree rings. To the best of our knowledge, there exists no R package that encompasses functions for automatically identifying pith

location, ring segmentation and computing average ring density for processing the CT-scan data of tree discs and logs.

In this manuscript, we present CTRing, a new R package that extends the capabilities of the XRing package to X-ray medical CT images; this novel package includes functions to automatically detect pith, produce a tree-ring density profile, delineate the EW–LW transition and allow for manual corrections. Pith detection is based on the HT method, which uses multiple arc segments; this approach should be robust when encountering defects found within a tree disc. Finally, we present results from samples collected from two plantation-grown white spruce (*Picea glauca* (Moench) Voss) trees.

2.3 Materials and methods

2.3.1 Computerized tomography (CT)

CT scans produce a series of X-ray images collected at different angles to enable visualizing an object's internal structures. These images, called projections, are then used to produce a 3D view of the volume using a filtered back projection (Hendee & Ritenour, 2003). The object is described by voxels (e.g., $100 \times 100 \times 400 \mu\text{m}$; in a 3D grid) that contain the attenuation of the X-ray signal. The attenuation is expressed in Hounsfield units (HU) and is calculated as the ratio of X-ray attenuation differences (Kalender, 2011; Vock, 2001) (Eq. 1).

$$HU = 1000 \frac{\mu_x - \mu_{\text{water}}}{\mu_{\text{water}} - \mu_{\text{air}}} \quad (1)$$

where μ_x , μ_{water} and μ_{air} are the linear attenuation coefficients for the tested specimen ($\text{length}\cdot\text{unit}^{-1}$), water ($\text{length}\cdot\text{unit}^{-1}$) and air ($\text{length}\cdot\text{unit}^{-1}$), respectively. HU is represented by grey levels (recorded at 8,

12 or 16 bits), as shown in [Figure 2-1](#), and its values fluctuate with wood density, as the attenuation coefficient is directly related to density ([Macedo et al., 2002](#)). To obtain density values, we selected middle slice from all the images in the z-direction, such that the voxels become pixels. Any slice can be used, or the slices can be averaged over the z-direction. The number of pixels per slice is always constant (512×512). Thus, the size of the pixel or the image resolution varies with specimen size (between 0.15 and $0.51 \text{ mm} \cdot \text{pixel}^{-1}$ for our sample discs).

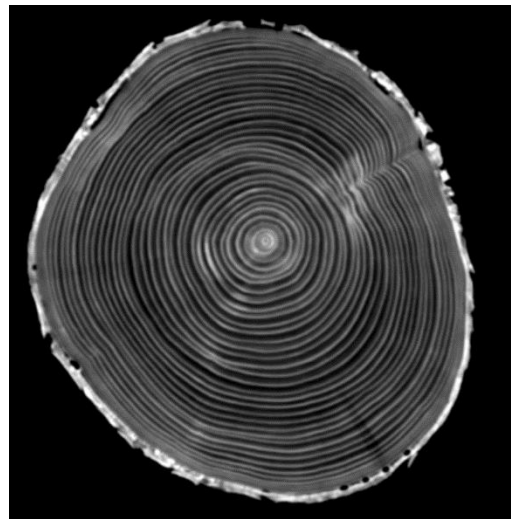


Figure 2-1: An X-ray computed tomography image of the cross-section of a white spruce log in which the densities at different positions in the object are shown in a greyscale format. The darker zones indicate earlywood, and the lighter ones indicate latewood.

2.3.2 Method overview

The pith-to-bark profile for a path of interest is obtained by:

1. Converting HU values to 8-bit greyscale (i.e., grey values between 0 and 255);
2. Applying a calibration curve to obtain density values for each voxel;

3. Identifying the pith of the disc;
4. Selecting the pixels along the pith-to-bark path of interest;
5. Delineating the rings, EW and LW along the path and averaging the density.

All steps were coded in R ([R Core Team, 2021](#)) and are presented in the CTRing package. The package will be available under the GPL-3 licensing. Each step is detailed in the following subsections.

2.3.2.1 Converting HU values to 8-bit greyscale

CT scanners store HU values as 8-bit (256 levels), 12-bit (4096 levels) or-16 bit (65,536 levels). To ensure portability and homogenize the workflow irrespective of CT scanner capacities, we rescale the grey values (GV_i , where i is the number of bits) to range between 0 and 255 (GV_8 , [Eq. 2](#)). The GV_8 values were not rounded to the integer value (i.e. all the decimals are kept). The downscaling to lower-bit scale is more convenient than rounding up to 16-bit, especially for CT scanners that store values in a lower-bit format.

$$GV_8 = GV_i \cdot \frac{2^8}{2^i} \quad (2)$$

2.3.2.2 Density values

Using the 8-bit grey values from samples of known density (acetal, heat glue, mosa, Teflon, and ultra-high molecular weight (UHMW) plastic), we developed a linear calibration equation ([Figure 2-2](#), intercept = -0.14 , slope = 0.018). This equation was then applied directly to determine the density of the wood. As X-ray absorption relies on atomic composition, we used calibration materials having density closely resembling that of wood. All samples were passed through a medical X-ray CT scanner (Siemens SOMATOM Definition AS+ 128) at INRS-ETE in Quebec City, Quebec. The X-ray tube of the CT scanner was operated at an energy level between 70 and 140 kV and a current of 300 to 700 mA. The equipment

was controlled by a workstation running Syngo CT VA48A software, which was originally designed for medical applications.

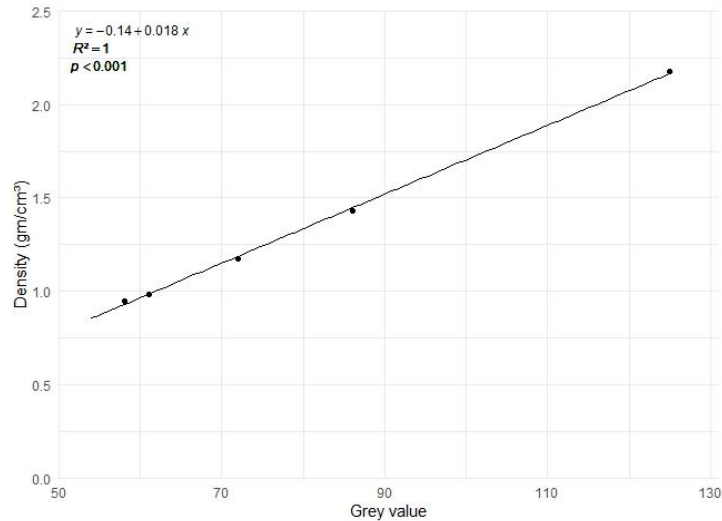


Figure 2-2: Calibration curve relating density to 8-bit grey values of known materials.

2.3.2.3 Pith identification

The location of the pith was found by iterating over several steps.

Step a: From a given point having coordinates x_1, y_1 (the starting value is the centre of the image and is updated at the end of each iteration), n number of line segments are traced from the centre to the tree-ring limits of the image (Figure 2-3a). The length of each line segment is less than half of the smallest dimension of the input image, and two adjacent line segments form an angle of $360/n$ between them.

A density profile for each individual segment is then obtained using a rotated rectangle between two points (x and y). The rotated rectangle serves as a moving window, extracting pixel values along the length and width of the rectangle and thus forms a matrix of profiles from the n segments. The length of this rectangle corresponds to the distance between x and y .

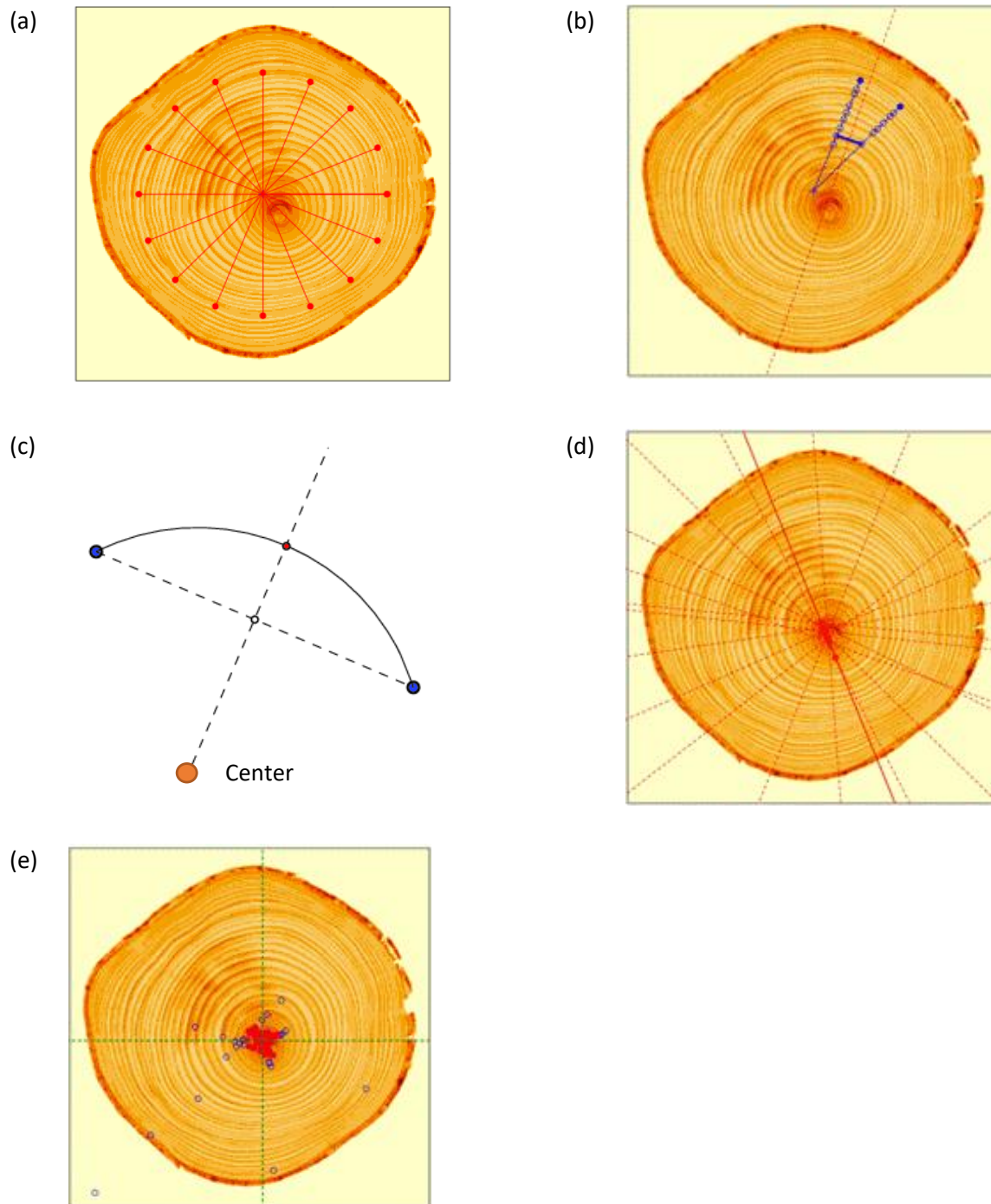


Figure 2-3: (a) Initial estimate of the pith location and segmentation of the image from pith location; (b) the location of two ring-edge points from adjacent segments; (c) estimation of the new pith based on the principal that the perpendicular bisector of any arc of a circle passes through the centre of the circle; (d) number of bisectors along which the pith should be located; and (e) positions for the pith estimated as the intersection of two bisectors (blue points are considered as outliers, and red points are used to estimate pith location; the intersection of the green dotted lines indicates the estimated pith location.)

Step b: The n mean density profiles obtained in the previous step are now used to detect tree-ring edges, using the internal “border()” function from the xRing package (Campelo et al., 2019). This function calculates the difference between the local k -point maximum and minimum values and compares it to a user-defined threshold, to identify tree-ring boundaries ($>$ threshold). The function simulates the kernel of the edge detectors, albeit in a horizontal 1D form. The argument k provides the length of the moving window used to calculate the local extreme values.

Step c: A new estimate of pith location is then obtained by using tree-ring edges. Our proposed technique is a modification of the original HT method. In the HT approach, the algorithm considers tree rings as a set of concentric circles, whereas our technique focuses on identifying specific pairs of points from two adjacent segments of the same ring (Figure 2-3b). The technique ensures the points are on the same ring by selecting pairs that are closest along the ring's edge. These pairs of points generate numerous arcs that should have the same centre, i.e., the tree pith. Geometrically, the perpendicular line that bisects the line segment connecting two endpoints of an arc passes from the centre of the circle, of which that arc is a segment (Figure 2-3c). Thus, the pith is then estimated as the intersection of all the lines obtained by the bisections of arcs (Figure 2-3d). The pith is assumed to be at the centroid of the intersections of all possible pairs of lines after dismissing outliers (Figure 2-3e).

Steps a to c are repeated (using the new estimate of pith location) until the previous coordinates are found or the maximum number of iterations (30) is reached. If the coordinates do not converge within 30 iterations, the position of the pith from the 30th iteration is taken as the final estimate.

2.3.2.4 Selecting the pixels along the pith-to-bark path of interest

The path corresponding to n -pixels wide is defined by the coordinates of the pith and an endpoint selected by the user (Figure 2-4a). The width of the line is set, and an average density perpendicular to the path is calculated to obtain the pith-to-bark density profile (Figure 2-4b).

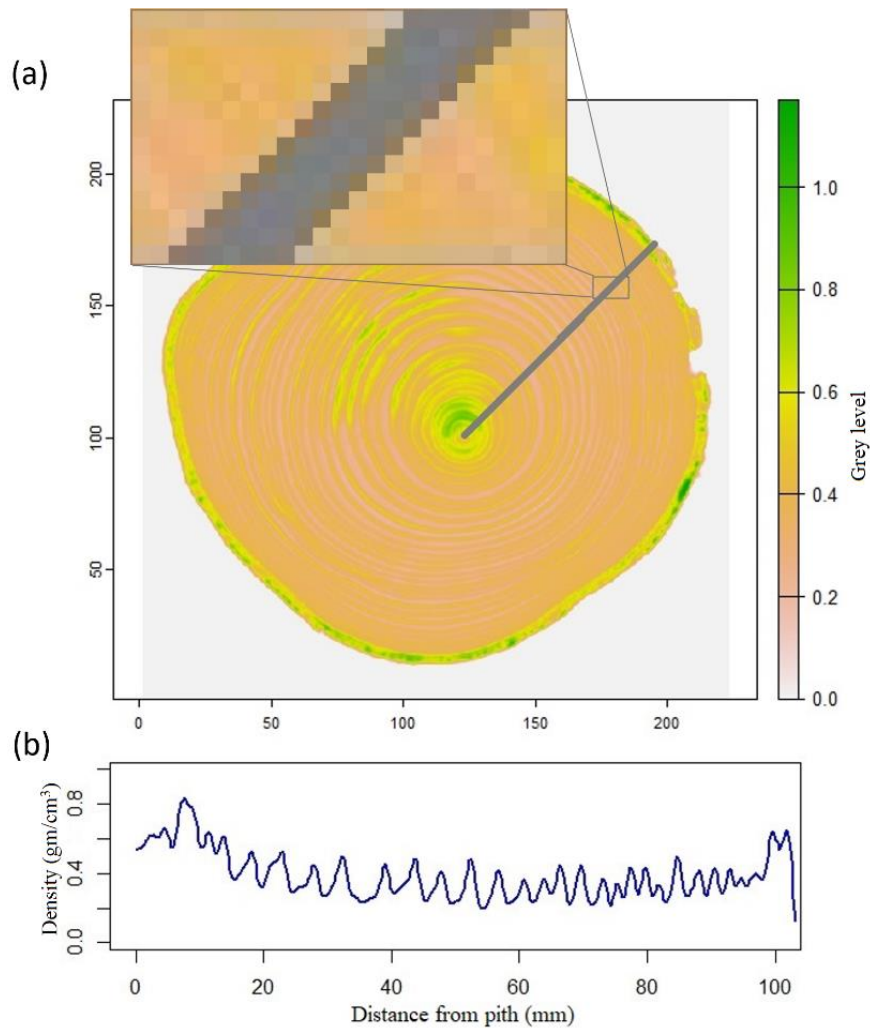


Figure 2-4: Profile path on the raster image, highlighting (a) the pixels through which the profile passes and (b) the plot of the profile from pith to the bark of the selected path.

2.3.2.5 Delineating the rings, earlywood and latewood along the path and averaging the density

Segmenting the profile path to rings relies on using a modified version of the “getBorders()” function from the xRing package, as discussed above. After the profile is segmented, the delineation of rings is

confirmed visually. The ring count calculated using the “getBorders()” function is subsequently compared with the manually counted rings on the disc or DICOM image. Rings are then added or removed accordingly using a graphical user interface (GUI).

The EW–LW transition is obtained using a 3rd-degree polynomial that is fitted to the density profile of each ring (Eq. 3).

$$\text{density} = a + b \cdot \text{dist} + c \cdot \text{dist}^2 + d \cdot \text{dist}^3 + \varepsilon \quad (3)$$

where a , b , c and d are the parameters estimated by the regression, dist represents the distance from the pith (in mm) and ε is the residual error.

The inflection point (e.g., $(-2c)/6d$) of the polynomial is assumed to correspond to the transition point between the EW and LW in the case that the polynomial is of the convex–concave form (Figure 2-5a). If the polynomial method fails, for instance, in cases with a low number of points within the ring, or when the minimum and maximum values fall outside the expected range, or when the inflection point is close to the minimum or maximum density of the ring, we use the mid-point method. In mid-point method, the EW-LW transition is established as the distance to the midway point between the minimum and maximum density of the ring (Figure 2-5b). Similarly, for the concave-convex polynomial form, the transition is determined as the distance to the midpoint between the minimum and maximum density of the ring (Figure 2-5c). Table 2-1 provides the approximate rates at which each transition type is encountered.

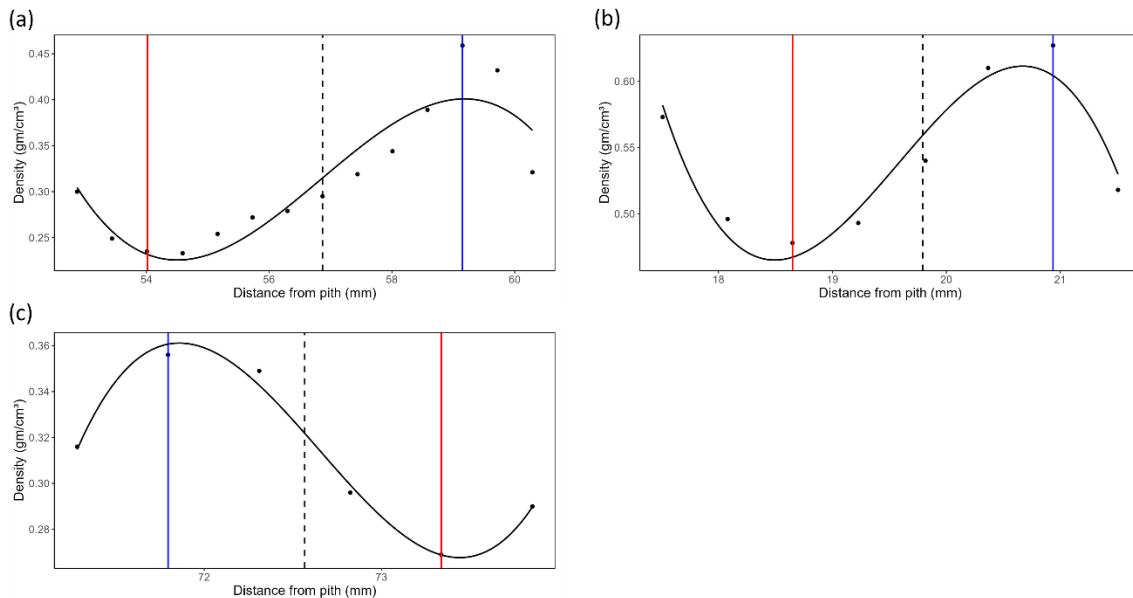


Figure 2-5: Earlywood-latewood transition (a) established by polynomial method when the form is convex-concave, (b) established by mid-point method when there are a low number of points within the ring, or when the minimum and maximum values fall outside the expected range, or when the inflection point is close to the minimum or maximum density of the ring and (c) established by mid-point method when the polynomial is concave-convex form. The black line is the fitted 3rd-degree polynomial function; the red and blue solid lines indicate the minimum and the maximum density points, respectively and the black dashed line indicates the earlywood-latewood transition.

Table 2-1: Earlywood-latewood transition types of the annual rings in percentage for the 60-disc samples representing different heights.

| Disc height | Transition type (in percentage) | | | | |
|-------------|---------------------------------|------|-----|------|-----|
| | 1 | 2 | 3 | 4 | 5 |
| 0% | 14.8 | 47.9 | 5.9 | 29.0 | 2.4 |
| 1.3m | 4.1 | 78.2 | 4.8 | 12.9 | 0 |
| 25% | 1.7 | 77.4 | 7.8 | 13.1 | 0 |
| 50% | 1.1 | 86.0 | 4.3 | 8.6 | 0 |
| 75% | 4.6 | 92.3 | 1.5 | 1.6 | 0 |

Transition types: 1 denotes a low number of points in the ring; 2 denotes the inflection point estimated by polynomial; 3 denotes minimum or maximum out of range; 4 denotes inflection point close to minimum or

maximum; 5 denotes convex to concave. The disc samples used here are the same ones used to validate the pith location.

Furthermore, the pixel size enables the determination of ring width. Thus, the final data frame for the selected path contains the following information for each tree ring: age, density, width, and also width and density for both EW and LW.

2.3.3 CT scan data

We destructively sampled 140 white spruce trees from two plantations established in the year 1990. Within each tree, five 2 cm thick discs were extracted at 0%, 25%, 50% and 75% of the total height, as well as at a fixed height of 1.3 m. These discs were preserved in a freezer until processing. Before undergoing scanning, the discs were placed in a conditioning room at a temperature of 20 to 22 °C and 65% relative humidity until constant weight was reached, implying a 12% moisture content (ISO 554, 2002). The samples were scanned in the same CT scanner using the same settings as those used for obtaining the calibration curve data set.

2.3.4 Validation of pith location

To assess the pith location functions, we randomly selected 60 sample discs representing all heights (0%, 25%, 50%, and 75% of the total height, as well as at 1.3 m) and social classes. The sample trees had an average diameter, height, and age of 18.4 cm, 13.4m and 31 years, respectively. The automatically identified pith (x_1, y_1) was compared against the actual pith position (x_0, y_0), the latter obtained by manual inspection of the CT images. We then calculated discrepancies (i.e., errors or distance from the actual pith (0, 0) in arbitrary x- and y-axes) and the Euclidean distance between the actual pith and automatically located pith (ED, Eq. 4):

$$ED = \sqrt{(x_1 - x_0)^2 + (y_1 - y_0)^2} \quad (4)$$

2.4 Results

The largest errors were observed for samples collected at the tree base—0% height—1.4 mm and 3.5 mm in the x- and y-directions, respectively (Fig. 2-6a). Figure 2-6b shows that more than two-thirds of the automatically detected pith was less than 1 mm from their manually located position and that the ED of 95% of the discs was less than 2 mm. Notably, the three sample discs featuring an ED above the 2 mm threshold exhibited more pronounced irregularities within the ring structures. Regarding ED variation with height within the tree (Fig. 2-6c), pith detection accuracy increased from the stump to the apex of the tree. The average ED of the discs at 75% was 0.42 mm, compared with 1.26 mm at 0%.

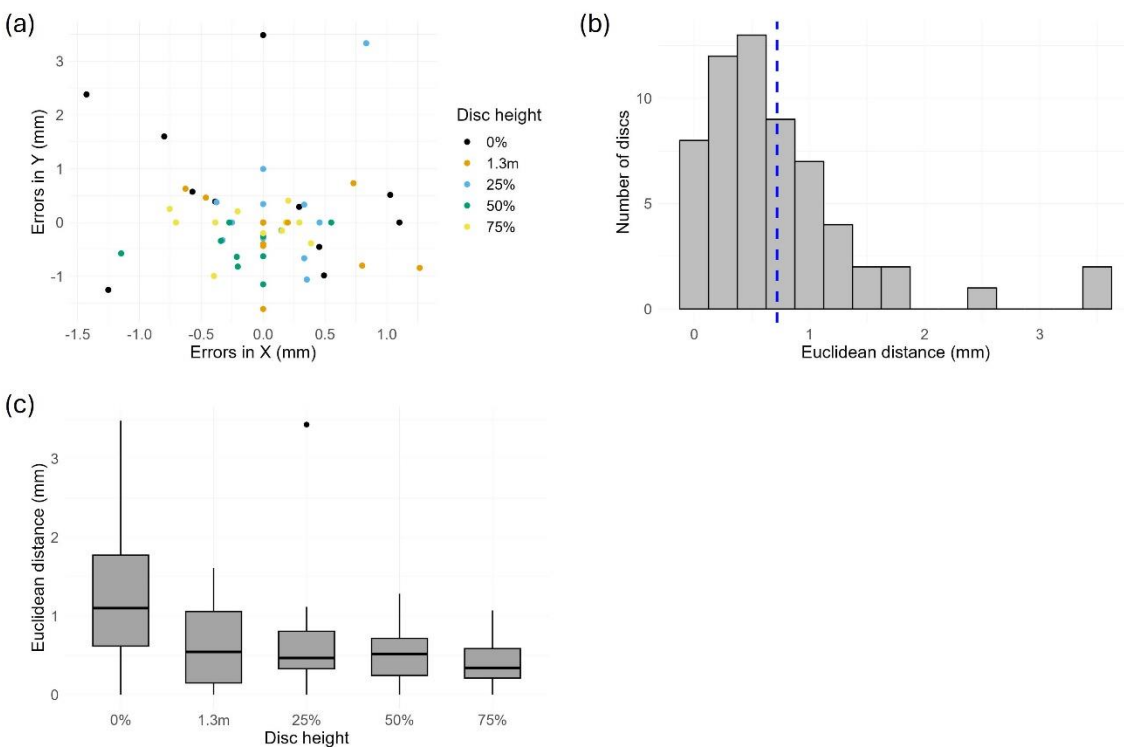


Figure 2-6: (a) Distances between the automatically and manually detected locations of pith in the x- and y-direction in terms of error (we considered all manually detected pith locations as 0, 0); (b) histograms showing the Euclidean distance between manually and automatically determined pith locations. The blue dashed line denotes the mean value (0.72 mm). (c) Boxplots presenting the Euclidean distances between manually and automatically determined pith locations for different disc heights.

2.5 Discussion

The CTRing package integrates three main steps to extract the tree-ring information from the CT-scan images: automatic detection of the pith, automatic delineation of tree rings and a graphical user interface (GUI) to correct the pith location and tree-ring edges. The good predictive performance and user-friendly interface make CTRing package a reliable alternative for CT-image analysis in dendrochronology and forest ecology.

We demonstrated that the developed algorithm located efficaciously the pith of various tree sizes and at different heights within the tree. Detection accuracy was lowest for discs collected closest to the stem base, as these samples exhibited more irregularities and “defects” in the tree-ring edges. Moreover, the number of pixels of an image is constant; thus, the pixels cover larger areas for the larger discs. Furthermore, in the upper stem of the tree, the annual rings become wider and more regular, and it is easier to obtain defect-free discs in the upper stem. [Boukadida et al. \(2012\)](#) reported errors in pith detection for hardwood species related to secondary pith produced by forking at the top of the tree. In our case, most of the trees exhibited a single, dominant straight trunk with small side branches, resulting in the absence of a secondary pith.

Overall, our mean discrepancy was 0.72 mm compared to 4.19 mm in [Andreu & Rinnhofer \(2001\)](#), 0.75 mm in [Longuetaud et al. \(2004\)](#), 1.69 mm in [Boukadida et al. \(2012\)](#), and 4.18 mm in [Gazo et al. \(2020\)](#), all using the HT method run on medical CT-scan data. Furthermore, in a related study, [Habite et al. \(2020\)](#) reported a mean error of 2.6 mm along the x-axis and 3.2 mm along the y-axis whereas, [Perlin et al. \(2018\)](#) observed an overall error of 5 mm when using images acquired through optical surface scanning and ultrasonic measurements, respectively. By using arcs rather than the complete ring, our method reduces the effect of possible abnormalities on estimates of pith location, thereby increasing

the accuracy for the images with defects, broken rings or where the ring direction changes rapidly and/or frequently. The accuracy of our method could be further improved by changing the settings or discarding those discs with obvious defects.

We applied a third-degree polynomial to delimit the EW–LW transition. The most widely used methods for identifying this zone are threshold densities, Mork’s Index (MI) and the inflection-point method. Threshold density relies on an arbitrary threshold value of wood density used to delimit EW and LW (Kumar, 2002). For example, Cown & Ball (2001) applied a threshold density of $400 \text{ kg}\cdot\text{m}^{-3}$ to define the EW–LW transition in Monterey (radiata) pine (*Pinus radiata* D. Don). Other studies have defined the EW–LW transition as the point where the density surpasses the halfway point between the minimum and maximum density values of a ring (Polge, 1978; Campelo et al., 2019). The first method is a more static approach, as it is based on a single predefined value for all rings, whereas the second method uses two density values (minimum and maximum) that vary from ring to ring and can lead to an EL–LW transition at quite different density values. On the other hand, MI is an anatomically based approach (Mork, 1928), which considers the wall thickness of the tracheid to define both types of wood. MI involves identifying the features (cell lumen diameter and cell wall thickness) of individual tracheid within a tree ring, thereby producing comprehensive anatomical data sets (Samusevich et al., 2020). When within-ring density varies substantially, both the threshold and MI approaches often misidentify the transition point (Björklund et al., 2017). Also, it was found that both methods tended to overestimate the proportion of EW, particularly for rings near the pith (Koubaa et al., 2002; Antony et al., 2012). All methods can erroneously identify the EW–LW transition when intra-annual density fluctuations (IADFs) are present.

Inflection-point methods, also known as derivative methods, rely on identifying points where the density vs. distance from the pith exhibits a change in slope for each individual ring. The inflection point

is defined as the maximum of the derivative function that describes the variability of intra-ring density (Koubaa et al., 2002). This point can be established by a polynomial or smooth function (Barbour et al., 1997; Koubaa et al., 2002) or through segmented regression (Nocetti et al., 2011; Franceschini et al., 2013). In our study, we opted for a third-degree polynomial rather than segmented regression because of the substantially lower number of measurements per ring compared with those obtained through micro-densitometry.

The profile is segmented into rings by comparing a threshold value with the minimum and maximum local k -points. The sensitivity can thus be adjusted but rarely permits identifying all the rings, by either over- or under detecting ring transitions. Narrow rings or wide rings having minimal LW (as in juvenile wood) are harder to segment because of the low contrast between the LW and EW of adjacent rings. IADFs or false rings—where short-term climate events cause tracheid having larger cell walls to be produced during EW forming (Palakit et al., 2012)—or cracks produced because of conditioning constraints can be inadequately detected. Therefore, correcting these possible errors in tree-ring edges and EW–LW transitions requires visually verifying these areas and then correcting manually; our package can perform these adjustments.

Further work should include improving the tree-ring detection accuracy of the CTRing package by controlling for multiple sources of noise. Moreover, noise that may arise from complex anatomical features could be reduced through image filtering, and thresholding could be applied to segment those images having a poor resolution (Sauvola & Pietikäinen, 2000). Threshold-based segmentation acts as a selective filter by isolating tree-ring features from the background, thus allowing for precise analysis even when using distorted images with some noise.

CTRing works well for white spruce, with the estimated pith location differing minimally from the observed position. It would be interesting to validate the package on species with similar structures to

better understand the limits and biases of the functions. This could then be extended to species that lack distinct ring transitions, such as diffuse-porous species like sugar maple (*Acer saccharum*) and trembling aspen (*Populus tremuloides*), or for species having less stable edges, such as European ash (*Fraxinus excelsior*) (Fabijańska et al., 2017).

The package source code is currently available at <https://gitlab.uqar.ca/schnro01/ctring> and will be available at the Comprehensive R Archive Network (CRAN) as well.

2.6 Acknowledgments

This work was funded by the Ministère des Ressources naturelles et des Forêts, Québec (Formerly Ministère des Forêts, de la Faune et des Parcs) and the Natural Sciences and Engineering Research Council of Canada. The authors would like to acknowledge Laval University and Institut National de la Recherche Scientifique, Québec for their support during sample storage and processing. We thank our reviewers for their comprehensive and insightful feedback, which greatly enhanced both the quality of this paper and the package.

2.7 Author contributions

Dipak Mahatara, Robert Schneider, and Filipe Campelo conceived the ideas and led the package development; Dipak Mahatara led the writing of the manuscript and Robert Schneider supervised the work; All authors worked on the advancement of the package, contributed critically to the draft, and gave final approval for the submission. The authors declare no conflict of interest.

2.8 References

Abedi, T. (2021). *Effects of some important genes, phytohormones, and abiotic factors on wood formation in trees; an overview.*

Andreu, J. P., & Rinshofer, A. (2001). Automatic detection of pith and annual rings on industrial

- computed tomography log images. *ScanTech, Seattle, Washington, USA*, 37–47.
- Antony, F., Schimleck, L. R., & Daniels, R. F. (2012). A comparison of earlywood–latewood demarcation methods—a case study in loblolly pine. *IAWA Journal*, *33*(2), 187–195.
- Baar, J., Tippner, J., & Rademacher, P. (2015). Prediction of mechanical properties—modulus of rupture and modulus of elasticity—of five tropical species by nondestructive methods. *Maderas. Ciencia y Tecnología*, *17*(2), 239–252.
- Babst, F., Bouriaud, O., Papale, D., Gielen, B., Janssens, I. A., Nikinmaa, E., Ibrom, A., Wu, J., Bernhofer, C., & Köstner, B. (2014). Above-ground woody carbon sequestration measured from tree rings is coherent with net ecosystem productivity at five eddy-covariance sites. *New Phytologist*, *201*(4), 1289–1303.
- Baker, T. R., Phillips, O. L., Malhi, Y., Almeida, S., Arroyo, L., Di Fiore, A., Erwin, T., Killeen, T. J., Laurance, S. G., & Laurance, W. F. (2004). Variation in wood density determines spatial patterns in Amazonian forest biomass. *Global Change Biology*, *10*(5), 545–562.
- Beaulieu, J., & Dutilleul, P. (2019). Applications of computed tomography (CT) scanning technology in forest research: a timely update and review. *Canadian Journal of Forest Research*, *49*(10), 1173–1188.
- Bhandarkar, S. M., Faust, T. D., & Tang, M. (1999). CATALOG: a system for detection and rendering of internal log defects using computer tomography. *Machine Vision and Applications*, *11*(4), 171–190.
- Björklund, J., Seftigen, K., Schweingruber, F., Fonti, P., von Arx, G., Bryukhanova, M. V., Cuny, H. E., Carrer, M., Castagneri, D., & Frank, D. C. (2017). Cell size and wall dimensions drive distinct variability of earlywood and latewood density in Northern Hemisphere conifers. *New Phytologist*, *216*(3), 728–740.
- Boden, S., Schinker, M. G., Duncker, P., & Spiecker, H. (2012). Resolution abilities and measuring depth of high-frequency densitometry on wood samples. *Measurement*, *45*(7), 1913–1921.
- Boukadida, H., Longuetaud, F., Colin, F., Freyburger, C., Constant, T., Leban, J. M., & Mothe, F. (2012). PithExtract: A robust algorithm for pith detection in computer tomography images of wood—Application to 125 logs from 17 tree species. *Computers and Electronics in Agriculture*, *85*, 90–98.

- Bouriaud, O., Leban, J.-M., Bert, D., & Deleuze, C. (2005). Intra-annual variations in climate influence growth and wood density of Norway spruce. *Tree Physiology*, *25*(6), 651–660.
- Bradley, R. S. (1985). Quaternary paleoclimatology; methods of paleoclimatic reconstruction. *Quaternary Paleoclimatology; Methods of Paleoclimatic Reconstruction*. <https://doi.org/10.2307/632972>
- Campelo, F., Mayer, K., & Grabner, M. (2019). xRing—An R package to identify and measure tree-ring features using X-ray microdensity profiles. *Dendrochronologia*, *53*, 17–21.
- Cerda, M., Hitschfeld-Kahler, N., & Mery, D. (2007). Robust tree-ring detection. *Pacific-Rim Symposium on Image and Video Technology*, 575–585.
- Cown, D. J., & Ball, R. D. (2001). Wood densitometry of 10 *Pinus radiata* families at seven contrasting sites: influence of tree age, site, and genotype. *New Zealand Journal of Forestry Science*, *31*(1), 88–100.
- De Micco, V., Campelo, F., De Luis, M., Bräuning, A., Grabner, M., Battipaglia, G., & Cherubini, P. (2016). Intra-annual density fluctuations in tree rings: how, when, where, and why? *IAWA Journal*, *37*(2), 232–259.
- Deng, G., Li, M., Hao, Z., & Shao, X. (2022). Responses to Climate Change of Maximum Latewood Density from *Larix speciosa* Cheng et Law and *Abies delavayi* Franch. in the Northwest of Yunnan Province, China. *Forests*, *13*(5), 720.
- Dolgova, E. (2016). June–September temperature reconstruction in the Northern Caucasus based on blue intensity data. *Dendrochronologia*, *39*, 17–23.
- Entacher, K., Planitzer, D., & Uhl, A. (2007). Towards an automated generation of tree ring profiles from CT-images. *2007 5th International Symposium on Image and Signal Processing and Analysis*, 174–179.
- Fabijańska, A., Danek, M., Barniak, J., & Piórkowski, A. (2017). Towards automatic tree rings detection in images of scanned wood samples. *Computers and Electronics in Agriculture*, *140*, 279–289.
- Flood, K., Danielsson, P. E., & Seger, M. M. (2003). On 3D segmentation of knots in 3D-volume data acquired from X-ray linear cone-beam scanning. *Fifth International Conference on Image Processing*

and Scanning of Wood, 23–26.

Ford, K. R., Breckheimer, I. K., Franklin, J. F., Freund, J. A., Kroiss, S. J., Larson, A. J., Theobald, E. J., & HilleRisLambers, J. (2017). Competition alters tree growth responses to climate at individual and stand scales. *Canadian Journal of Forest Research*, *47*(1), 53–62.

Franceschini, T., Longuetaud, F., Bontemps, J.-D., Bouriaud, O., Caritey, B.-D., & Leban, J.-M. (2013). Effect of ring width, cambial age, and climatic variables on the within-ring wood density profile of Norway spruce *Picea abies* (L.) Karst. *Trees*, *27*, 913–925.

Fritts, H. (2012). *Tree rings and climate*. Elsevier.

Gauli, A., Neupane, P. R., Mundhenk, P., & Köhl, M. (2022). Effect of climate change on the growth of tree species: Dendroclimatological analysis. *Forests*, *13*(4), 496.

Gazo, R., Vanek, J., Abdul_Massih, M., & Benes, B. (2020). A fast pith detection for computed tomography scanned hardwood logs. *Computers and Electronics in Agriculture*, *170*, 105107.

Habite, T., Olsson, A., & Oscarsson, J. (2020). Automatic detection of pith location along norway spruce timber boards on the basis of optical scanning. *European Journal of Wood and Wood Products*, *78*(6), 1061–1074.

Harold, F. M. (1990). To shape a cell: an inquiry into the causes of morphogenesis of microorganisms. *Microbiological Reviews*, *54*(4), 381–431.

Hendee, W. R., & Ritenour, E. R. (2003). *Medical imaging physics*. John Wiley & Sons.

Hietz, P. (2011). A simple program to measure and analyse tree rings using Excel, R and SigmaScan. *Dendrochronologia*, *29*(4), 245–250.

Hounsfield, G. N. (1973). Computerized transverse axial scanning (tomography): Part 1. Description of system. *The British Journal of Radiology*, *46*(552), 1016–1022.

ISO 554. (2002). *Standard atmospheres for conditioning and/or testing – specifications*.

Jaeger, M., Leban, J.-M., Borianne, P., Chemouny, S., & Saint André, L. (1999). *3D stem reconstruction from CT scan exams. From log external shape to internal structures*.

- Kalender, W. A. (2011). *Computed tomography: fundamentals, system technology, image quality, applications*. John Wiley & Sons.
- Kalle, M., Petteri, O., & Martti, M. (2009). *SPECTRAL REFLECTANCES OF LOG ENDS FOR CAMERA BASED ANNUAL RING WIDTH MEASUREMENTS*.
- Koprowski, M. (2013). Spatial distribution of introduced Norway spruce growth in lowland Poland: The influence of changing climate and extreme weather events. *Quaternary International*, 283, 139–146.
- Koubaa, A., Zhang, S. Y. T., & Makni, S. (2002). Defining the transition from earlywood to latewood in black spruce based on intra-ring wood density profiles from X-ray densitometry. *Annals of Forest Science*, 59(5–6), 511–518.
- Kozłowski, T. T., & Pallardy, S. G. (1997). *Growth control in woody plants*. Elsevier.
- Kumar, S. (2002). Earlywood-Latewood Demarcation Criteria and Their Effect on Genetic Parameters of Growth Ring Density Components and Efficiency of Selection for End-of-Rotation Density of Radia Pine. *Silvae Genetica*, 51(5–6), 241–245.
- Lara, W., Bravo, F., & Sierra, C. A. (2015). measuRing: an R package to measure tree-ring widths from scanned images. *Dendrochronologia*, 34, 43–50.
- Li, M., Duan, J., Wang, L., & Zhu, H. (2018). Late summer temperature reconstruction based on tree-ring density for Sygera Mountain, southeastern Tibetan Plateau. *Global and Planetary Change*, 163, 10–17.
- Longuetaud, F., Leban, J.-M., Mothe, F., Kerrien, E., & Berger, M.-O. (2004). Automatic detection of pith on CT images of spruce logs. *Computers and Electronics in Agriculture*, 44(2), 107–119.
- Macedo, A., Vaz, C. M. P., Pereira, J. C. D., Naime, J. M., Cruvinel, P. E., & Crestana, S. (2002). *Wood density determination by X-and gamma-ray tomography*.
- Mannes, D., Lehmann, E., Cherubini, P., & Niemz, P. (2007). Neutron imaging versus standard X-ray densitometry as method to measure tree-ring wood density. *Trees*, 21, 605–612.

- Martinez-Garcia, J., Stelzner, I., Stelzner, J., Gwerder, D., & Schuetz, P. (2021). Automated 3D tree-ring detection and measurement from X-ray computed tomography. *Dendrochronologia*, *69*, 125877.
- Morel, H., Lehnebach, R., Cigna, J., Ruelle, J., Nicolini, E. A., & Beauchêne, J. (2018). Basic wood density variations of *Parkia velutina* Benoist, a long-lived heliophilic Neotropical rainforest tree. *Bois et Forêts Des Tropiques*, *335*(1), 59–69.
- Mork, E. (1928). Die qualitaat des fichtenholzes unter besonderer rucsichtnahme auf schleif-und papierholz. *Papier Fabrikant*, *26*, 741–747.
- Nocetti, M., Rozenberg, P., Chaix, G., & Macchioni, N. (2011). Provenance effect on the ring structure of teak (*Tectona grandis* Lf) wood by X-ray microdensitometry. *Annals of Forest Science*, *68*, 1375–1383.
- Norell, K. (2009). An automatic method for counting annual rings in noisy sawmill images. *International Conference on Image Analysis and Processing*, 307–316.
- Norell, K., & Borgefors, G. (2008). Estimation of pith position in untreated log ends in sawmill environments. *Computers and Electronics in Agriculture*, *63*(2), 155–167.
- Palakit, K., Siripattanadilok, S., & Duangsathaporn, K. (2012). False ring occurrences and their identification in teak (*Tectona grandis*) in north-eastern Thailand. *Journal of Tropical Forest Science*, 387–398.
- Perlin, L. P., do Valle, Â., & de Andrade Pinto, R. C. (2018). New method to locate the pith position in a wood cross-section based on ultrasonic measurements. *Construction and Building Materials*, *169*, 733–739.
- Phillips, E. W. J. (1960). The beta ray method of determining the density of wood and the proportion of summer wood. *Journal of the Institute of Wood Science*, *5*, 16–28.
- Poláček, M., Arizpe, A., Hüther, P., Weidlich, L., Steindl, S., & Swarts, K. (2023). Automation of tree-ring detection and measurements using deep learning. *Methods in Ecology and Evolution*, *14*(9), 2233–2242.
- Polge, H. (1978). Fifteen years of wood radiation densitometry. *Wood Science and Technology*, *12*(3),

187–196.

- Polge, Hubert. (1966). Établissement des courbes de variation de la densité du bois par exploration densitométrique de radiographies d'échantillons prélevés à la tarière sur des arbres vivants: applications dans les domaines Technologique et Physiologique. *Annales Des Sciences Forestières*, 23(1), 1–206.
- Pothong, T., Elliott, S., Chairuang Sri, S., Chanthorn, W., Shannon, D. P., & Wangpakapattanawong, P. (2022). New allometric equations for quantifying tree biomass and carbon sequestration in seasonally dry secondary forest in northern Thailand. *New Forests*, 53, 17–36.
- Rathgeber, C. B. K., Cuny, H. E., & Fonti, P. (2016). Biological basis of tree-ring formation: a crash course. *Frontiers in Plant Science*, 7, 734.
- RJ, B. (1997). New methods for evaluating intra-ring X-ray densitometry data: maximum derivative methods as compared to Mark's index. *Timber Management Toward Wood Quality and End-Product Value: Proceedings of the CTIA/IUFRO International Wood Quality Workshop, Quebec City, Canada, August 18-22*.
- Saint-André, L., & Leban, J.-M. (2001). A model for the position and ring eccentricity in transverse sections of Norway spruce logs. *European Journal of Wood and Wood Products*, 59(1–2), 137–144.
- Samusevich, A., Lexa, M., Vejpusťková, M., Altman, J., & Zeidler, A. (2020). Comparison of methods for the demarcation between earlywood and latewood in tree rings of Norway spruce. *Dendrochronologia*, 60, 125686.
- Sauvola, J., & Pietikäinen, M. (2000). Adaptive document image binarization. *Pattern Recognition*, 33(2), 225–236.
- Schneider, R., Zhang, S. Y., Swift, D. E., Begin, J., & Lussier, J.-M. (2008). Predicting selected wood properties of jack pine following commercial thinning. *Canadian Journal of Forest Research*, 38(7), 2030–2043.
- Sundari, P. M., & Kumar, S. B. R. (2014). An approach for dendroclimatology using image processing techniques. *2014 World Congress on Computing and Communication Technologies*, 234–236.

- Team, R. C. (2016). R: A language and environment for statistical computing. R Foundation for Statistical Computing, Vienna, Austria. [Http://Www. R-Project. Org/](http://www.R-project.org/).
- Vaganov, E. A., Hughes, M. K., & Shashkin, A. V. (2006). Introduction and factors influencing the seasonal growth of trees. *Growth Dynamics of Conifer Tree Rings: Images of Past and Future Environments*, 1–20.
- Visser, R. M. (2021). Dendrochronological Provenance Patterns. Network Analysis of Tree-Ring Material Reveals Spatial and Economic Relations of Roman Timber in the Continental North-Western Provinces. *Journal of Computer Applications in Archaeology*, 4(1).
- Vock, P. (2001). WA Kalender: Computed tomography: fundamentals, system technology, image quality, applications (with CD-ROM). *European Radiology*, 11(9), 1855.
- Wei, Q., Leblon, B., & La Rocque, A. (2011). On the use of X-ray computed tomography for determining wood properties: a review. *Canadian Journal of Forest Research*, 41(11), 2120–2140.
- Woods, F. W., & Lawhon, W. T. (1974). Gamma densitometry of increment cores. *Forest Science*, 20(3), 269–271.
- Wu, Z., Fan, C., Zhang, C., Zhao, X., & von Gadow, K. (2022). Effects of biotic and abiotic drivers on the growth rates of individual trees in temperate natural forests. *Forest Ecology and Management*, 503, 119769.
- Zobel, B. J., & Van Buijtenen, J. P. (2012). *Wood variation: its causes and control*. Springer Science & Business Media.
- Żywiec, M., Muter, E., Zielonka, T., Delibes, M., Calvo, G., & Fedriani, J. M. (2017). Long-term effect of temperature and precipitation on radial growth in a threatened thermo-Mediterranean tree population. *Trees*, 31, 491–501.

CHAPTER III

Influence of commercial thinning on wood density and carbon sequestration in white spruce (*Picea glauca* (Moench) Voss) plantations

Authors: Dipak Mahatara, Julie Barrette, Boris Dufour, Pierre Francus, Luc Sirois, Alexis Achim,
Robert Schneider

Copy of the manuscript

To be submitted to the Forest Ecology and Management

3.1 Abstract

Effective forest management could play a crucial nature-based solution for climate change mitigation. Commercial thinning, often included in silvicultural scenarios applied to plantations, influences tree growth and wood properties, and consequently can modify the carbon sequestration rate. The consensus on whether thinning increases or decreases carbon storage is unclear. Carbon sequestration is influenced by factors such as thinning timing and intensity, tree species, and, notably, wood density. The present study considered the inter and intra-tree density variations to estimate carbon dioxide (CO₂) sequestration rates under four treatments (control, thinning from below, early crop tree release (CTR) of 50/ha, and CTR of 100/ha) conducted in white spruce (*Picea glauca* (Moench) Voss) plantations in eastern Quebec. The plantations dating from 1990 were thinned in 2008. Firstly, the disc samples collected in 2021 from 140 trees across the 4 thinning intensities were used to construct a model that predicts ring density (RD) after thinning. Secondly, the plot inventory data from 2008, 2014, and 2021, combined with RD model were used to estimate individual tree carbon sequestration, which was then summed up to the plot level. The findings show: (1) RD displayed higher values near the pith, followed by a rapid decline, after which RD slightly increased towards the bark; (2) thinned and control treatments showed similar average RD chronologies throughout the study period, constraining the generalization of RD trends post-thinning; (3) thinned plots exhibited lower CO₂ sequestration rates than control plots, with the estimates of 5.17, 5.35, 4.75, and 5.84 tons/ha/year for 100 CTR, 50 CTR, thinning from below, and control respectively. The growth of residual trees did not sufficiently compensate for the stock loss during thinning, even after 13 years. This study showed the importance of considering inter and intra-tree density variations for accurate carbon estimation. However, an extended follow-up period is necessary to discern the direction of changes in growth.

Keywords: Thinning, CO₂ sequestration, Ring density modeling, Crop tree release, intra-tree density variation, White spruce

3.2 Introduction

Climate change, driven by rising carbon dioxide (CO₂) emissions, stands as one of the most pressing global challenges of our time. Forests, that are one of the major carbon sinks recognized by the Intergovernmental Panel on Climate Change (IPCC), store 40-60% of terrestrial carbon and play a crucial role in the global carbon cycle (Brown & Lugo, 1982; Nabuurs et al., 2007; Pan et al., 2011). Intensive forest management is considered as the third largest natural pathway to mitigate climate change (Griscom et al., 2017), although it has yet to be fully quantified. A better understanding of forest carbon dynamics in diverse management scenarios is crucial for advancing sustainable practices and improving projections of future atmospheric CO₂ concentrations.

Under certain circumstances, well-managed forest ecosystems can serve as stable carbon sinks (Jandl et al., 2007; Thürig & Kaufmann, 2010; Noormets et al., 2015; Ontl et al., 2020). Among different forest management practices, thinning is the most important and widely used silvicultural tool that directly influences tree growth, wood quality, and carbon content (Ruiz-Peinado et al., 2013; Russo et al., 2019). In general, it has been suggested that radial growth and earlywood percentage of conifer species increase with spacing (Zhang, 1995; Tasissa & Burkhardt, 1997; Mäkinen et al., 2002). Thinning diminishes competition among remaining trees, promotes increased availability of water, nutrients, and solar radiation, thereby enhances growth and vigor of the residual trees (Eriksson, 2006; Geng et al., 2021). Several studies suggest that thinning, by promoting increased growth of remaining trees and enhancing undergrowth vegetation and regeneration, may contribute to higher carbon sequestration rates within the stand (Briceño-Elizondo et al., 2006; Garcia-Gonzalo et al., 2007; Zhang et al., 2019; Zhang et al., 2023). In contrast, some studies showed that thinning significantly alters the stand density and hence decreases aboveground carbon storage both immediately and over the long-term (Ruiz-Peinado et al., 2016; Kariuki, 2008; Lin et al., 2018). Schaedel et al. (2017) reported that precommercial or early

thinning might have positive impact on long-term carbon sequestration, proposing it as an alternative to achieve climate change mitigation objective. These findings show that thinning indeed increases the growth and quality of individual trees, but it does not always lead to an increase in total carbon storage of a stand. Furthermore, it has been reported that thinning has a lesser impact in relative terms on dominant and codominant trees, while smaller (suppressed) trees exhibit a greater relative response (Pukkala et al., 1998; Peltola et al., 2002). Larson (1963) observed that the stem's shape is related to the crown, implying that ring growth is affected by the foliage and branches above the measurement point. So, the extent of post-thinning carbon storage is intricately influenced by factors such as the intensity of thinning and its type (Hoover & Stout, 2007), tree species and their status in the stand (Peltola et al., 2002; Zhang et al., 2018), age during thinning (Schroeder, 1991) and environmental conditions (Downes & Drew, 2008; Gonzalez-Benecke et al., 2010), making it challenging to generalize the consequences of thinning on above-ground carbon dynamics.

Various thinning strategies are used to achieve diverse forest management objectives (Ashton & Kelty, 2018). In Quebec, since 2014, forest management plans must reduce the differences between managed and unmanaged forests, in order to maintain natural ecosystem properties—composition, structure and function (Government of Quebec, 2013). Commercial thinning by early crop tree release (CTR) has been recommended as a way to initiate structural conversion and accelerate the development of uneven aged forest stand over the long run (Singer & Lorimer, 1997; Gagné et al., 2016, 2019). CTR provides density control at the individual level to release competition of certain dominant trees, allowing them to grow more vigorously (Schütz, 1997; Grenon et al., 2007; Miller et al., 2010). Although a growing concern exists on growth and stand structure following CTR (Trimble, 1971; Ward, 2002, 2013; Ward et al., 2008; Lafèche et al., 2013; Dupont-Leduc et al., 2020), the short and long-term effects of CTR on forest productivity, wood quality and carbon sequestration potential is still poorly understood.

The carbon content of a tree is generally determined by multiplying dry biomass and carbon conversion factor (Houghton et al., 1990; Pan et al., 2011; Nizami, 2012). A value of 0.5 has widely been used as a conversion factor (Hollinger et al., 1993; Matthews, 1993; Brown, 2002; Chave et al., 2005; IPCC, 2006; Zhang et al., 2015; Fahey et al., 2010). The dry biomass can be estimated either using biomass equations or by multiplying cubic volume by the wood density for a given species (Wood Handbook, 1999; Jenkins, 2004). However, the biomass equations assume the same dry weights for trees of the same size, ignoring the effects of wood density variations associated with age, treatment, and the growing environment.

Basic wood density, refers to the ratio of oven-dried weight to green volume and, is recognized as a primary indicator of wood quality (Ortega Rodriguez & Tomazello-Filho, 2019). There exists a distinct wood density patterns along the bole, among individuals and among species (Wiemann & Williamson, 1989; Woodcock, 2000; Muller-Landau, 2004), and ignoring this variability can lead to substantial inaccuracies in carbon estimations (Laurance et al., 2007). In fact, the variability in density exists both in radial and vertical dimensions, and becomes more evident with changes in forest management practices (Zubizarreta Gerendiain et al., 2007; Downes & Drew, 2008; D'Amato et al., 2011). In pioneer and early successional species, wood density increases from pith to bark, while an opposite pattern is observed for late-successional species showing a clear adaptive strategy (Van Gelder et al., 2006). Vertical variations in wood density are less explored than radial patterns due to challenges in sample acquisition. Generally, wood density decreases from the tree's base to its top, attributed to the changing proportion of juvenile wood (Zobel & Van Buijtenen, 2012). Wood density values reported in the literature are often obtained from a single defect-free core sample at breast height (Williamson & Wiemann, 2010). Thus, use of generic wood density value of tree species can produce misleading carbon estimates as the average might not capture the full complexity of the wood density variability within a tree. Methods that incorporate intra wood density variations have been shown to enhance the accuracy of carbon estimates

(Muller-Landau, 2004; Repola, 2006; Chave et al., 2014; Wiemann & Williamson, 2014; Bastin et al., 2015).

There has long been an interest in the development of models to predict annual ring density (RD), thereby enhancing our understanding of the consequences of silvicultural interventions on wood quality. These models can be used to convert volume to dry biomass, and subsequently to carbon and energy content of a stand, using volume equations, yield tables, and growth models. Most of the previous studies have employed cambial age as a key variables to characterize RD (Ikonen et al., 2008; Schneider et al., 2008; Ivković et al., 2013; Auty et al., 2014; Kimura & Fujimoto, 2014; Xiang et al., 2014) as it captures the complexity of tree growth patterns and physiological changes. Nevertheless, applying models reliant on cambial age might be challenging when cambial age is not available (e.g. inventory data without increment cores).

To test how different thinning regimes influence wood quality, growth and carbon content of white spruce (*Picea glauca* (Moench) Voss), we used a thinning trial in plantations that follows a randomized block design with four thinning intensities (Gagné et al., 2016; Dupont-Leduc et al., 2020): 1) control: only the skid trails were harvested, 2) thinning from below: uniform removal of small, diseased, or deformed stems, 3) 50 CTR: early release of 50 crop trees (CT) per hectare from competition on all sides within a 3-m radius from the bole and 4) 100 CTR: early release of 100 CT per hectare from competition on all sides within a 3-m radius from the bole. The growth and productivity of white spruce following various silvicultural scenarios have been relatively well-studied (Pelletier & Pitt, 2008; Ott, 2010; Olson et al., 2014; Dupont-Leduc et al., 2020), as has been the examination of wood properties, including genetic effects on wood quality traits, acoustic velocity and modulus of elasticity (Zhou & Smith, 1991; Hernandez et al., 2001; Park et al., 2012; Bérubé-Deschênes et al., 2016; Tony et al., 2019). However, there is limited understanding of the consequences of thinning on wood density and CO₂ sequestration of white spruce. Thus, our study asked: (1) does thinning decrease the RD of white spruce? (2) does the

ability of stands and individual trees to sequester CO₂ vary with the intensity of thinning? (3) is it necessary to account for inter and intra-tree density variations for accurately estimating carbon? To answer these questions, we first developed a mixed-effects model for predicting RD following thinning, applied the established model to estimate RD of trees in the permanent sample plots and subsequently calculated CO₂ sequestration based on volume and the predicted density. The concept of CTR has been recently applied to softwood stands in Eastern Canada and determining the effects of this innovative approach on carbon density can assist in evaluating the applicability of CTR for global carbon mitigation.

3.3 Materials and methods

3.3.1 Sampling Design

The study used a thinning trial located in the Bas-Saint-Laurent region of the province of Quebec, Canada (47.0° to 48.5° N latitude and 68.0° to 69.0° W longitude). The climate is characterized by a mean annual temperature of 2.0°C and an average annual precipitation of 1032 mm. The duration of the growing season ranges between 130 and 140 days with about 92 frost-free days ([Environnement Canada, 2015](#)).

The trial was established in 2008 in two white spruce plantations (Lechasseur and Humqui) and consists of a randomized block design with the plantation sites as the blocks ([Dupont-Leduc et al., 2020](#)). In each block, there were four thinning types as treatments: 1) control units, 2) thinning from below, 3) thinning with 50 CTR per hectare, and 4) thinning with 100 CTR per hectare. All four thinning types had 5 replicats leading to a total of 20 experimental units (EU; 99 m × 76 m, 7,500 m²) per block. Furthermore, each EU was subdivided into three experimental subunits of around 2,500 m² area: no gap, small gap, and large gap ([Figure 3-1](#)). In the subunits with no gap, permanent sample plots (PSP) spanning the distance between 2 skid trials with approximate dimensions of 33 m x 15 m (area ranging from 379 to 633 m²) were established 6 years after thinning (i.e., in 2014).

The trees removed during the thinning from below had a diameter at breast height (DBH) less than 12.0 cm and at least one 2.44-m log with a top-end outside bark diameter of at least 9.1 cm (Gagné et al., 2016). In the CTR, the CT were freed from all the competitors. A tree was considered a competitor when its branches touched the CT and were at least half the height of the CT. A tree was considered as CT when it 1) was dominant or codominant, 2) vigorous with no signs of defoliation, 3) had branch of maximum diameters <2 cm on the first 2 m of the bottom log, 4) had a crown with a regular form and no defects, and 5) maintained a live crown ratio of 40–60 percent (Gagné et al., 2016).

3.3.2 Data Collection

From all 40 PSPs, the DBH (mm, at 1.3 m above the ground) of all the trees (≥ 5 cm) and the total tree height (m) of every 15th tree were measured in the years 2014, and 2021. Since the PSPs were established in 2014, tree level information before the thinning year was not available. Increment cores collected at BH in 2014 from all the trees in PSPs were used to interpolate the DBH at the time of thinning (Dupont-Leduc et al., 2020).

Three to four white spruce trees were selected for destructive sampling from each EU. For this, three points were positioned randomly in the subunits with a small gap (Figure 3-1). In the field, the closest CT and codominant competitor to point 1 were selected. Likewise, a codominant tree closest to point 2 and an intermediate tree with a DBH ≥ 9.1 cm closest to point 3 were chosen. In this way, 40 codominant trees and 40 intermediate trees from all 40 EUs were sampled. Whereas we only sampled 30 CT and 30 codominant competitors from 40 EUs (10 CT and 10 codominant competitors from the EUs of 50 CTR/ha and 100 CTR/ha, and 10 CT and 10 codominant competitors from both the control and thinning from below EUs). This was done to maintain the proportion of the same number of CTs per treatment, as the release of the CTs was the same in both the 50 and 100 CT per ha. 140 trees were thus destructively felled in the summer of 2021. At first, the DBH of the sample trees was measured and after felling, total

tree height and trunk diameter at an interval of 1 m from base to top of the tree were measured. Also, the DBH, azimuth, and distance of all trees in a 5 m radius around the sample trees were recorded. Two cm thick discs were cut from five positions along the stem, at 0% tree height, BH (1.3m), 25% of tree height, 50% of tree height and 75% of tree height. On each disc, the north was indicated.

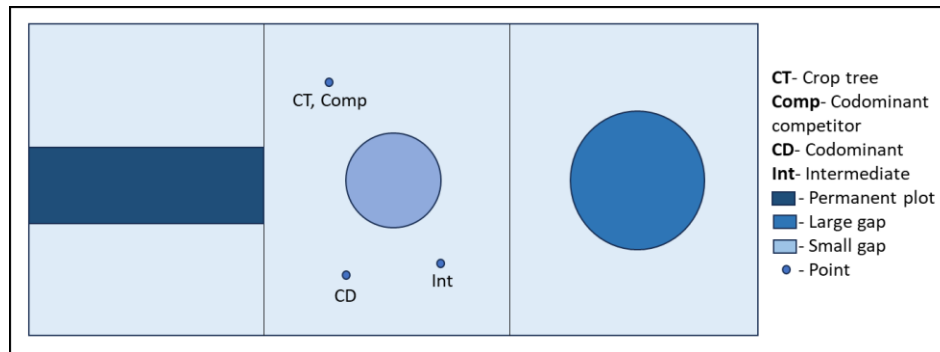


Figure 3-1: Layout of the experimental unit (EU) with three sub-units; no gap, small gap, and large gap

3.3.3 Wood density measurements

The collected discs were frozen and placed in a conditioning room at a temperature of 22–23°C and 58% relative humidity until constant weight was reached, implying 12% moisture content (ISO 554, 2002). Following this, the cross-sectional discs were passed through a medical X-ray Computed Tomography (CT) scanner, the Siemens SOMATOM Definition AS+ 128, with a workstation with Syngo CT VA48A software, the latter primarily intended for medical purposes at INRS-ETE located in Quebec City. The X-ray tube of the CT scanner was set to operate within an energy range of 70 to 140 kV and a current ranging from 300 to 700 mAs.

The CTRing package was used to extract the ring-level information from the CT images. In summary, the package adapts the Hough Transform method to locate the pith position and modified version of “getBorders” function from the xRing package (Campelo et al., 2019) for ring segmentation of the

selected path. Two pith to bark density profiles were obtained from two radial directions (North and East) for each disc. The profile paths were adjusted, if necessary, to avoid knots, cracks, or unclear ring boundaries. The number of rings of each disc were manually counted and rings were added or removed accordingly using the Graphical User Interface (GUI) of the CTRing package. We did not include the outermost ring (ring formed in the year 2021) in the density profile due to its incomplete formation. The yearly RW and RD were averaged over each profile, to obtain one series of RW and RD for every disc. The acquired series of RW were then cross dated within individual trees and across the entire experimental unit using the 'corr.rwl.seg' and 'ccf.series.rwl' functions available in the 'dplr' package (Bunn, 2010). We excluded damaged and broken discs from scanning, so our dataset consisted of density profiles from 678 discs with 13254 annual rings. The obtained density values were expressed as relative density or specific gravity, defined as the ratio of a substance's density to that of pure water at 4°C. Summary of tree and ring-level characteristics before and after thinning is given in [Table 3-1](#).

Table 3-1: Tree and ring level characteristics of sampled trees before and after thinning treatment

| Block | Treatment | Relative ring density | | Ring width (mm) | | DBH in 2021 (cm) | Height in 2021 (m) | Competition index* |
|-------|-----------|-----------------------|----------------|-----------------|----------------|------------------|--------------------|--------------------|
| | | Before thinning | After thinning | Before thinning | After thinning | | | |
| HU | 100 CTR | 0.395 (0.089) | 0.360 (0.044) | 3.58 (1.17) | 2.81 (1.12) | 18.50 (4.38) | 13.09 (2.09) | 1.20 (0.26) |
| | 50 CTR | 0.387 (0.078) | 0.343 (0.043) | 3.56 (1.11) | 2.79 (1.14) | 16.76 (4.16) | 12.89 (2.12) | 1.11 (0.27) |
| | Below | 0.383 (0.089) | 0.346 (0.053) | 3.60 (1.27) | 2.94 (1.15) | 18.37 (4.55) | 13.11 (2.66) | 1.10 (0.35) |
| | Control | 0.397 (0.096) | 0.356 (0.053) | 3.75 (1.22) | 2.86 (1.15) | 17.50 (4.35) | 13.26 (2.53) | 1.02 (0.26) |
| LE | 100 CTR | 0.378 (0.080) | 0.357 (0.054) | 3.85 (1.41) | 2.69 (1.18) | 19.28 (4.89) | 13.70 (2.38) | 0.94 (0.44) |
| | 50 CTR | 0.377 (0.081) | 0.353 (0.052) | 3.64 (1.32) | 2.48 (1.01) | 16.65 (4.84) | 12.84 (1.71) | 0.93 (0.31) |
| | Below | 0.379 (0.071) | 0.356 (0.044) | 3.88 (1.18) | 2.59 (1.02) | 20.35 (4.61) | 13.94 (2.21) | 0.99 (0.25) |
| | Control | 0.378 (0.080) | 0.354 (0.056) | 3.89 (1.26) | 2.61 (1.05) | 18.90 (4.54) | 13.75 (1.83) | 1.03 (0.27) |

Values shown are the mean and standard deviation in parentheses. HU and LE denote the site Humqui and Lechasseur respectively. () Table 3-3 provides the formula for calculating the competition index.*

3.3.4 Predicting post-thinning ring density profiles

Unlike many similar studies (Ivković et al., 2013; Auty et al., 2014; Filipescu et al., 2014; Xiang et al., 2014; Franceschini et al., 2018), we chose years after thinning as the primary predictor variable instead of cambial age to model mean RD. This is because the RD model will be applied to the PSP data to assess CO₂ sequestration following thinning, and the age of the individual trees is unknown. We thus considered 2009 as the first year after thinning, and this progression culminated with 2020 as the twelfth year. Rings formed in the year of thinning and prior to the thinning were omitted from the final modeling dataset. The model was thus established utilizing RD data derived from a total of 7804 annual rings of 678 discs from 140 trees.

We applied mixed-effects models to align with the longitudinal structure of the data: discs were nested within trees; trees were nested within plots and plots within sites. We used the 'lmer' function from the 'lme4' package (Pinheiro, 2009) in R, utilizing the maximum likelihood method to fit the models. At first, we examined various variance-covariance structures of random effects with all possible combinations of hierarchical levels and found discs nested within trees as the best structure. Secondly, for model specification, we employed a two-stage modeling approach in order to account the distinctive trends in the RD of individual discs. In the first stage, we developed a disc-level model (Eq. 1) with year after thinning as a predictor variable and in the second stage the parameters of the disc-level model were regressed with all possible tree and ring level covariates (Table 3-3). Subsequently, the variance-covariance structure was added to the Eq. 1 and the parameters α_0 , α_1 , and α_2 of Eq. 1 were substituted by their respective linear model developed in stage 2, resulting in the formulation of the final model (Eq. 2). The summary of the parameter values obtained from disc-level model can be found in Table 3-2 and definitions and the abbreviations used for the candidate tree and ring level covariates can be found in Table 3-3. Detailed information for each step of model development is available in the supplementary document (Appendix I).

$$RD_{ijk} = \alpha_0 + \alpha_1 \cdot \ln(TY_{ijk}) + \alpha_2 \cdot TY_{ijk}^2 + \varepsilon_{ijk} \quad (1)$$

Where TY_{ijk} denotes the year after thinning for the k^{th} annual ring of the j^{th} disc from the i^{th} tree, α_0 , α_1 , and α_2 are the parameters to be estimated.

$$RD_{ijk} = \left(\beta_0 + \beta_1 \cdot DBH_i^2 + \beta_2 \cdot \sqrt{RW_i} + \beta_3 \cdot h_{\text{disc}_{ij}} \right) + \left\{ \left(\beta_4 + \frac{\beta_5}{DBH_i^2} + \beta_6 \cdot h_{\text{disc}_{ij}} \right) * \ln(TY_{ijk}) \right\} + \left\{ (\beta_7 + \beta_8 \cdot CI_i + \beta_9 \cdot h_{\text{disc}_{ij}}) * TY_{ijk}^2 \right\} + \mu_i + \mu_{ij} + \varepsilon_{ijk} \quad (2)$$

Where, β_0 , β_1 , β_2 , β_3 , β_4 , β_5 , β_6 , β_7 , β_8 , and β_9 are the parameters to be estimated, μ_i the tree random effect, μ_{ij} the disc nested in tree random effect and ε_{ijk} the error term.

Table 3-2: Descriptive statistics for parameters α_0 , α_1 and α_2 obtained by fitting Eq. 1 to 678 individual discs

| Parameters | Mean (Range) |
|------------|------------------------------|
| α_0 | 0.325 (0.179 – 0.467) |
| α_1 | 2.227 (-0.28 – 123.37) |
| α_2 | 0.00043 (-0.00075 – 0.00175) |

Table 3-3: Definitions of the abbreviations for the candidate variables used to develop final ring density model

| Abbreviations | Description |
|-------------------------|---|
| <i>DBH</i> | Tree diameter at breast height in cm |
| <i>Ht</i> | Total height of the tree in meter |
| <i>RW</i> | Average ring width of the tree at breast height in mm |
| <i>h_{disc}</i> | Disc position along the stem from stem base as a factor |
| <i>CI</i> | Quadratic diameter competition index, $\frac{DBH_i}{\sqrt{\frac{1}{N} \sum_{j=1}^N (DBH_j^2)}}$ |

Where: DBH_i is the diameter at breast height (DBH) of the subject tree in cm, DBH_j is the DBH of j -th neighboring tree in cm and N is the total number of neighboring trees in 5 m radius around the subject tree.

3.3.5 Assessing post-thinning CO₂ sequestration

3.3.5.1 Mean post-thinning wood density

The RD model uses year since thinning, RW, h_{disc} , and DBH and CI after 12 years of thinning as input variables (Eq. 2). Individual RW was obtained from the PSP data as the average radial increment for each period (period 1: $RW = (DBH_{2014} - DBH_{2008}) / (2 \times 6)$, period 2: $RW = (DBH_{2021} - DBH_{2014}) / (2 \times 7)$), CI was calculated as found in Table 3-3, i.e. the ratio between DBH_{2021} and the mean quadratic DBH in 2021. Finally, the RD for each ring was calculated for 5-disc heights (0%, 1.3 m, 25%, 50% and 75% of the total height of the tree in 2021).

All relative ring density values were converted to ring density unit (Kg/m³) at 12% moisture content. Furthermore, average wood density per growth period (2008-2014, 2014-2021) was calculated as follows.

1. Between the rings of one disc for each period

The outermost ring contributes more to the volume than the innermost ring, rendering a simple averaging of densities between the rings imprecise. To address this, we quantified the ring area at each disc height for each year after thinning and utilized these areas (or increments) as weights to compute the average density between the rings. For the disc at BH (BH, 1.3m), we calculated the area increment for each year by using the DBH measured in years 2008, 2014, and 2021, and assuming that the yearly growth between two measurements was equal. This calculation enabled us to compute the area-weighted density of each ring at BH for each growth period. For the discs other than at BH, the stem increment data were unavailable, so we utilized the ring area per year for all discs from the sample trees

(140 trees). We determined the area weight for each year by averaging all the discs at each height, and subsequently calculated the weighted mean wood density per growth period and height.

2. Between the discs of one tree for each period

Given that different disc heights represent varying proportions of the tree volume, we assigned weights to each disc based on their respective heights. To get the weight, we used the taper measurement of our samples. For this, we first defined the proportions of tree height represented by each disc: disc from 0% height (0 – 0.65 m), disc from BH (0.65 – 1.95 m), disc from 25% height (1.95 m to 37.5% of total height), disc from 50% height (37.5% to 62.5% of total height), and disc from 75% height (62.5% of total height to top of the tree). The volume percentage of each section was then obtained and averaged over all the sample trees. Finally, we used the average volume percentages as weight for the respective discs and got the average wood density for the two growth periods for each tree.

3.3.5.2 Volume increment and CO₂ sequestration

As not all tree heights were measured, a height - DBH equation (Eq. 3) based on Fortin et al. (2009) was calibrated for each block, treatment and year (Appendix II). As no height measurements were available for 2008, we applied the height – DBH equation calibrated for 2014 to the 2008 PSP data.

$$Ht_i = a + b \cdot \ln(DBH_i + 1) + c \cdot \ln(DBH_i + 1)^2 + \varepsilon_i \quad (3)$$

Where, a, b and c are the parameters of the model.

Tree volume for each inventory year was calculated from the measured DBH in 2008, 2014 and 2021 and estimated height from Eq. 3 in combination with the volume equation (Eq. 4) developed by (Prégent et al., 2010). The summary statistics of the DBH and height for all three inventoried years are presented in Table 3-6.

$$V_i = 0.0344 \cdot DBH_i^{1.8329} \cdot Ht_i^{1.1793} \quad (4)$$

Where V_i is the total tree volume without bark (cubic decimeter, dm^3).

Finally, tree volume increment was obtained by subtracting the volume at t from the one at $t+1$. C -sequestration was then estimated for each tree as (Eq. 5):

$$C_{seq_{ip}} = 3.67 \cdot (V_{ip} \cdot \rho_{ip} \cdot E \cdot C_0) \quad (5)$$

Where, $C_{seq_{ip}}$ is the amount of CO_2 sequestered (kilogram, Kg), V_{ip} is the volume increment (m^3) and ρ_{ip} is the mean wood density (Kg/m^3) of tree i for the growth period p . The term E denotes the density conversion factor (to convert wood density at 12% moisture content to basic wood density, constant value of 0.828 (Vieilledent et al., 2018)) and the term C_0 denotes the coefficient of carbon content (to convert dry biomass to carbon, constant value of 0.5). Finally, to determine the equivalent amount of CO_2 , the carbon content was multiplied by a stoichiometric conversion factor of 3.67 (44/12).

The effects of stand density index (SDI) thinning types (stand structure) and growth period on stand level variables (volume increment and CO_2 sequestration) were analyzed using analysis of variance (ANOVA). SDI (Eq. 6) characterizes the density of stands based on a quadratic mean diameter (d in cm) and the number of trees per hectare (N) by calculating the number of stems per hectare in relation to a mean diameter of 25 cm (Pretzsch & Biber, 2005). There was a high degree of correlation between SDI and thinning types, thus we did separate analysis—one for stand level variables vs SDI and another for stand level variables vs thinning types. The site effect was also considered as blocks, and thus added as a fixed term.

$$\text{SDI} = N \cdot \left(\frac{25}{d}\right)^{-1.605} \quad (6)$$

Finally, to assess the robustness of the average wood density at BH, we calculated total CO_2 sequestration per hectare over the 13 years studied by utilizing intra-tree density variations (actual CO_2 sequestration) and compared with the value obtained utilizing average wood density at BH of this study.

Again, to provide evidence for the necessity of accounting for the effects of treatments and growing conditions in carbon estimation, we compared the actual CO₂ sequestration with values obtained using the published wood density of white spruce (412 kg/m³; [De Araujo et al., 2015](#)).

3.4 Results

Among the 13 254 annual rings assessed, the relative RD ranged from 0.198 to 0.724, with a mean value of 0.366. There was a negative correlation between relative RD and annual RW, and this correlation was more pronounced before thinning (-0.50 and -0.39 before and after thinning respectively). When averaging the pith-to-bark density profiles for five different disc heights, we observed higher mean relative RD near the pith with a rapid decrease followed by a gradual increase towards the bark ([Figure 3-2A](#)). This observed trend was consistent across all social classes ([Figure 3-2C](#)) and thinning types ([Figure 3-2E](#)). In the vertical direction, the mean relative density remained almost consistent up to 50%-disc height (0.364, 0.362, 0.359 and 0.361 for disc heights 0%, BH, 25% and 50% respectively), with a slight increase observed at the topmost disc (0.373) ([Figure 3-2G](#)). For a given growth year, intermediate trees exhibited higher mean relative RD (0.390), while the other three dominance classes showed nearly identical average relative RD (0.362, 0.357, and 0.358 for codominant, competitor, and crop trees respectively) ([Figure 3-2C](#)). Tree growth rate and average relative RD in both study blocks remained consistent between control and thinned stands, with a slow rise after thinning. The average relative RD chronologies within the thinned and control stands displayed increased variability near the pith, which gradually followed identical trend after a few years. Eventually, 4-5 years after thinning treatment, control stands showed a slightly higher relative RD value than thinned plots ([Figure 3-2E](#)). Since the control and thinned treatments exhibited a similar trend in relative RD chronologies —characterized by a

decline until 2008 followed by an upward trend from 2009—it was difficult to attribute the observed relative RD patterns of thinned plots as only a consequence of thinning.

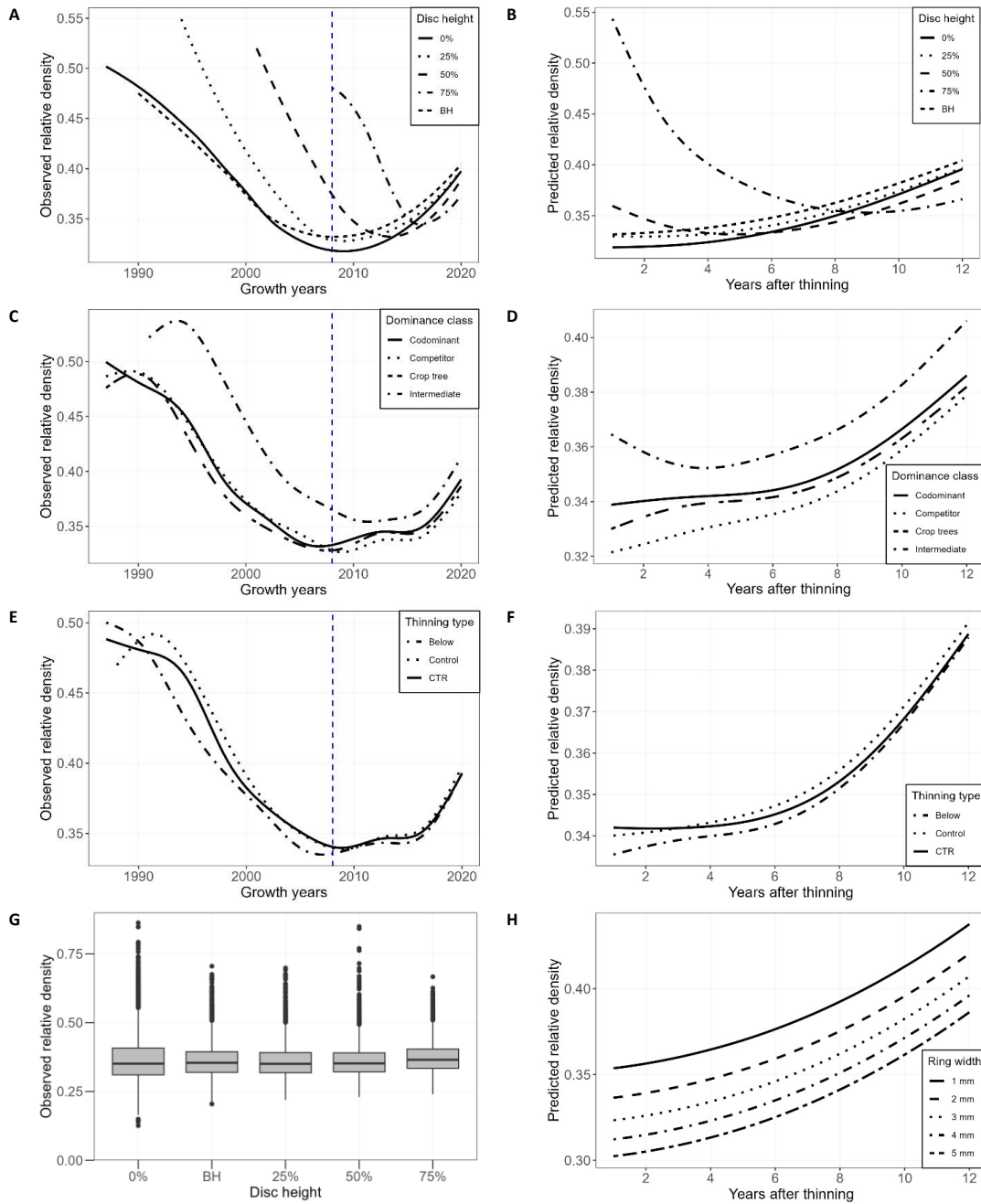


Figure 3-2: Model predictions for relative density for different disc heights, dominance classes, thinning types, and ring widths. Plots A, C and E denote the observed spline-smoothed relative density of the annual rings plotted against disc heights, social classes, and thinning types respectively and plot G denotes the axial pattern of observed

relative density, whereas plots B, D, F and H denote the predicted relative density with years after thinning from final model (Eq. 2) for different disc heights, social classes, thinning types and ring widths respectively. To plot the predicted curves, all the remaining tree-level and disc level variables were set to their respective mean values. The blue vertical dotted line in the plots of left panel represents the year of thinning (i.e., 2008).

3.4.1 Model fitting

Approximately 5% of RD profiles showed a consistent increasing trend, while the remaining 95% showed no discernible systematic trend in density within their respective RD profiles. The disc level models' (stage 1) accuracy was evaluated by comparing predicted and observed values, as well as by fitting model curves to their respective observed density profiles. The curves for the density profiles of individual discs were unbiased, indicating the effective representation of data patterns by Eq. 1 (not shown). The precision of the disc level model is highlighted by root mean square error (RMSE) of 0.015, mean absolute error (|ME|) of 0.012, and absolute percentage mean error (|ME|%) of 3.57%, all of which were calculated as averages over the 678 discs (Table 3-4).

Table 3-4: Fit indices and error statistics calculated from the disc level model (Eq. 1) and final model (Eq. 2)

| Model | | AIC | R-squared | Model errors | | |
|------------------|------|----------|---------------|--------------|-------|------|
| | | | | RMSE | ME | ME % |
| Disc-level Model | Min. | -140.1 | 0.056 | 0.004 | 0.003 | 0.98 |
| | Mean | -56.51 | 0.716 | 0.015 | 0.012 | 3.57 |
| | Max. | -25.65 | 0.988 | 0.044 | 0.033 | 9.32 |
| Final Model | | 32918.14 | 0.386 (0.759) | 0.025 | 0.018 | 5.23 |

The value in the parenthesis for final model indicates the R-squared value with both fixed and random terms.

The final model (stage 2) showed that RD can be best described with the addition of ring (RW at BH), disc (disc height), and tree (DBH and competition index (CI)) level covariates as fixed terms and disc nested within the tree as random terms. The fixed effects parameter estimates and standard deviation of the random effects for the final model are presented in Table 3-5. The prediction of RD using the final model

initially resulted in a 38% explained variability, which significantly increased to 76% with the inclusion of random effects. Error statistics obtained for the final model were 0.025, 0.018, and 5.23% for RMSE, |ME| and |ME|%, respectively (Table 3-4). The plot of the standardized residuals indicated no obvious residual trend in predicted RD (Figure 3-3). The variance components of the random effects in the final model accounted for approximately 39% and 24% of the total variance at the tree and disc levels, respectively, leaving the remaining 37% attributed to residuals (Table 3-5). Additionally, the final model's predicted average RD (0.354) closely approximated the observed post-thinning average RD (0.353), aligning well with the observed RD trends (Figure 3-2). The trends showed a slight increase in RD with years after thinning for discs at 0% and 25% tree height, as well as for those at BH. Conversely, discs at 50% and 75% of total height showed a decreasing trend followed by an increase (Figure 3-2B). The average values predicted for RD based on the final model were also higher for intermediate trees than the other three dominance classes (Figure 3-2D). Interestingly, the trees in the intermediate class required additional few years following thinning to reach the lowest mean RD, while the other three dominance classes displayed a gradual post-thinning increase (Figure 3-2D) from the first year. Finally, thinning intensity did not result in a significant enhancement of the model's fit statistics (not shown). In other words, the relationship between RD and the years post-thinning at a given growth rate, competition, and disc height remained unchanged. The average RD chronologies following thinning showed initial stability for the first few years, followed by a gradual increase for all the thinned and control stands (Figure 3-2F). Moreover, a consistent increase in RD was observed after thinning for a given ring width (Figure 3-2H).

Table 3-5: Parameter estimates, standard errors (SE), t-values and standard deviation of the random effects estimates for the final model of ring density given by Eq. 2.

| Fixed parameters | Estimate | SE | t-value |
|------------------|----------|-------|---------|
| β_0 | 0.427 | 0.024 | 17.48 |

| | | | |
|-----------------------------------|-------------------|------------------|--------|
| β_1 | -0.0001 | $1.59 * 10^{-5}$ | -8.52 |
| β_2 | -0.041 | 0.017 | -2.37 |
| β_3 : h _{disc} 25% | 0.013 | 0.003 | 3.94 |
| β_3 : h _{disc} 50% | 0.048 | 0.003 | 14.25 |
| β_3 : h _{disc} 75% | 0.261 | 0.005 | 45.88 |
| β_3 : h _{disc} BH | 0.013 | 0.003 | 3.73 |
| β_4 | 0.011 | 0.001 | 5.96 |
| β_5 | -3.91 | 0.202 | -19.33 |
| β_6 : h _{disc} 25% | -0.002 | 0.002 | -0.96 |
| β_6 : h _{disc} 50% | -0.028 | 0.002 | -11.64 |
| β_6 : h _{disc} 75% | -0.129 | 0.003 | -32.34 |
| β_6 : h _{disc} BH | 0.002 | 0.002 | 0.97 |
| β_7 | 0.0009 | $3.77 * 10^{-5}$ | 25.16 |
| β_8 | -0.0003 | $2.59 * 10^{-5}$ | -12.88 |
| β_9 : h _{disc} 25% | $-3.14 * 10^{-5}$ | $3.76 * 10^{-5}$ | -0.83 |
| β_9 : h _{disc} 50% | $8.73 * 10^{-5}$ | $3.79 * 10^{-5}$ | 2.29 |
| β_9 : h _{disc} 75% | 0.0002 | $4.67 * 10^{-5}$ | 4.57 |
| β_9 : h _{disc} BH | $-6.23 * 10^{-5}$ | $3.83 * 10^{-5}$ | -1.62 |
| Random parameters | Std. Dev | Level | |
| μ_i | 0.0276 | <i>Tree</i> | |
| μ_{ij} | 0.0171 | <i>Disc</i> | |
| ϵ_{ijk} | 0.0261 | <i>Residual</i> | |

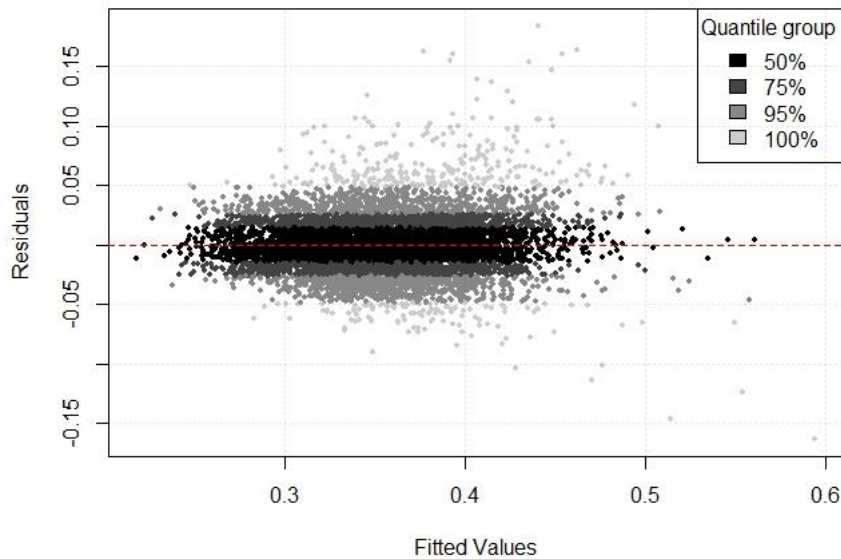


Figure 3-3: Model residuals of the final model plotted against the fitted values of ring density. The gray levels represent the percentiles of the residuals.

3.4.2 Tree volume and CO₂ sequestration

Before thinning, the average basal area in the research plots ranged from 26.72 to 29.22 m²/ha (Dupont-Leduc et al., 2020). Following thinning, basal area varied from 21.52 to 29.22 m²/ha, and the total standing volume ranged from 91.58 m³/ha in the thinning from below treatment to 132.48 m³/ha for the control. Since plots differ in their initial volumes, straightforward comparisons among treatments are most easily made using annual increment and volume increment percentages. Expressed as a percentage relative to the control, the plots with 50 CTR exhibited the highest volume percentage followed by 100 CTR for both the years, i.e., immediately after the thinning (2008) and the end of study period (2021). In all cases, the volume of thinned plots was always lower than that of the control plot. Nevertheless, the percentage volume change from 2008 to 2021 was higher for plots with greater thinning intensity (Table 3-6).

Table 3-6: Average tree characteristics (standard deviation in parenthesis) of three inventory periods for each thinning treatment and their respective total volume, carbon sequestration and increment rates during the 13 years study period.

| Variables | Thinning types | | | |
|---|----------------|--------------|--------------|--------------|
| | 100 CTR | 50 CTR | Below | Control |
| DBH (cm) 2008 | 12.28 (4.54) | 12.44 (4.23) | 13.01 (4.69) | 12.57 (4.38) |
| DBH (cm) 2014 | 14.72 (5.13) | 14.73 (4.86) | 15.89 (5.30) | 14.88 (4.93) |
| DBH (cm) 2021 | 16.27 (6.11) | 16.09 (6.11) | 17.77 (6.24) | 16.02 (6.45) |
| Height (m) 2008 | 10.41 (2.26) | 10.27 (2.62) | 10.18 (2.26) | 10.35 (2.20) |
| Height (m) 2014 | 11.35 (2.20) | 11.22 (2.14) | 11.56 (2.54) | 11.26 (2.00) |
| Height (m) 2021 | 12.44 (3.19) | 12.25 (3.22) | 12.56 (3.38) | 12.23 (3.53) |
| BA (m ² /ha) before thinning | 26.72 | 28.92 | 26.83 | 29.22 |
| BA (m ² /ha) after thinning in 2008 | 23.39 | 27.48 | 21.51 | 29.22 |
| Total volume (m ³ /ha) in 2008 as a % of control | 82.83% | 92.22% | 69.12% | 100% |
| Total volume (m ³ /ha) in 2014 as a % of control | 85.05% | 92.37% | 77.09% | 100% |
| Total volume (m ³ /ha) in 2021 as a % of control | 87.27% | 93.23% | 77.30% | 100% |
| Annual volume increment during the study period (m ³ /ha/year) | 9.36 | 9.54 | 8.83 | 10.34 |
| Annual Co ₂ sequestration during the study period (tons/ha/year) | 5.17 | 5.35 | 4.75 | 5.84 |

The control plots had the highest annual volume increments per hectare for both growth periods, followed by thinning from below for growth period 1 and 50 CTR for growth period 2 (Figure 3-4A, 4B). Overall, for 13 years, plots thinned from below exhibited the lowest total growth in volume, with an annual increment of 8.83 m³/ha. Unthinned or control plots demonstrated the highest volume increment at 10.34 m³/ha per year, while treatments with 100 CTR and 50 CTR had volume increment of 9.36 and 9.54 m³/ha per year, respectively (Table 3-6). At the stand level, there were no statistical differences observed in the annual volume increment among the silvicultural treatments for both growth periods

and sites (Table 3-7). Nevertheless, variations are noticeable in the annual volume increment concerning both the stand density index and the growth periods (Table 3-8). As expected, treatments with higher stand density exhibited a higher volume increment, and the stand density index uniformly rose for all plots, regardless of the treatments, during the transition from growth period 1 to growth period 2 (Figure 3-4). Although statistically insignificant, the annual volume increment rate for plots thinned from below was found to be lower in growth period 2 than in growth period 1, despite an increase in the stand density index (Figure 3-4).

Table 3-7: F-values (P-values in parentheses) for the analysis of variance of stand level variables (volume increment and CO₂ sequestration) with silvicultural treatments (control, thinned from below, thinned by CTR), growth periods (period 1 and period 2) and site.

| Source of variation | Response = volume increment | | | Response = CO ₂ sequestration | | |
|---------------------------|-----------------------------|-----|---------------------|--|-----|---------------------|
| | ndf | ddf | F-values (P-values) | ndf | ddf | F-values (P-values) |
| Site | 1 | 71 | 0.08 (0.77) | 1 | 71 | 0.70 (0.40) |
| Treatment | 3 | 71 | 0.69 (0.56) | 3 | 71 | 0.72 (0.54) |
| Growth period | 1 | 71 | 0.54 (0.46) | 1 | 71 | 2.39 (0.12) |
| Treatment x growth period | 3 | 71 | 1.74 (0.16) | 3 | 71 | 1.55 (0.20) |

Note: ddf, denominator degrees of freedom; ndf, numerator degrees of freedom.

Table 3-8: F-values (P-values in parentheses) for the analysis of variance of stand level variables (volume increment and CO₂ sequestration) with stand density index (SDI) just before the start of the respective growth periods, growth periods (period 1 and period 2) and site.

| Source of variation | Response = volume increment | | | Response = CO ₂ sequestration | | |
|---------------------|-----------------------------|-----|-----------------------|--|-----|-----------------------|
| | ndf | ddf | F-values (P-values) | ndf | ddf | F-values (P-values) |
| Site | 1 | 75 | 0.12 (0.72) | 1 | 75 | 0.01 (0.90) |
| SDI | 1 | 75 | 4.30 (<.05) | 1 | 75 | 6.30 (<.05) |
| Growth period | 1 | 75 | 9.39 (<.05) | 1 | 75 | 6.42 (<.05) |
| SDI x growth period | 1 | 75 | 0.37 (0.54) | 1 | 75 | 0.32 (0.57) |

Note: Bold values denote significance at $P < 0.05$; ddf, denominator degrees of freedom; ndf, numerator degrees of freedom.

Our results indicated that changes in stand structure can affect CO₂ sequestration rate, with the control treatments storing the most carbon and the thinning from below treatment storing the least (Table 3-6). Annual CO₂ sequestration for both growth periods showed similar trends to the volume increment results with the highest values for control. In contrast, plots thinned from below exhibited the lowest CO₂ sequestration compared to plots with a 50 CTR, which is the opposite of the volume increment trend (Figure 3-5A, 5B). The annual CO₂ sequestration across all treatments demonstrated uniform increases of approximately 13-14% from growth period 1 to growth period 2, except for plots thinned from below, which experienced a 6% reduction (Figure 3-5A, 5B).

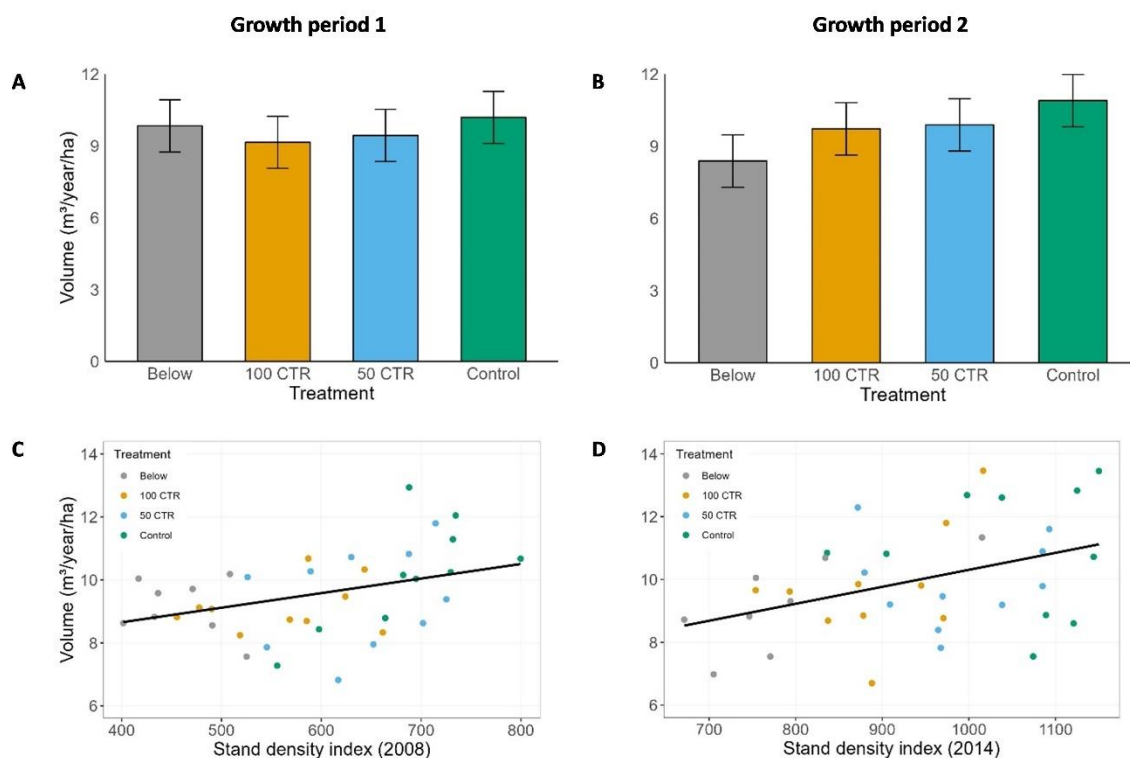


Figure 3-4: Figures in the upper panel denote the annual volume increment per hectare for four thinning treatments at (A) growth period 1 (2008-2014) and (B) growth period 2 (2014-2021). Error bars are the standard error of the mean. Figures in the lower panel represent the annual volume increment per hectare during (C)

growth period 1 and (D) growth period 2, as a function of the stand density index (Pretzsch & Biber, 2005) calculated just before the start of the respective growth periods.

Throughout the study period, annual CO₂ sequestration was highest in the control plots, reaching 5.84 tons/ha per year, and lowest in the plots thinned from below, with a rate of 4.75 tons/ha per year. Plots with 50 CTR showed a slightly higher CO₂ sequestration rate (5.35 tons/ha per year) compared to those with 100 CTR (5.17 tons/ha per year) (Table 3-6). The lack of differences in both annual volume increment and CO₂ sequestration trends among the various treatment plots suggested a minimal effect of inter and intra-ring density variations. The analysis of variance results of CO₂ sequestration among stand structures (silviculture treatments), stand density and growth periods mirrored the observations for annual volume increment differences: no significant difference was observed between thinning modalities (Table 3-7), while a significant difference was noted between stand density index and growth period (Table 3-8). The CO₂ sequestration rates for all the plots, except those thinned from below, were found to be higher in growth period 2 than in growth period 1 (Figure 3-5).

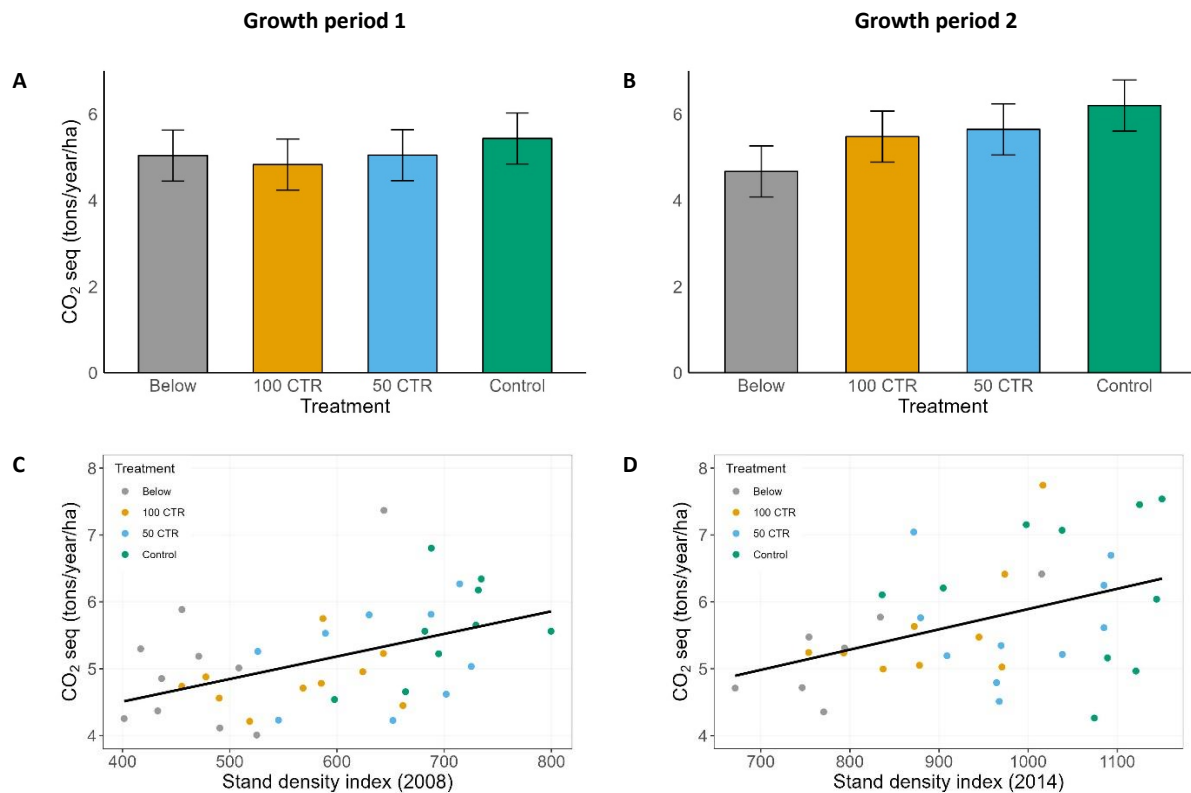


Figure 3-5: Figures in the upper panel denote the annual CO₂ sequestration per hectare for four thinning treatments at (A) growth period 1 (2008-2014) and (B) growth period 2 (2014-2021). Error bars are the standard error of the mean. Figures in the lower panel represent the annual CO₂ sequestration per hectare during (C) growth period 1 and (D) growth period 2, as a function of the stand density index (Pretzsch & Biber, 2005) calculated just before the start of the respective growth periods.

Total CO₂ sequestration over the studied 13 years estimated with the average wood density at BH (367 kg/m³) from our study closely aligned with the value obtained using the intra-tree density variations. The projection based on the average density at BH resulted in a slight overestimation of total CO₂ sequestration per hectare, ranging from 0.54% to 4.24% across various thinning plots (Figure 3-6). Interestingly, the distinctions between treatments appeared to be less pronounced when considering the average density at BH. Whereas the total CO₂ sequestration using the published wood density value

(412 kg/m³) for white spruce, as provided by De Araujo et al. (2015), exceeded the actual value by up to 15% (Figure 3-6).

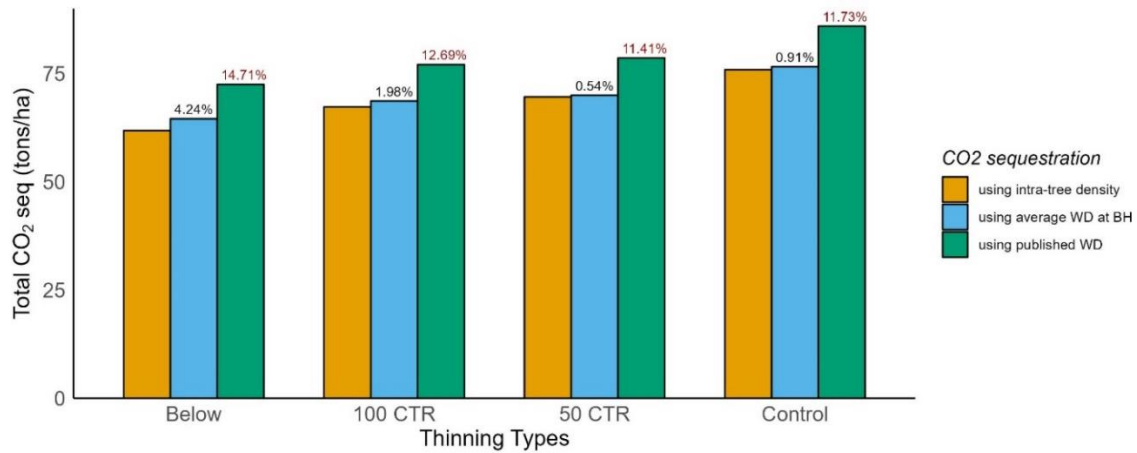


Figure 3-6: Total CO₂ sequestration per hectare over the 13-year study period computed utilizing intra-tree density variation, average wood density at breast height and a published wood density of 412 kg/m³ for four thinning types. The numerical values presented above the bars represent the percentage difference between the total CO₂ sequestration obtained using respective wood density and that derived from intra-tree density variations. (The WD and BH in the figure represent wood density and breast height respectively).

3.5 Discussion

In the context of climate change, carbon mitigation is more often being integrated as explicitly stated forest management and silvicultural objectives. In this regard, our study aimed to assess how CTR influences growth ring characteristics and carbon sequestration capacity of white spruce plantations. Overall, it was found that (1) thinned and unthinned plots exhibited similar RD chronologies both before and after thinning; (2) stand productivity, measured by either volume increment or carbon sequestration, was found to be invariant to thinning type, but increased with SDI; (3) although statistically non-significant, CTR seems to limit loss in sequestration capacity, if thinning has to be carried out.

3.5.1 Variations in ring density

The radial density variation in conifers typically exhibits one of the three patterns: a gradual increase in average RD from juvenile wood to mature wood (type I), high initial density near the pith with a rapid decrease followed by a gradual increase (type II), or a consistent decrease in density from pith to bark (John, 1980; Schimleck et al., 2022). In this study, the radial variation of wood density showed a type II pattern, typical of spruces (Saranpää, 2003; Alteyrac et al., 2005; Gardiner et al., 2011; Xiang et al., 2014). This type II pattern has been attributed to the higher earlywood density with low earlywood proportion near the pith (Koubaa et al., 2005), which is a clear adaptive strategy of conifers to respond to complex loading patterns at a young age (Telewski, 1989; Van Gelder et al., 2006). In the vertical direction, the mean density exhibited a flattened U-shaped pattern of fluctuation with height, indicating a minimal decline up to one-fourth of the tree's height, followed by a slight rise towards the apex. The U-shaped pattern of vertical density variation was also reported by Repola (2006) for pine and birch Wassenberg et al. (2015) for *Quercus* and Longuetaud et al. (2017) for temperate tree species. Typically, variations in wood density with height correlate with vertical changes in the proportion of juvenile wood, growth ring width, and cambial age, particularly in species displaying pronounced radial density variations. Indeed, in tree species where there is a significant density difference between juvenile and mature wood, we naturally observe a variation in wood density with height. This variation occurs because of the proportion of juvenile wood which increases from the base to the top of the tree (Zobel & Buijtenen, 1989). Often, the pattern of radial variations of wood density contributes to explaining the vertical trends, as the composition of wood within the stem—whether it's juvenile versus mature wood or the proportion of narrow rings—exhibits variations with tree height. For instance, we observed "pattern a" vertical variation as described by Longuetaud et al. (2017), where average wood density increases from the bottom to the top of the stem due to the decrease in wood density with distance from the pith. In other words, this occurs when wood density increases along the stem for the same

cambial age, likely due to the maturity of the apical meristem (Jyske et al., 2008). Conversely, if density increases from pith to bark, an opposite vertical density pattern would have been evident. Moreover, most of the discs that were studied had a high composition of juvenile wood, where the transition is estimated at 10 to 20 years (Zobel & Sprague, 2012). Thus, caution is warranted when generalizing the axial density pattern of white spruce solely from our study, as our results were derived from trees with a maximum age of 34 years.

The higher average RD noted for intermediate trees aligns with the conclusions drawn by Lindström (1996) and Deng et al. (2014). The decline in RD as tree dominance increases is observed because trees with slower growth rates tend to develop denser wood (Johansson, 1993; Pape, 1999a). In fact, trees under higher competition produce proportionally more latewood, distinguished by thicker cell walls, a smaller lumen, and increased density (John, 1980; Tsoumis & Panagiotidis, 1980; Peltola et al., 2007). Additionally, Pukkala et al. (1998) and Peltola et al. (2002) found that suppressed trees exhibited a faster and more pronounced response (in relative terms) to thinning compared to dominant trees, which might explain the observed temporary decline in the average RD of the intermediate class following thinning. With reduced competition, intermediate trees may have utilized available resources for quicker but potentially less dense growth, aiming to establish themselves in the canopy.

The response of RD to thinning was found to vary between species. For instance, a slight reduction in wood density was observed after thinning in Norway spruce (*Picea abies* L.) (Herman et al., 1998; Jaakkola et al., 2005) and Scots pine (*Pinus sylvestris*, L.) (Mörling, 2002) whereas, an increase in wood density was observed after thinning in loblolly pine (*Pinus taeda* L.) (Megraw, 1985) and red pine (*Pinus resinosa* Sol.) (Paul, 1958). Sudden release from high competition through intense thinning can lead to a temporary drop in wood density (Pape, 1999b). Also, a limited change in wood density was observed following pre-commercial thinning, in black spruce (Tong et al., 2009; Vincent et al., 2011) and Scots pine (Tasissa & Burkhart, 1997; Peltola et al., 2009), which are in line with our results. Our findings revealed

that two rings with the same ring width, one from a thinned tree and the other from an unthinned tree, have the same RD values. Thinning-induced alterations in competition and resource availability can lead to diverse growth patterns among remaining trees (Hannrup et al., 2000), ultimately impacting the relationship between RD and RW. This indicates that changes in RD following thinning could be explained by changes in growth rates, such that thinning influences RD indirectly. For instance, thinning results in an increased ring width, which subsequently contributes to a proportional change in RD (Barbour et al., 1994; Schneider et al., 2008). Also, as cambial ages increases, there is a tendency for the proportion of latewood to increase, leading to a corresponding rise in RD towards the bark (Moore, 2011). Koubaa et al. (2000) illustrated a declining correlation between RD and RW in black spruce as wood transitions from juvenile to mature stages, aligning with the observed rise in RD for the same ring width after thinning.

The large random effect estimate of tree level, compared to vertical disc height level, suggests a consistent RD value at each disc height position with more noticeable variation among the trees. This larger tree level variations is most likely due to the high genetic variation among the individual trees (Hannrup et al., 2000; Saranpää, 2003). While the residual variance in the random effects might indicate the year-to-year variability in climatic conditions (D'Arrigo et al., 1992; Bouriaud et al., 2004) or the significant intra-ring differences (Barbour et al., 1994). Although the constructed model accurately captures the observed patterns in white spruce wood density, there remains some unaccounted variability, which might be linked to biological or environmental factors specific to the sites (Zobel & Buijtenen, 1989; Piutti & Cescatti, 1997; Downes et al., 2000; Björklund et al., 2017). In a recent study on white spruce wood properties and heritability, Soro et al. (2022) examined the genetic control of traits to discern the extent of inter-tree variability attributed to genetic and environmental factors, and found that the variation from pith to bark was more strongly governed by genetics compared to year-to-year variability.

3.5.2 Post-thinning CO₂ sequestration

The impacts of thinning on stand-level productivity depend on thinning intensity, and the remaining tree's capacity to compensate for the removed carbon through enhanced uptake (Saunders et al., 2012). In our study, during thinning treatment, the stand densities of 50 CTR, 100 CTR, and thinning from below plots were reduced by an average of 4%, 11%, and 23%, respectively (Dupont-Leduc et al., 2020). The lower annual volume increment and CO₂ sequestration rate observed for 100 CTR and plots thinned from below are thus attributed to the stand density following thinning. This aligns with findings from other similar studies, indicating that thinning significantly reduces stand density, thereby immediately decreasing net carbon stocks (Dewar & Cannell, 1992; Vesterdal et al., 1995; Campbell et al., 2009; Powers et al., 2011; Ruiz-Peinado et al., 2016; Lin et al., 2018). A recent study by Allen et al. (2021) found that the annual volume increment follows an optimum relationship with stand density. They also highlighted that the differences in cumulative net volumes between thinned and unthinned plots is strongly influenced by the rotation period. On the contrary, certain studies have demonstrated that despite a decrease in stand density, thinning can still lead to an increase in carbon storage over the long run. For instance, Schroeder (1991) reported a 11% increase in carbon stocks over 50 years in Douglas fir plantations due to thinning, while Balboa-Murias et al. (2006) found that extending rotation, coupled with suitable thinning intensity, could enhance carbon pools in radiata pine. Higher stand density reduction led to an increased growth rate at the individual level, likely due to the concentration of limited resources on fewer trees.

Although statistically insignificant, our findings suggest that the selection of thinning methods could have the potential to influence the stand's capacity to sequester carbon. It seems that retaining abundant trees that grow slowly like in the control and 50 CTR groups, is more important than having just a few fast-growing trees, as seen in the 100 CTR group, is crucial for maintaining high levels of growing stock or CO₂ sequestration. Moreover, we found evidence that the SDI affects stand-level productivity, with higher stand-level volume increment and CO₂ sequestration rates observed in the plots

with higher SDI. Higher SDI values typically indicate denser forests, which can lead to increased CO₂ sequestration through enhanced photosynthetic capacity and greater biomass accumulation (Waring et al., 2020; Zhao et al., 2022). However, this increased capacity seems to depend on the forest type. In a study across China's forested regions, Wang et al. (2024) reported that increasing SDI leads to a reduction in biomass carbon and soil organic carbon in natural forests by 231.7 tC/ha, while in planted forests, it results in an increase of 74.7 tC/ha. This suggests that specific forest management strategies should be tailored to the specific forest types to optimize carbon sequestration. In the case of white spruce plantations, if the goal is to maximize stand level volume increment or CO₂ sequestration, maintaining higher stand density without thinning would be advisable. It should also be noted that thinning practices may initially reduce stand productivity but can ultimately lead to a surge in growth and an increase in sawtimber volume. Additionally, it enhances forest health and mitigates the risk of climatic uncertainties, such as fire, by reducing stand density (Alvarez et al., 2016; Moreau et al., 2022). Therefore, if the management aims to achieve an optimal balance between CO₂ sequestration and financial return, the CTR treatment, which minimizes reduction in stand density and thus CO₂ sequestration compared to thinning from below treatment, would be the preferable option. Furthermore, at the beginning of growth period 1, 100 CTR has 82% of volume to control but at the end of growth period 2, it has 87% of volume to control, suggesting that the stands are offsetting the volume lost during thinning. The response of thinning treatments could still be in their early stages as the full impact of thinning may take 7-10 years to manifest. Over time, it's possible that thinned stands may fully compensate for the initial carbon loss incurred during thinning treatments until the end of the final rotation. Nevertheless, current carbon stocks are not the sole indicators of CO₂ sequestration, as the biomass harvested during thinning, with the potential for substituting fossil fuels, can substantially contribute to CO₂ sequestration. Moreover, effective thinning practices could enhance the carbon storage capacity of the understory and soil. For instance, Zhang et al. (2023) observed the highest carbon

storage in surface soil, the highest tree diversity, and an increased carbon pool in litter under a thinning intensity of 30%. Thus, the carbon dynamics of the forest stand following thinning would be viewed more comprehensively when we integrate the forest carbon pool with the product pool of stored carbon, along with the dead and belowground carbon pools.

In response to the growing concern for natural climate solutions and the gradual acceptance of carbon credit markets, there is an increasing demand for enhanced accuracy in estimating forest carbon levels. The significant overestimations in total CO₂ sequestration, arising from the utilization of published wood density values, highlights the importance to account the effects of treatments and growing conditions on wood density. [Kantavichai et al. \(2010\)](#) calculated carbon content using treatment-specific average wood density of Douglas-fir and compared the results to estimates based on the Wood Handbook ([Forest Products Laboratory \(US\), 2021](#)) average density and [Gholz et al. \(1979\)](#) and [Jenkins \(2004\)](#) biomass equations. They found that the use of Wood Handbook average density underestimated carbon storage by up to 14%, whereas the use of biomass equations led to a more pronounced underestimation, reaching up to 52%. The differences between total CO₂ sequestration estimated utilizing intra-tree density variations and average wood density at BH was negligible, with only a noticeable difference for plots thinned from below. However, studies have highlighted significant differences between tree density at BH and average wood density ([Wiemann & Williamson, 2014](#); [Kimberley et al., 2015](#); [Longuetaud et al., 2017](#)) and suggested to consider variations in density to have more refined biomass estimates ([Rueda & Williamson, 1992](#); [Wassenberg et al., 2015](#)). In our case, to estimate the CO₂ sequestration, we employed only the rings formed after thinning which exhibited more stable density both in the radial and vertical directions. Often, higher variability in wood density exists near the pith ([Saranpää, 2003](#)), so it might be necessary to consider intra-tree variability while estimating carbon gain in all growth years. Furthermore, intra-tree density variability patterns and magnitudes are species-specific, with some

exhibiting homogeneous variation, while others display high variability throughout the stem ([Wassenberg et al., 2015](#)).

3.6 Conclusions

Forests are the primary terrestrial carbon reservoir and play a major role in CO₂ exchange, underscoring the importance of managing them for climate change mitigation. Our findings do provide some robust evidence to consider new insights to manage forests for carbon objectives. Firstly, we found that the unthinned plots exhibit higher volume and CO₂ sequestration increment rates due to their higher initial stand density, indicating that thinning may not be suitable when the management objective is solely to maximize carbon benefits. Our results also indicate that the CTR, although reduces the net productivity of the stand, has the potential to compensate for the loss of stock until the final rotation. When thinning is necessary, CTR should be considered over thinning from below as the loss of CO₂ sequestration following CTR was not notably high. Moreover, crop trees can yield high-quality wood products that store carbon for 70-100 years, providing a means to offset emissions from fossil fuels ([Lindroth et al., 2018](#)). Finding the right balance between thinning intensity and stand-level aboveground net primary productivity requires a compromise that balances adequate stocking of large dominant trees, while also allowing younger trees to grow in the stand. Adopting CTR with moderate stand density reduction (not exceeding 20%) could serve as a balanced tradeoff, enhancing long-term carbon storage potential while mitigating the risk of stand-level net stock loss. This tradeoff could also be balanced through early thinning, promoting accelerated individual tree growth and encouraging the development of understory vegetation from an early stage ([He et al., 2012](#)). To grasp the long-term effects on carbon stock and identify the point at which stands could recover the carbon loss, necessitates additional years of

investigation. For this, the established mixed-effect model could be employed to predict the RD of upcoming growth years.

This study also holds significance in exploring carbon allocation along the stem, challenging the conventional approach of treating density as a constant value independent of site, age, and treatment. Finally, the employed RD modeling approach and carbon estimation method have broadened the scope for future studies, thereby enhancing the accurate evaluation of forest carbon dynamics.

3.7 References

- Akaike, H. (1974). A new look at the statistical model identification." *IEEE transactions on automatic control*, 19(6), 716–723.
- Allen, M., Brunner, A., Antón-Fernández, C., & Astrup, R. (2021). The relationship between volume increment and stand density in Norway spruce plantations. *Forestry: An International Journal of Forest Research*, 94(1), 151–165.
- Alteyrac, J., Zhang, S. Y., Cloutier, A., & Ruel, J.-C. (2005). Influence of stand density on ring width and wood density at different sampling heights in black spruce (*Picea mariana* (Mill.) BSP). *Wood and Fiber Science*, 37(1), 83–94.
- Ashton, M. S., & Kelty, M. J. (2018). *The practice of silviculture: applied forest ecology*. John Wiley & Sons.
- Auty, D., Achim, A., Macdonald, E., Cameron, A. D., & Gardiner, B. A. (2014). Models for predicting wood density variation in Scots pine. *Forestry: An International Journal of Forest Research*, 87(3), 449–458.
- Balboa-Murias, M. A., Rodríguez-Soalleiro, R., Merino, A., & Álvarez-González, J. G. (2006). Temporal variations and distribution of carbon stocks in aboveground biomass of radiata pine and maritime pine pure stands under different silvicultural alternatives. *Forest Ecology and Management*, 237(1–3), 29–38.

- Barbour, R. J., Fayle, D. C. F., Chauret, G., Cook, J., Karsh, M. B., & Ran, S. (1994). Breast-height relative density and radial growth in mature jack pine (*Pinus banksiana*) for 38 years after thinning. *Canadian Journal of Forest Research*, *24*(12), 2439–2447.
- Bastin, J.-F., Fayolle, A., Tarelkin, Y., Van den Bulcke, J., De Haulleville, T., Mortier, F., Beeckman, H., Van Acker, J., Serckx, A., & Bogaert, J. (2015). Wood specific gravity variations and biomass of central African tree species: The simple choice of the outer wood. *PloS One*, *10*(11), e0142146.
- Bérubé-Deschênes, A., Franceschini, T., & Schneider, R. (2016). Factors affecting plantation grown white spruce (*Picea glauca*) acoustic velocity. *Journal of Forestry*, *114*(6), 629–637.
- Björklund, J., Seftigen, K., Schweingruber, F., Fonti, P., von Arx, G., Bryukhanova, M. V, Cuny, H. E., Carrer, M., Castagneri, D., & Frank, D. C. (2017). Cell size and wall dimensions drive distinct variability of earlywood and latewood density in Northern Hemisphere conifers. *New Phytologist*, *216*(3), 728–740.
- Bouriaud, O., Bréda, N., Le Moguedec, G., & Nepveu, G. (2004). Modelling variability of wood density in beech as affected by ring age, radial growth and climate. *Trees*, *18*(3), 264–276.
- Brown, S. (2002). Measuring carbon in forests: current status and future challenges. *Environmental Pollution*, *116*(3), 363–372.
- Bunn, A. G. (2010). Statistical and visual crossdating in R using the dplR library. *Dendrochronologia*, *28*(4), 251–258.
- Campbell, J., Alberti, G., Martin, J., & Law, B. E. (2009). Carbon dynamics of a ponderosa pine plantation following a thinning treatment in the northern Sierra Nevada. *Forest Ecology and Management*, *257*(2), 453–463.
- Campelo, F., Mayer, K., & Grabner, M. (2019). xRing—An R package to identify and measure tree-ring features using X-ray microdensity profiles. *Dendrochronologia*, *53*, 17–21.
- Chave, J., Andalo, C., Brown, S., Cairns, M. A., Chambers, J. Q., Eamus, D., Fölster, H., Fromard, F., Higuchi, N., & Kira, T. (2005). Tree allometry and improved estimation of carbon stocks and balance in tropical forests. *Oecologia*, *145*, 87–99.

- Chave, J., Réjou-Méchain, M., Búrquez, A., Chidumayo, E., Colgan, M. S., Delitti, W. B. C., Duque, A., Eid, T., Fearnside, P. M., & Goodman, R. C. (2014). Improved allometric models to estimate the aboveground biomass of tropical trees. *Global Change Biology*, *20*(10), 3177–3190.
- Cohen, J., Cohen, P., West, S. G., & Aiken, L. S. (2013). *Applied multiple regression/correlation analysis for the behavioral sciences*. Routledge.
- D'Amato, A. W., Troumbly, S. J., Saunders, M. R., Puettmann, K. J., & Albers, M. A. (2011). Growth and survival of *Picea glauca* following thinning of plantations affected by eastern spruce budworm. *Northern Journal of Applied Forestry*, *28*(2), 72–78.
- D'Arrigo, R. D., Jacoby, G. C., & Free, R. M. (1992). Tree-ring width and maximum latewood density at the North American tree line: parameters of climatic change. *Canadian Journal of Forest Research*, *22*(9), 1290–1296.
- De Araujo, F., Hart, J. F., & Mansfield, S. D. (2015). Variation in Trembling Aspen and White Spruce Wood Quality Grown in Mixed and Single Species Stands in the Boreal Mixedwood Forest. *Forests*, *6*(5), 1628–1648.
- Deng, X., Zhang, L., Lei, P., Xiang, W., & Yan, W. (2014). Variations of wood basic density with tree age and social classes in the axial direction within *Pinus massoniana* stems in Southern China. *Annals of Forest Science*, *71*(4), 505–516.
- Dewar, R. C., & Cannell, M. G. R. (1992). Carbon sequestration in the trees, products and soils of forest plantations: an analysis using UK examples. *Tree Physiology*, *11*(1), 49–71.
- Downes, G. M., & Drew, D. M. (2008). Climate and growth influences on wood formation and utilisation. *Southern Forests: A Journal of Forest Science*, *70*(2), 155–167.
- Downes, G. M., Evans, R., Schimleck, L. R., & Fritts, H. C. (2000). The commercial cambium: understanding the origin of wood property variation. *Cell and Molecular Biology of Wood Formation*, *BIOS Sci., Oxford*, 325–336.
- Dupont-Leduc, L., Schneider, R., & Sirois, L. (2020). Preliminary results from a structural conversion thinning trial in Eastern Canada. *Journal of Forestry*, *118*(5), 515–533.

- Environnement Canada, A. S. (2015). Normales climatiques au Canada 1980–2010 (Region d'Amqui). Available Online at https://Climate.Weather.Gc.ca/Climate_Normals/Results_1981_2010_e.html.
- Eriksson, E. (2006). Thinning operations and their impact on biomass production in stands of Norway spruce and Scots pine. *Biomass and Bioenergy*, 30(10), 848–854.
- Fahey, T. J., Woodbury, P. B., Battles, J. J., Goodale, C. L., Hamburg, S. P., Ollinger, S. V., & Woodall, C. W. (2010). Forest carbon storage: ecology, management, and policy. *Frontiers in Ecology and the Environment*, 8(5), 245–252.
- Filipescu, C. N., Lowell, E. C., Koppelaar, R., & Mitchell, A. K. (2014). Modeling regional and climatic variation of wood density and ring width in intensively managed Douglas-fir. *Canadian Journal of Forest Research*, 44(3), 220–229.
- Forest Products Laboratory (US). (2021). *Wood handbook: wood as an engineering material* (p. No. 72).
- Fortin, M., Bernier, S., Saucier, J.-P., & Labbé, F. (2009). *Une relation hauteur-diamètre tenant compte de l'influence de la station et du climat pour 20 espèces commerciales du Québec*. Gouvernement du Québec. Direction de la recherche forestière.
- Fox, J., & Weisberg, S. (2011). *An R companion to applied regression*. Sage publications.
- Franceschini, T., Bontemps, J.-D., Gelhaye, P., Rittie, D., Herve, J.-C., Gegout, J.-C., & Leban, J.-M. (2010). Decreasing trend and fluctuations in the mean ring density of Norway spruce through the twentieth century. *Annals of Forest Science*, 67, 816.
- Franceschini, T., Gauthray-Guyénet, V., Schneider, R., Ruel, J.-C., Pothier, D., & Achim, A. (2018). Effect of thinning on the relationship between mean ring density and climate in black spruce (*Picea mariana* (Mill.) BSP). *Forestry: An International Journal of Forest Research*, 91(3), 366–381.
- Gagné, L., Sirois, L., & Lavoie, L. (2016). Comparison of volume and value of softwoods from downslope and elite tree clearance in eastern Canada. *Canadian Journal of Forest Research*, 46(11), 1320–1329.
- Gagné, L., Sirois, L., & Lavoie, L. (2019). Seed rain and seedling establishment of *Picea glauca* and *Abies balsamea* after partial cutting in plantations and natural stands. *Forests*, 10(3), 221.

- Garcia-Gonzalo, J., Peltola, H., Briceno-Elizondo, E., & Kellomäki, S. (2007). Changed thinning regimes may increase carbon stock under climate change: A case study from a Finnish boreal forest. *Climatic Change*, *81*, 431–454.
- Gardiner, B., Leban, J.-M., Auty, D., & Simpson, H. (2011). Models for predicting wood density of British-grown Sitka spruce. *Forestry*, *84*(2), 119–132.
- Geng, Y., Yue, Q., Zhang, C., Zhao, X., & von Gadow, K. (2021). Dynamics and drivers of aboveground biomass accumulation during recovery from selective harvesting in an uneven-aged forest. *European Journal of Forest Research*, *140*(5), 1163–1178.
- Gholz, H. L., Grier, C. C., Campbell, A. G., & Brown, A. T. (1979). *Equations for estimating biomass and leaf area of plants in the Pacific Northwest*.
- Gonzalez-Benecke, C. A., Martin, T. A., Cropper Jr, W. P., & Bracho, R. (2010). Forest management effects on in situ and ex situ slash pine forest carbon balance. *Forest Ecology and Management*, *260*(5), 795–805.
- Government of Quebec. (2013). Sustainable Forest Development Act, CQLR. Available Online at [Http://Canlii.ca/t/Ks3n., c, A-18.1](http://Canlii.ca/t/Ks3n.,c,A-18.1).
- Grenon, F., Lussier, J. M., & Sirois, L. (2007). Conversion de jeunes forêts du Bas-St-Laurent en peuplements inéquiennes dans un contexte d'aménagement forestier écosystémique. *UQAR Serv Can Cent Can Sur Fibre Bois*, *80*.
- Griscom, B. W., Adams, J., Ellis, P. W., Houghton, R. A., Lomax, G., Miteva, D. A., Schlesinger, W. H., Shoch, D., Siikamäki, J. V, & Smith, P. (2017). Natural climate solutions. *Proceedings of the National Academy of Sciences*, *114*(44), 11645–11650.
- Handbook, W. (1999). Wood Handbook-Wood as an engineering material. *US Department of Agriculture, Forest Service, Forest Products Laboratory, Madison, WI, USA. Gen. Tech. Rep. FPLGTR-113*.
- Hannrup, B., Ekberg, I., & Persson, A. (2000). Genetic correlations among wood, growth capacity and stem traits in *Pinus sylvestris*. *Scandinavian Journal of Forest Research*, *15*(2), 161–170.
- He, L., Chen, J. M., Pan, Y., Birdsey, R., & Kattge, J. (2012). Relationships between net primary

- productivity and forest stand age in US forests. *Global Biogeochemical Cycles*, 26(3).
- Hedeker, D., & Gibbons, R. D. (2006). *Longitudinal data analysis*. Wiley-Interscience.
- Herman, M., Dutilleul, P., & Avella-Shaw, T. (1998). Growth rate effects on temporal trajectories of ring width, wood density, and mean tracheid length in Norway spruce (*Picea abies* (L.) Karst.). *Wood and Fiber Science*, 30(1), 6–17.
- Hernandez, R. E., Bustos, C., Fortin, Y., & Beaulieu, J. (2001). Wood machining properties of white spruce from plantation forests. *Forest Products Journal*, 51(6), 82.
- Hollinger, D. Y., Maclaren, J. P., Beets, P. N., & Turland, J. (1993). Carbon sequestration by New Zealand's plantation forests. *New Zealand Journal of Forestry Science*, 23(2), 194–208.
- Hoover, C., & Stout, S. (2007). The carbon consequences of thinning techniques: stand structure makes a difference. *Journal of Forestry*, 105(5), 266–270.
- Houghton, J. T., Jenkins, G. J., & Ephraums, J. J. (1990). Climate change: the IPCC scientific assessment. *American Scientist;(United States)*, 80(6).
- Ikonen, V.-P., Peltola, H., Wilhelmsson, L., Kilpeläinen, A., Väisänen, H., Nuutinen, T., & Kellomäki, S. (2008). Modelling the distribution of wood properties along the stems of Scots pine (*Pinus sylvestris* L.) and Norway spruce (*Picea abies* (L.) Karst.) as affected by silvicultural management. *Forest Ecology and Management*, 256(6), 1356–1371.
- ISO 554. (2002). *Standard atmospheres for conditioning and/or testing – specifications*.
- Ivković, M., Gapare, W., Wu, H., Espinoza, S., & Rozenberg, P. (2013). Influence of cambial age and climate on ring width and wood density in *Pinus radiata* families. *Annals of Forest Science*, 70(5), 525–534.
- Jaakkola, T., Mäkinen, H., & Saranpää, P. (2005). Wood density in Norway spruce: changes with thinning intensity and tree age. *Canadian Journal of Forest Research*, 35(7), 1767–1778.
- Jandl, R., Lindner, M., Vesterdal, L., Bauwens, B., Baritz, R., Hagedorn, F., Johnson, D. W., Minkinen, K., & Byrne, K. A. (2007). How strongly can forest management influence soil carbon sequestration?

Geoderma, 137(3–4), 253–268.

- Jenkins, J. C. (2004). *Comprehensive database of diameter-based biomass regressions for North American tree species* (Issue 319). United States Department of Agriculture, Forest Service, Northeastern Research Station; 2004.
- John, P. A. (1980). Textbook of wood technology: structure, identification, properties, and uses of the commercial woods of the United States and Canada. *McGraw-Hill Series in Forest Resources (USA)*.
- Jyske, T., Mäkinen, H., & Saranpää, P. (2008). Wood density within Norway spruce stems. *Silva Fennica*, 42(3).
- Kantavichai, R., Briggs, D. G., & Turnblom, E. C. (2010). Effect of thinning, fertilization with biosolids, and weather on interannual ring specific gravity and carbon accumulation of a 55-year-old Douglas-fir stand in western Washington. *Canadian Journal of Forest Research*, 40(1), 72–85.
- Kariuki, M. (2008). Modelling the impacts of various thinning intensities on tree growth and survival in a mixed species eucalypt forest in central Gippsland, Victoria, Australia. *Forest Ecology and Management*, 256(12), 2007–2017.
- Kimberley, M. O., Cown, D. J., McKinley, R. B., Moore, J. R., & Dowling, L. J. (2015). Modelling variation in wood density within and among trees in stands of New Zealand-grown radiata pine. *New Zealand Journal of Forestry Science*, 45, 1–13.
- Kimura, J., & Fujimoto, T. (2014). Modeling the effects of growth rate on the intra-tree variation in basic density in hinoki cypress (*Chamaecyparis obtusa*). *Journal of Wood Science*, 60(5), 305–312.
- Koubaa, A., Isabel, N., Zhang, S. Y., Beaulieu, J., & Bousquet, J. (2005). Transition from juvenile to mature wood in black spruce (*Picea mariana* (Mill.) BSP). *Wood and Fiber Science*, 445–455.
- Koubaa, A., Zhang, S. Y., Isabel, N., Beaulieu, J., & Bousquet, J. (2000). Phenotypic correlations between juvenile-mature wood density and growth in black spruce. *Wood and Fiber Science*, 61–71.
- Lafèche, V., Larouche, C., & Guillemette, F. (2013). L'éclaircie commerciale, in: Le Guide Sylvicole Du Québec, Les Concepts et l'application de La Sylviculture. *Les Publications Du Québec, Québec*, 300-327 p.

- Larson, P. R. (1963). Stem form development of forest trees. *Forest Science*, 9(suppl_2), a0001-42.
- Laurance, W. F., Nascimento, H. E. M., Laurance, S. G., Andrade, A., Ewers, R. M., Harms, K. E., Luizao, R. C. C., & Ribeiro, J. E. (2007). Habitat fragmentation, variable edge effects, and the landscape-divergence hypothesis. *PLoS One*, 2(10), e1017.
- Lin, J.-C., Chiu, C.-M., Lin, Y.-J., & Liu, W.-Y. (2018). Thinning effects on biomass and carbon stock for young Taiwania plantations. *Scientific Reports*, 8(1), 3070.
- Lindroth, A., Holst, J., Heliasz, M., Vestin, P., Lagergren, F., Biermann, T., Cai, Z., & Mölder, M. (2018). Effects of low thinning on carbon dioxide fluxes in a mixed hemiboreal forest. *Agricultural and Forest Meteorology*, 262, 59–70.
- Lindström, H. (1996). Basic density in Norway spruce, Part III. Development from pith outwards. *Wood and Fiber Science*, 391–405.
- Longuetaud, F., Mothe, F., Santenoise, P., Diop, N., Dlouha, J., Fournier, M., & Deleuze, C. (2017). Patterns of within-stem variations in wood specific gravity and water content for five temperate tree species. *Annals of Forest Science*, 74(3), 1–19.
- Mäkinen, H., Hynynen, J., & Penttilä, T. (2015). Effect of thinning on wood density and tracheid properties of Scots pine on drained peatland stands. *Forestry: An International Journal of Forest Research*, 88(3), 359–367.
- Mäkinen, H., Saranpää, P., & Linder, S. (2002). Wood-density variation of Norway spruce in relation to nutrient optimization and fibre dimensions. *Canadian Journal of Forest Research*, 32(2), 185–194.
- Matthews, G. (1993). *The carbon content of trees*. No. 4, 4–21.
- Megraw, R. A. (1985). *Wood quality factors in loblolly pine: the influence of tree age, position in tree, and cultural practice on wood specific gravity, fiber length, and fibril angle*. Tappi Press.
- Miller, C., Grayson, S., Houser, A., Clatterbuck, W., & Kuers, K. (2010). Thirty-year assessment of released, overtopped white oaks. *Proceedings of the 17th Central Hardwood Forest Conference, Lexington, KY, USA*, 5–7.

- Moore, J. (2011). *Wood properties and uses of Sitka spruce in Britain*. (Issue 015). Forestry Commission.
- Moreau, G., Chagnon, C., Achim, A., Caspersen, J., D'Orangeville, L., Sánchez-Pinillos, M., & Thiffault, N. (2022). Opportunities and limitations of thinning to increase resistance and resilience of trees and forests to global change. *Forestry*, 95(5), 595–615.
- Mörling, T. (2002). Evaluation of annual ring width and ring density development following fertilisation and thinning of Scots pine. *Annals of Forest Science*, 59(1), 29–40.
- Muller-Landau, H. C. (2004). Interspecific and inter-site variation in wood specific gravity of tropical trees. *Biotropica*, 36(1), 20–32.
- Nabuurs, G. J., Masera, O., Andrasko, K., Benitez-Ponce, P., Boer, R., Dutschke, M., Elsiddig, E., Ford-Robertson, J., Frumhoff, P., & Karjalainen, T. (2007). *Forestry. Climate Change 2007: Mitigation. Contribution of Working Group III to the Fourth Assessment Report of the Intergovernmental Panel on Climate Change*, eds Metz B, et al.
- Nizami, S. M. (2012). The inventory of the carbon stocks in sub tropical forests of Pakistan for reporting under Kyoto Protocol. *Journal of Forestry Research*, 23(3), 377–384.
- Noormets, A., Epron, D., Domec, J.-C., McNulty, S. G., Fox, T., Sun, G., & King, J. S. (2015). Effects of forest management on productivity and carbon sequestration: A review and hypothesis. *Forest Ecology and Management*, 355, 124–140.
- Olson, M. G., Meyer, S. R., Wagner, R. G., & Seymour, R. S. (2014). Commercial thinning stimulates natural regeneration in spruce-fir stands. *Canadian Journal of Forest Research*, 44(3), 173–181. <https://doi.org/10.1139/cjfr-2013-0227>
- Ontl, T. A., Janowiak, M. K., Swanston, C. W., Daley, J., Handler, S., Cornett, M., Hagenbuch, S., Handrick, C., McCarthy, L., & Patch, N. (2020). Forest management for carbon sequestration and climate adaptation. *Journal of Forestry*, 118(1), 86–101.
- Ortega Rodriguez, D. R., & Tomazello-Filho, M. (2019). Clues to wood quality and production from analyzing ring width and density variabilities of fertilized *Pinus taeda* trees. *New Forests*, 50(5), 821–843.

- Ott, R. A. (2010). *Effects of Pre-Commercial Thinning on Stand Composition, Stand Structure, and White Spruce Diameter Growth in White Spruce Stands in Interior Alaska*. January, 16.
- Pan, Y., Birdsey, R. A., Fang, J., Houghton, R., Kauppi, P. E., Kurz, W. A., Phillips, O. L., Shvidenko, A., Lewis, S. L., & Canadell, J. G. (2011). A large and persistent carbon sink in the world's forests. *Science*, 333(6045), 988–993.
- Pape, R. (1999a). Effects of thinning on wood properties of Norway spruce on highly productive sites. *Doctoral Thesis. Swedish University of Agricultural Sciences. Uppsala, Sweden*.
- Pape, R. (1999b). Effects of thinning regime on the wood properties and stem quality of *Picea abies*. *Scandinavian Journal of Forest Research*, 14(1), 38–50.
- Park, Y.-S., Weng, Y., & Mansfield, S. D. (2012). Genetic effects on wood quality traits of plantation-grown white spruce (*Picea glauca*) and their relationships with growth. *Tree Genetics & Genomes*, 8(2), 303–311.
- Parresol, B. R. (1999). Assessing tree and stand biomass: a review with examples and critical comparisons. *Forest Science*, 45(4), 573–593.
- Paul, B. H. (1958). Specific gravity changes in southern pines after release. *South. Lumberman*, 163, 122–124.
- Peltola, H., Gort, J., Pulkkinen, P., Zubizarreta Gerendiain, A., Karppinen, J., & Ikonen, V.-P. (2009). Differences in growth and wood density traits in Scots pine (*Pinus sylvestris* L.) genetic entries grown at different spacing and sites. *Silva Fennica*, 43(3).
- Peltola, H., Kilpeläinen, A., Sauvala, K., Räisänen, T., & Ikonen, V.-P. (2007). Effects of early thinning regime and tree status on the radial growth and wood density of Scots pine. *Silva Fennica*, 41(3), 489–505.
- Peltola, H., Miina, J., Rouvinen, I., & Kellomäki, S. (2002). Effect of early thinning on the diameter growth distribution along the stem of Scots pine. *Silva Fennica*, 36(4).
- Pinheiro, J. (2009). nlme: linear and nonlinear mixed effects models. R package version 3.1-96. [Http://Cran. r-Project. Org/Web/Packages/Nlme/](http://cran.r-project.org/web/packages/nlme/).

- Pinheiro, J. C., & Bates, D. M. (2000). Linear mixed-effects models: basic concepts and examples. *Mixed-Effects Models in S and S-Plus*, 3–56.
- Piutti, E., & Cescatti, A. (1997). A quantitative analysis of the interactions between climatic response and intraspecific competition in European beech. *Canadian Journal of Forest Research*, 27(3), 277–284.
- Powers, M., Kolka, R., Palik, B., McDonald, R., & Jurgensen, M. (2011). Long-term management impacts on carbon storage in Lake States forests. *Forest Ecology and Management*, 262(3), 424–431.
- Prégent, G., Picher, G., & Auger, I. (2010). *Tarif de cubage, tables de rendement et modèles de croissance pour les plantations d'épinette blanche au Québec*. Gouvernement du Québec, Ministère des Ressources naturelles et de la Faune, Direction de la recherche forestière. Mémoire de recherche foresti.
- Pretzsch, H., & Biber, P. (2005). A re-evaluation of Reineke's rule and stand density index. *Forest Science*, 51(4), 304–320.
- Pukkala, T., Miina, J., & Kellomäki, S. (1998). Response to different thinning intensities in young *Pinus sylvestris*. *Scandinavian Journal of Forest Research*, 13(1–4), 141–150.
- Rawlings, J. O., Pantula, S. G., & Dickey, D. A. (1998). *Applied regression analysis: a research tool*. Springer.
- Repola, J. (2006). Models for vertical wood density of Scots pine, Norway spruce and birch stems, and their application to determine average wood density. *Silva Fennica*, 40(4).
- Rueda, R., & Williamson, G. B. (1992). Radial and vertical wood specific gravity in *Ochroma pyramidale* (Cav. ex Lam.) Urb.(Bombacaceae). *Biotropica*, 512–518.
- Ruiz-Peinado, R., Bravo-Oviedo, A., López-Senespleda, E., Montero, G., & Río, M. (2013). Do thinnings influence biomass and soil carbon stocks in Mediterranean maritime pinewoods? *European Journal of Forest Research*, 132(2), 253–262.
- Ruiz-Peinado, Ricardo, Bravo-Oviedo, A., Montero, G., & Del Río, M. (2016). Carbon stocks in a Scots pine afforestation under different thinning intensities management. *Mitigation and Adaptation Strategies for Global Change*, 21, 1059–1072.

- Russo, D., Marziliano, P. A., Macri, G., Proto, A. R., Zimbalatti, G., & Lombardi, F. (2019). Does thinning intensity affect wood quality? An analysis of Calabrian Pine in Southern Italy using a non-destructive acoustic method. *Forests*, *10*(4), 303.
- Saranpää, P. (2003). Wood density and growth. *Wood Quality and Its Biological Basis*, 87–117.
- Saunders, M., Tobin, B., Black, K., Gioria, M., Nieuwenhuis, M., & Osborne, B. A. (2012). Thinning effects on the net ecosystem carbon exchange of a Sitka spruce forest are temperature-dependent. *Agricultural and Forest Meteorology*, *157*, 1–10.
- Schaedel, M. S., Larson, A. J., Affleck, D. L. R., Belote, R. T., Goodburn, J. M., & Page-Dumroese, D. S. (2017). Early forest thinning changes aboveground carbon distribution among pools, but not total amount. *Forest Ecology and Management*, *389*, 187–198.
- Schimleck, L. R., Dahlen, J., & Auty, D. (2022). Radial patterns of specific gravity variation in North American conifers. *Canadian Journal of Forest Research*, *52*(6), 889–900.
- Schneider, R., Zhang, S. Y., Swift, D. E., Begin, J., & Lussier, J.-M. (2008). Predicting selected wood properties of jack pine following commercial thinning. *Canadian Journal of Forest Research*, *38*(7), 2030–2043.
- Schroeder, P. (1991). Can intensive management increase carbon storage in forests? *Environmental Management*, *15*(4), 475–481.
- Singer, M. T., & Lorimer, C. G. (1997). Crown release as a potential old-growth restoration approach in northern hardwoods. *Canadian Journal of Forest Research*, *27*(8), 1222–1232.
- Soro, A., Lenz, P., Hasegawa, M., Roussel, J.-R., Bousquet, J., & Achim, A. (2022). Genetic influence on components of wood density variation in white spruce. *Forestry*, *95*(2), 153–165.
- Tasissa, G., & Burkhart, H. E. (1997). Modeling thinning effects on ring width distribution in loblolly pine (*Pinus taeda*). *Canadian Journal of Forest Research*, *27*(8), 1291–1301.
- Telewski, F. W. (1989). Structure and function of flexure wood in *Abies fraseri*. *Tree Physiology*, *5*(1), 113–121.

- Thürig, E., & Kaufmann, E. (2010). Increasing carbon sinks through forest management: a model-based comparison for Switzerland with its Eastern Plateau and Eastern Alps. *European Journal of Forest Research*, *129*, 563–572.
- Tong, Q.-J., Fleming, R. L., Tanguay, F., & Zhang, S. Y. (2009). Wood and lumber properties from unthinned and precommercially thinned black spruce plantations. *Wood and Fiber Science*, 168–179.
- Tony, F., Thibaut, F., Guillaume, G., Julie, B., & Robert, S. (2019). Modelling wood density and modulus of elasticity in white spruce plantations in Eastern Québec. *The Forestry Chronicle*, *95*(3), 196–206.
- Trimble, G. R. (1971). *Early crop-tree release in even-aged stands of Appalachian hardwoods* (Vol. 203). Northeastern Forest Experiment Station.
- Tsoumis, G., & Panagiotidis, N. (1980). Effect of growth conditions on wood quality characteristics of black pine (*Pinus nigra* Arn.). *Wood Science and Technology*, *14*(4), 301–310.
- Van Gelder, H. A., Poorter, L., & Sterck, F. J. (2006). Wood mechanics, allometry, and life-history variation in a tropical rain forest tree community. *New Phytologist*, *171*(2), 367–378.
- Vesterdal, L., Dalsgaard, M., Felby, C., Raulund-Rasmussen, K., & Jørgensen, B. B. (1995). Effects of thinning and soil properties on accumulation of carbon, nitrogen and phosphorus in the forest floor of Norway spruce stands. *Forest Ecology and Management*, *77*(1–3), 1–10.
- Vieilledent, G., Fischer, F. J., Chave, J., Guibal, D., Langbour, P., & Gérard, J. (2018). New formula and conversion factor to compute basic wood density of tree species using a global wood technology database. *American Journal of Botany*, *105*(10), 1653–1661.
- Vincent, M., Krause, C., & Koubaa, A. (2011). Variation in black spruce (*Picea mariana* (Mill.) BSP) wood quality after thinning. *Annals of Forest Science*, *68*(6), 1115–1125.
- Wang, T., Dong, L., & Liu, Z. (2024). Factors driving carbon accumulation in forest biomass and soil organic carbon across natural forests and planted forests in China. *Frontiers in Forests and Global Change*, *6*, 1333868.
- Ward, J. S. (2002). Crop tree release increases growth of mature red oak sawtimber. *Northern Journal of*

- Applied Forestry*, 19(4), 149–154.
- Ward, J. S. (2013). Precommercial crop tree release increases upper canopy persistence and diameter growth of oak saplings. *Northern Journal of Applied Forestry*, 30(4), 156–163.
- Waring, B., Neumann, M., Prentice, I. C., Adams, M., Smith, P., & Siebert, M. (2020). Forests and decarbonization—roles of natural and planted forests. *Frontiers in Forests and Global Change*, 3, 534891.
- Wassenberg, M., Chiu, H.-S., Guo, W., & Spiecker, H. (2015). Analysis of wood density profiles of tree stems: incorporating vertical variations to optimize wood sampling strategies for density and biomass estimations. *Trees*, 29(2), 551–561.
- Wiemann, M. C., & Williamson, G. B. (1989). Radial gradients in the specific gravity of wood in some tropical and temperate trees. *Forest Science*, 35(1), 197–210.
- Wiemann, M. C., & Williamson, G. B. (2014). Wood specific gravity variation with height and its implications for biomass estimation. *USDA Forest Service, Forest Products Laboratory, Research Paper, FPL-RP-677, 2014; 12 P., 677, 1–12.*
- Williamson, G. B., & Wiemann, M. C. (2010). Measuring wood specific gravity... correctly. *American Journal of Botany*, 97(3), 519–524.
- WOODCOCK, D. W. (2000). Wood specific gravity of trees and forest types in the southern Peruvian Amazon. *Acta Amazonica*, 30, 589.
- Xiang, W., Leitch, M., Auty, D., Duchateau, E., & Achim, A. (2014). Radial trends in black spruce wood density can show an age-and growth-related decline. *Annals of Forest Science*, 71, 603–615.
- Zhang, B., Dong, X., Qu, H., Gao, R., & Mao, L. (2023). Effects of thinning on ecosystem carbon storage and tree-shrub-herb diversity of a low-quality secondary forest in NE China. *Journal of Forestry Research*, 34(4), 977-991.
- Zhang, C., Ju, W., Chen, J. M., Wang, X., Yang, L., & Zheng, G. (2015). Disturbance-induced reduction of biomass carbon sinks of China's forests in recent years. *Environmental Research Letters*, 10(11), 114021.

- Zhang, H., Zhou, G., Wang, Y., Bai, S., Sun, Z., Berninger, F., Bai, Y., & Penttinen, P. (2019). Thinning and species mixing in Chinese fir monocultures improve carbon sequestration in subtropical China. *European Journal of Forest Research*, *138*, 433–443.
- Zhang, S. Y. (1995). Effect of growth rate on wood specific gravity and selected mechanical properties in individual species from distinct wood categories. *Wood Science and Technology*, *29*(6), 451–465.
- Zhang, X., Guan, D., Li, W., Sun, D., Jin, C., Yuan, F., Wang, A., & Wu, J. (2018). The effects of forest thinning on soil carbon stocks and dynamics: A meta-analysis. *Forest Ecology and Management*, *429*, 36–43.
- Zhao, M., Sun, M., Xiong, T., Tian, S., & Liu, S. (2022). On the link between tree size and ecosystem carbon sequestration capacity across continental forests. *Ecosphere*, *13*(6), e4079.
- Zhou, H., & Smith, I. (1991). Factors influencing bending properties of white spruce lumber. *Wood and Fiber Science*, *23*(4), 483–500.
- Zobel, B. J., & Sprague, J. R. (2012). *Juvenile wood in forest trees*. Springer Science & Business Media.
- Zobel, B. J., & Van Buijtenen, J. P. (2012). *Wood variation: its causes and control*. Springer Science & Business Media.
- Zubizarreta Gerendiain, A., Peltola, H., Pulkkinen, P., Jaatinen, R., Pappinen, A., & Kellomäki, S. (2007). Differences in growth and wood property traits in cloned Norway spruce (*Picea abies*). *Canadian Journal of Forest Research*, *37*(12), 2600–2611.

3.8 Annex I: Supplementary information for RD model development

Model selection:

Model selection was done by visual examination of normalized residuals against fitted and explanatory variables, assessment of bias and homoscedasticity of the residuals and with Akaike's Information Criterion (AIC; model with lower value is preferred, [Akaike \(1974\)](#)). We also used χ^2 -based likelihood-ratio tests to assess the significance of terms in both the fixed and the random effects structure and also to evaluate the significance of the variance function and correlation structure ([Pinheiro & Bates, 2000](#)). In addition, pseudo- R^2 was also computed following [Parresol \(1999\)](#) to estimate the proportion of variance explained by both fixed and random effects.

Determining the variance–covariance structure of random effects:

We first established the variance-covariance structure by fitting several null models with all possible combinations of hierarchical levels and compared them using the log-likelihood ratio test and AIC. With the fit statistics, model with discs nested within trees was the best among different variance-covariance structure of random effects (Eq. 1).

$$RD_{ijk} = \mu_0 + \mu_i + \mu_{ij} + \varepsilon_{ijk} \quad (1)$$

Where μ_0 is the fixed effect intercept, RD_{ijk} the mean RD, μ_i the tree random effect, μ_{ij} the disc nested in tree random effect and ε_{ijk} the within-group errors. The i , j , and k are associated with the tree, the disc, and the annual tree ring respectively. The random effects and within-group errors were assumed to be independent and normally distributed, with $\mu_i \sim N(0, \Psi_1)$ and $\mu_{ij} \sim N(0, \Psi_2)$ and $\varepsilon_{ijk} \sim N(0, \sigma_e^2)$. The Ψ_1 and Ψ_2 are the variance-covariance matrices for the tree and disc level random effects ([Pinheiro & Bates, 2000](#)) respectively.

Model specification:

From an initial examination by plotting RD of individual discs against year after thinning, we observed many distinctive trends for individual discs since it is always important to look at the trends per individual and not the overall trend in such data (Hedeker & Gibbons, 2006). Considering this, we employed a two-stage modeling approach, in which the first stage was to obtain the parameter estimates of the base model for individual discs and the second stage consisted in modeling these parameter estimates as functions of possible tree and ring level covariates.

Stage 1:

To develop a base model, we first reviewed several existing linear model forms from similar studies (Franceschini et al., 2010; Gardiner et al., 2011; Kimura & Fujimoto, 2014) with year after thinning as a predictor variable. Nevertheless, none of them demonstrated satisfactory performance in representing RD patterns of all individual discs. This could be attributed to the variations within the data as well as the variable being used. We observed that the radial density pattern was best represented by a model with logarithmic or exponential function of year after thinning, with the additional inclusion of another form. So, various parameterizations of the logarithmic, exponential, and quadratic function, both individually and in combination, were fitted to all the 678 discs individually, and the following form showed the best fit (i.e., the average AIC over all the discs was the lowest).

$$RD_{ijk} = \alpha_0 + \alpha_1 \cdot \ln(TY_{ijk}) + \alpha_2 \cdot TY_{ijk}^2 + \varepsilon_{ijk} \quad (2)$$

Where TY_{ijk} denotes the year after thinning for the k^{th} annual ring of the j^{th} disc from the i^{th} tree, α_0 , α_1 , and α_2 are the parameters to be estimated. The model combines a diminishing effect linked to a logarithmic term with curvature introduced by a quadratic term. While the logarithmic part suggests decreasing impact with increasing TY_{ijk} , the quadratic term counteracts this, resulting in a more intricate relationship between TY_{ijk} and RD_{ijk} and thus, does not allow the model to exhibit an asymptotic behavior.

Stage 2:

In this stage, the parameter estimates from Eq. 2 for individual discs were regressed against possible tree and ring level variables. We performed correlation tests to establish the logical link between candidate variables and parameter estimates. From the correlation test, it was observed that the parameter α_0 was linked to the DBH, RW and h_{disc} , while parameters α_1 and α_2 were found to be related to DBH, h_{disc} and CI. Subsequently, various mathematical forms, including linear, quadratic, square root, inverse, of the individual candidate variables associated with each parameter estimate were screened and the best forms were identified. Then, all possible combinations of linear models with those chosen mathematical forms of candidate variables for α_0 , α_1 , and α_2 were fitted and the best with lowest AIC were selected. The Ht and D_{class} were not included in any of the models, as they did not demonstrate a significant contribution based on the AIC analysis. This procedure led to three individual linear models f_{α_0} , f_{α_1} , and f_{α_2} for parameters α_0 , α_1 , and α_2 respectively:

$$f_{\alpha_0} = \beta_0 + \beta_1 \cdot DBH_i^2 + \beta_2 \cdot \sqrt{RW_i} + \beta_3 \cdot h_{disc_{ij}} + \epsilon_{ij} \quad (3)$$

$$f_{\alpha_1} = \beta_4 + \frac{\beta_5}{DBH_i^2} + \beta_6 \cdot h_{disc_{ij}} + \epsilon_{ij} \quad (4)$$

$$f_{\alpha_2} = \beta_7 + \beta_8 \cdot CI_i + \beta_9 \cdot h_{disc_{ij}} + \epsilon_{ij} \quad (5)$$

Where, β_0 , β_1 , β_2 , β_3 , β_4 , β_5 , β_6 , β_7 , β_8 , and β_9 are the parameters to be estimated.

Finally, the parameters α_0 , α_1 , and α_2 of Eq. 2 were replaced by Eq. 3, Eq. 4, and Eq. 5 respectively and variance-covariance structure of the random terms from Eq. 1 were added to the disc-level model (Eq. 2) to get our final model (Eq. 6). All the error terms from Eqs. 1-5 were assumed to be independent and represented by ϵ_{ijk} of the final model.

$$RD_{ijk} = f_{\alpha_0} + f_{\alpha_1} \cdot \ln(TY_{ijk}) + f_{\alpha_2} \cdot TY_{ijk}^2 + \mu_i + \mu_{ij} + \epsilon_{ijk} \quad (6)$$

One potential issue in multiple linear regression is the influence of correlated predictor variables on parameter estimates and hypothesis tests. We conducted multicollinearity assessment of our final model, focusing on the Variance Inflation Factor (VIF) for each predictor, including interaction terms. This was performed using the ‘vif’ function from the ‘car’ package (Fox & Weisberg, 2011). The interaction terms exhibited relatively higher VIF values compared to the individual predictor variables. This was expected, as interaction terms involve multiplicative combinations of predictor variables and can amplify collinearity effects (Cohen et al., 2013). However, considering the study context, the elevated VIFs were likely tolerable as we applied the model to a dataset that possessed a similar correlation structure among the predictors (Rawlings et al., 1998).

3.9 Annex II: Supplementary information for Height-DBH (HD) relationships

We utilized the equation developed by Fortin et al. (2009) for the prediction of tree height for all trees within each site, treatment, and inventory year. We also considered the plot as a random effect and assessed its performance based on AIC. We did not have height information for trees in 2008, so we employed the same HD relationships developed for the inventory year 2014 to predict the height of trees in 2008. The HD equations for all treatments from the Humqui (HU) site in 2014 exhibited a plot random effect, whereas no plot effect was evident for Lechasseur (LE). Likewise, in 2021, HD equations for all treatments from both sites, except for the control, showed plot random effects.

$$Ht_i = a + b \cdot \ln(DBH_i + 1) + c \cdot \ln(DBH_i + 1)^2 + \varepsilon_i$$

Where, a, b, and c are the parameters of the model.

Parameter estimates of the HD equations for the trees in the years 2014.

| | |
|------------------------------------|-----------|
| Parameter estimates (fixed effect) | Intercept |
|------------------------------------|-----------|

| Site | Treatment | Plot | a | b | c | (random effect) |
|------|-----------|-------|--------|--------|-------|-----------------|
| HU | 100 CTR | HU-01 | | | | -1.35 |
| | | HU-02 | | | | 0.80 |
| | | HU-08 | 4.98 | -0.41 | 0.97 | -0.20 |
| | | HU-09 | | | | -0.05 |
| | | HU-14 | | | | 0.80 |
| | 50 CTR | HU-04 | | | | -0.27 |
| | | HU-05 | | | | 0.58 |
| | | HU-15 | -6.65 | 6.88 | -0.12 | 0.77 |
| | | HU-16 | | | | -0.24 |
| | | HU-19 | | | | -0.84 |
| | Below | HU-03 | | | | -0.07 |
| | | HU-06 | | | | 0.43 |
| | | HU-10 | 23.1 | -17.99 | 4.97 | -0.22 |
| | | HU-17 | | | | -0.07 |
| | | HU-20 | | | | -0.05 |
| | Control | HU-07 | | | | 0.11 |
| | | HU-11 | | | | -0.81 |
| | | HU-12 | -12.37 | 12.61 | -1.41 | 0.56 |
| | | HU-13 | | | | 0.12 |
| | | HU-18 | | | | 0.01 |
| LE | 100 CTR | | -15.14 | 13.15 | -1.19 | |
| | 50 CTR | | -30.83 | 27.06 | -4.15 | |
| | Below | | 0.82 | 0.73 | 1.07 | |
| | Control | | 0.06 | 2.25 | 0.67 | |

Parameter estimates of the HD equations for the trees in the year 2021.

| Site | Treatment | Plot | Parameter estimates (fixed effect) | | | Intercept (random effect) |
|------|-----------|-------|------------------------------------|-------|-------|------------------------------|
| | | | a | b | c | |
| | | HU-01 | | | | 0.21 |
| | | HU-02 | | | | 0.15 |
| | 100 CTR | HU-08 | -17.32 | 15.75 | -1.82 | 0.45 |
| | | HU-09 | | | | -0.46 |

| | | | | | | |
|---------|---------|-------|--------|-------|-------|-------|
| | | HU-14 | | | | -0.35 |
| HU | 50 CTR | HU-04 | | | | 0.19 |
| | | HU-05 | | | | 0.15 |
| | | HU-15 | -30.08 | 24.76 | -3.37 | 0.45 |
| | | HU-16 | | | | -0.46 |
| | | HU-19 | | | | -0.35 |
| | Below | HU-03 | | | | 0.23 |
| | | HU-06 | | | | 1.15 |
| | | HU-10 | -26.28 | 18.77 | -1.80 | -1.03 |
| | | HU-17 | | | | -1.08 |
| | | HU-20 | | | | 0.73 |
| Control | | -7.85 | 8.95 | -0.60 | | |
| LE | 100 CTR | LE-04 | | | | 0.02 |
| | | LE-08 | | | | 0.08 |
| | | LE-13 | -2.71 | 3.31 | 0.78 | 0.08 |
| | | LE-14 | | | | 0.009 |
| | | LE-18 | | | | -0.19 |
| | 50 CTR | LE-06 | | | | -0.20 |
| | | LE-07 | | | | -0.10 |
| | | LE-11 | -23.06 | 20.41 | -2.67 | 0.94 |
| | | LE-15 | | | | -0.40 |
| | | LE-19 | | | | -0.23 |
| | Below | LE-02 | | | | -0.01 |
| | | LE-03 | | | | 0.01 |
| | | LE-16 | -19.12 | 15.03 | -1.35 | -0.08 |
| | | LE-17 | | | | 0.04 |
| | | LE-20 | | | | -0.03 |
| Control | | 12.09 | -5.35 | 2.01 | | |

CHAPTER IV: CONCLUSIONS AND FUTURE WORKS

4.1 Conclusions

In addressing climate change, decisions in forest management and silviculture must incorporate a global carbon mitigation objective alongside ecological and economic goals. CTR, considering its positive response to convert the managed stands to uneven-aged or irregular structures (Dupont-Leduc et al., 2020), could potentially safeguard the stands' ability to sequester carbon in long run. This is because functionally diverse multi-aged stands, characterized by higher productivity (Paquette & Messier, 2011), also display greater resistance and resilience to disturbances (O'Hara & Ramage, 2013).

This study, at first, established a mixed-effect model for predicting RD of white spruce and subsequently employed this model to investigate the impact of various thinning treatments on white spruce CO₂ sequestration. Our results suggest that specific forest management strategies should be adapted to achieve specific goals. For instance, if the goal is to maximize carbon benefits, avoiding thinning or stand density reduction may be preferred. However, if thinning is necessary for achieving an optimal balance between carbon and financial benefits, implementing CTR appears suitable. Moreover, CTR with moderate intensity seems worth considering as it not only promotes the growth of released trees but also minimizes the risk of stand-level net stock loss. Releasing crop trees at early ages could also be considered as it promotes accelerated individual tree growth and encourages the development of understory vegetation from an early stage. However, understanding the long-term effects of CTR on carbon stock, including the point at which stands could balance or exceed the carbon lost during treatment, necessitates additional years of investigation. For this, the established mixed-effect model could be employed to predict the RD of upcoming growth years and assess the carbon gain of CTR or the

gap with the control. However, the present aboveground carbon stock alone does not serve as the exclusive indicator of a stand's CO₂ sequestration, as the biomass extracted during thinning and the dead and below-ground carbon pools collectively constitute a substantial portion of the forest's carbon pool.

A series of specific conclusions can be drawn from this study.

1. The first part is an R package, CTRing, which excels in accurately extracting tree-ring information, including automatic pith location, using X-ray medical CT images. Its precision in pith detection and getting ring density profiles, coupled with user-friendly manual correction feature, will help forest ecologists and dendrochronologists to better understand how trees grow, react to their environment and management prescriptions and record past events. Its potential applications extend to measure tree-ring widths from images by adding a scale function.
2. Following thinning, a gradual increase in RD was observed, contrary to the initial hypothesis, where a decline in RD was expected. Nevertheless, the consistent RD pattern observed between thinned and unthinned plots over the studied growth years implies a stronger association of RD with cambial age, given that the proportion of latewood tends to increase with older cambial ages (Moore, 2011). Additionally, a type II ring density pattern was observed radially, but the limited ages of the studied trees constrained the illustration of a RD variation pattern in the axial direction. The observed results lead to some potential implications; (I) Our findings revealed that two rings with the same ring width, one from a thinned tree and the other from an unthinned tree, have the same RD values, suggesting that thinning can be implemented without compromising the wood density of white spruce trees, (II) carbon accounting could be inaccurate if the wood density of white spruce is assumed to be a constant value in allometric equations, and also (III) the recognized density pattern can act as a valuable reference for wood industries, assisting in the optimal allocation of logs to maximize resource value and ensure the quality of end products.

3. We considered RD of individual disc by employing a two-stage modeling approach, taking into account the interrelated effects of years after thinning, growth rate, size of the tree, height along the stem and competition within the stand. The inclusion of disc height position in the model facilitated the prediction of wood density distribution in trees subjected to diverse silvicultural scenarios. Certainly, ring width and years after thinning elucidated a significant portion of the variation sources, capturing stand characteristics, growth patterns, and climatic influences. However, the detailed knowledge about the complete variability of wood density is still lacking which is assumed to be associated with climatic and environmental sources. For instance, the inclusion of potential climatic determinants could enhance model performance, as the proportion of earlywood and latewood is primarily regulated by temperature and precipitation ([Franceschini et al., 2013](#)). In any case, as the purpose of the developed model was to predict the RD of trees grown on same sites, caution should be taken when extrapolating its use beyond the sampled tree range.
4. Contrary to our hypothesis, no difference was observed in both the annual volume increment and CO₂ sequestration rate between thinned and control plots. The control plots, with higher stand density, showed a greater annual increment rate, but thinned plots also demonstrated to have the potential to eventually match the stock level of the control plots over time. These implications suggest that carefully planned thinning interventions have the capacity not only to influence immediate growth dynamics but also to shape the trajectory of carbon sequestration in forests over extended periods. Thinning may not be advisable if the goal is to sequester more carbon, but, if necessary, attention should be paid to the timing and intensity of the thinning. To sum up, even if thinning diminishes total stand stocks, it remains crucial in forest management, yielding larger, economically valuable trees, meeting immediate product needs, preserving wood quality, and maintaining overall carbon sequestration capacity.

5. Accurate forest carbon measurement aids global carbon cycle understanding and provides insights for sustainable forest management. This study advances conventional carbon estimation by integrating variations in site quality, age, silvicultural treatment, and tree and stand level attributes through the incorporation of tree height and intra-tree density into our analysis. Although our study demonstrates the robust representation of average density at breast height for carbon estimation, this may not hold true when accounting for rings with higher density fluctuations. Incorporating the intra-tree and inter-tree density variations during carbon estimation may not always be feasible; however, knowledge of this information facilitates the adoption of improved sampling strategies to achieve more accurate wood density determination.

4.2 Perspectives and future research

In Quebec, it is emphasized to employ an ecosystem-based approach in forest management to address the discrepancies in structure and functions between natural and managed forests. CTR, given the structuring roles played by released trees to accelerate the development of irregular stands (De Potter et al., 2012), has been under consideration for structural conversion. Nevertheless, many forest stakeholders hesitate to embrace this shift in silvicultural practices, questioning uncertainty regarding the growth, yield, and carbon sequestration rate of stands (Bédard et al., 2003; Laflèche et al., 2013). To address these questions, our study detailed stand-level volume and carbon sequestration increment rates following thinning using a highly precise method and elaborated possible growth scenarios to propose a pathway that could balance both structure conversion and carbon mitigation objectives. However, it has generated numerous questions from different perspectives that could be explored and addressed in future studies.

We employed trees aged 33 years or younger to generalize variation patterns in RD and subsequently examined the impact of thinning on wood density and carbon sequestration within a 13-year timeframe. The observed RD pattern could differ if the sampled trees were fully mature. Furthermore, although our study highlights significant changes in growth dynamics, it is advisable to assess a complete rotation before deciding to change silvicultural practices. So, evaluating the volume and carbon sequestration rate of the stands utilizing next inventories data or growth simulators is recommended.

Secondly, changes in forest structure after thinning can alter below-ground carbon dynamics by affecting root biomass, soil structure, and microbial activity. Therefore, to draw a more valid conclusion, it is recommended to assess how CTR influences the accumulation of dead and below-ground carbon pools. Additionally, incorporating the carbon sequestered by wood products removed during thinning would provide a more holistic perspective on the outcomes.

4.3 References for chapter I and chapter IV

- Alteyrac, J., Zhang, S. Y., Cloutier, A., & Ruel, J.-C. (2005). Influence of stand density on ring width and wood density at different sampling heights in black spruce (*Picea mariana* (Mill.) BSP). *Wood and Fiber Science*, 37(1), 83–94.
- Auty, D., Achim, A., Macdonald, E., Cameron, A. D., & Gardiner, B. A. (2014). Models for predicting wood density variation in Scots pine. *Forestry: An International Journal of Forest Research*, 87(3), 449–458.
- Beer, C., Reichstein, M., Tomelleri, E., Ciais, P., Jung, M., Carvalhais, N., Rödenbeck, C., Arain, M. A., Baldocchi, D., & Bonan, G. B. (2010). Terrestrial gross carbon dioxide uptake: global distribution and covariation with climate. *Science*, 329(5993), 834–838.
- Bergsten, U., Lindeberg, J., Rindby, A., & Evans, R. (2001). Batch measurements of wood density on intact or prepared drill cores using x-ray microdensitometry. *Wood Science and Technology*, 35(5), 435–452.
- Bérubé-Deschênes, A., Franceschini, T., & Schneider, R. (2016). Factors affecting plantation grown white spruce (*Picea glauca*) acoustic velocity. *Journal of Forestry*, 114(6), 629–637.
- Bhandarkar, S., Faust, T. D., & Tang, M. (1996). A system for detection of internal log defects by computer analysis of axial CT images. *Proceedings Third IEEE Workshop on Applications of Computer Vision. WACV'96*, 258–263.
- Briffa, K. R., Jones, P. D., & Schweingruber, F. H. (1992). Tree-ring density reconstructions of summer temperature patterns across western North America since 1600. *Journal of Climate*, 5(7), 735–754.
- Campelo, F., Mayer, K., & Grabner, M. (2019). xRing—An R package to identify and measure tree-ring features using X-ray microdensity profiles. *Dendrochronologia*, 53, 17–21.
- Chatterjee, A., Vance, G. F., & Tinker, D. B. (2009). Carbon pools of managed and unmanaged stands of ponderosa and lodgepole pine forests in Wyoming. *Canadian Journal of Forest Research*, 39(10), 1893–1900.
- Chave, J., Réjou-Méchain, M., Búrquez, A., Chidumayo, E., Colgan, M. S., Delitti, W. B. C., Duque, A., Eid, T., Fearnside, P. M., & Goodman, R. C. (2014). Improved allometric models to estimate the

- aboveground biomass of tropical trees. *Global Change Biology*, 20(10), 3177–3190.
- Chudnoff, M. (1984). *Tropical timbers of the world* (Issue 607). US Department of Agriculture, Forest Service.
- Conkey, L. E. (1988). Decline in old-growth red spruce in western Maine: an analysis of wood density and climate. *Canadian Journal of Forest Research*, 18(8), 1063–1068.
- Cown, D. J. (1973). Effects of severe thinning and pruning treatments on the intrinsic wood properties of young radiata pine. *NZ J Forest Sci*, 3, 370–389.
- D’Amato, A. W., Bradford, J. B., Fraver, S., & Palik, B. J. (2011). *Forest management for mitigation and adaptation to climate change: insights from long-term silviculture experiments*. *For Ecol Manag* 262: 803–816.
- D’Amato, A. W., Troumbly, S. J., Saunders, M. R., Puettmann, K. J., & Albers, M. A. (2011). Growth and survival of *Picea glauca* following thinning of plantations affected by eastern spruce budworm. *Northern Journal of Applied Forestry*, 28(2), 72–78.
- Davis, S. C., Hessler, A. E., Scott, C. J., Adams, M. B., & Thomas, R. B. (2009). Forest carbon sequestration changes in response to timber harvest. *Forest Ecology and Management*, 258(9), 2101–2109.
- De Potter, B., Perin, J., Ponette, Q., & Claessens, H. (2012). Détourage d’arbres-objectif: enseignements des dispositifs installés en Wallonie après six années. *Forêt Wallonne*, 119.
- del Río, M., Calama, R., Cañellas, I., Roig, S., & Montero, G. (2008). Thinning intensity and growth response in SW-European Scots pine stands. *Annals of Forest Science*, 65(3), 1.
- Dobner, M., Huss, J., & Tomazello Filho, M. (2018). Wood density of loblolly pine trees as affected by crown thinnings and harvest age in southern Brazil. *Wood science and technology*, 52, 465-485.
- Downes, G. M., & Drew, D. M. (2008). Climate and growth influences on wood formation and utilisation. *Southern Forests: A Journal of Forest Science*, 70(2), 155–167.
- Dupont-Leduc, L., Schneider, R., & Sirois, L. (2020). Preliminary results from a structural conversion thinning trial in Eastern Canada. *Journal of Forestry*, 118(5), 515–533.
- Dvinskikh, S. V., Henriksson, M., Berglund, L. A., & Furó, I. (2011). A multinuclear magnetic resonance imaging (MRI) study of wood with adsorbed water: estimating bound water concentration and

- local wood density. *Holzforschung*, 65(1), 103–107.
- Eyre, F. H. (1980). Forest cover types. *Washington, DC: Society of American Foresters*.
- Fabijańska, A., Danek, M., Barniak, J., & Piórkowski, A. (2017). Towards automatic tree rings detection in images of scanned wood samples. *Computers and Electronics in Agriculture*, 140, 279–289.
- Finkral, A. J., & Evans, A. M. (2008). The effects of a thinning treatment on carbon stocks in a northern Arizona ponderosa pine forest. *Forest Ecology and Management*, 255(7), 2743–2750.
- Fonti, P., von Arx, G., García-González, I., Eilmann, B., Sass-Klaassen, U., Gärtner, H., & Eckstein, D. (2010). Studying global change through investigation of the plastic responses of xylem anatomy in tree rings. *New Phytologist*, 185(1), 42–53.
- Franceschini, T., Gauthray-Guyénet, V., Schneider, R., Ruel, J.-C., Pothier, D., & Achim, A. (2018). Effect of thinning on the relationship between mean ring density and climate in black spruce (*Picea mariana* (Mill.) BSP). *Forestry: An International Journal of Forest Research*, 91(3), 366–381.
- Franceschini, T., Longuetaud, F., Bontemps, J.-D., Bouriaud, O., Caritey, B.-D., & Leban, J.-M. (2013). Effect of ring width, cambial age, and climatic variables on the within-ring wood density profile of Norway spruce *Picea abies* (L.) Karst. *Trees*, 27, 913–925.
- Habite, T., Olsson, A., & Oscarsson, J. (2020). Automatic detection of pith location along norway spruce timber boards on the basis of optical scanning. *European Journal of Wood and Wood Products*, 78(6), 1061–1074.
- Harmon, M. E., Moreno, A., & Domingo, J. B. (2009). Effects of partial harvest on the carbon stores in Douglas-fir/western hemlock forests: a simulation study. *Ecosystems*, 12(5), 777–791.
- Hasegawa, M., Savard, M., Lenz, P. R. N., Duchateau, E., Gélinas, N., Bousquet, J., & Achim, A. (2020). White spruce wood quality for lumber products: priority traits and their enhancement through tree improvement. *Forestry: An International Journal of Forest Research*, 93(1), 16–37.
- Haygreen, J. G., & Bowyer, J. L. (1996). *Forest products and wood science: an introduction*. (Issue Ed. 3). Iowa state university press.
- Herman, M., Dutilleul, P., & Avella-Shaw, T. (1998). Growth rate effects on temporal trajectories of ring width, wood density, and mean tracheid length in Norway spruce (*Picea abies* (L.) Karst.). *Wood and Fiber Science*, 30(1), 6–17.

- Hernandez, R. E., Bustos, C., Fortin, Y., & Beaulieu, J. (2001). Wood machining properties of white spruce from plantation forests. *Forest Products Journal*, 51(6), 82.
- Hoffman, G. R. (1987). *Forest vegetation of the Black Hills National Forest of South Dakota and Wyoming: a habitat type classification* (Vol. 276). US Department of Agriculture, Forest Service, Rocky Mountain Forest and Range Experiment Station; 1987.
- Houghton, J. T., Jenkins, G. J., & Ephraums, J. J. (1990). Climate change: the IPCC scientific assessment. *American Scientist;(United States)*, 80(6).
- Jaakkola, T., Mäkinen, H., & Saranpää, P. (2005). Wood density in Norway spruce: changes with thinning intensity and tree age. *Canadian Journal of Forest Research*, 35(7), 1767–1778.
- Jacquin, P., Longuetaud, F., Leban, J.-M., & Mothe, F. (2017). X-ray microdensitometry of wood: A review of existing principles and devices. *Dendrochronologia*, 42, 42–50.
- Jacquin, P., Mothe, F., Longuetaud, F., Billard, A., Kerfriden, B., & Leban, J.-M. (2019). CarDen: a software for fast measurement of wood density on increment cores by CT scanning. *Computers and Electronics in Agriculture*, 156, 606–617.
- John, P. A. (1980). Textbook of wood technology: structure, identification, properties, and uses of the commercial woods of the United States and Canada. *McGraw-Hill Series in Forest Resources (USA)*.
- Keyser, T. L., & Zarnoch, S. J. (2012). Thinning, age, and site quality influence live tree carbon stocks in upland hardwood forests of the Southern Appalachians. *Forest Science*, 58(5), 407–418.
- Kharrat, W., Koubaa, A., Khlif, M., & Bradai, C. (2019). Intra-ring wood density and dynamic modulus of elasticity profiles for black spruce and Jack pine from X-ray densitometry and ultrasonic wave velocity measurement. *Forests*, 10(7), 569.
- Koga, S., & Zhang, S. Y. (2002). Relationships between wood density and annual growth rate components in balsam fir (*Abies balsamea*). *Wood and Fiber Science*, 34(1), 146–157.
- Koubaa, A., Isabel, N., Zhang, S. Y., Beaulieu, J., & Bousquet, J. (2005). Transition from juvenile to mature wood in black spruce (*Picea mariana* (Mill.) BSP). *Wood and Fiber Science*, 445–455.
- Kozlowski, T. T., & Pallardy, S. G. (2002). Acclimation and adaptive responses of woody plants to environmental stresses. *The Botanical Review*, 68(2), 270–334.

- Kuprevicius, A., Auty, D., Achim, A., & Caspersen, J. P. (2013). Quantifying the influence of live crown ratio on the mechanical properties of clear wood. *Forestry*, *86*(3), 361–369.
- Larson, P. R. (1963). Stem form development of forest trees. *Forest Science*, *9*(suppl_2), a0001-42.
- Larson, P. R. (1969). Wood formation and the concept of wood quality. In *Bull. No. 74, School of Forestry, Yale University, USA*.
- Laurance, W. F., Nascimento, H. E. M., Laurance, S. G., Andrade, A., Ewers, R. M., Harms, K. E., Luizao, R. C. C., & Ribeiro, J. E. (2007). Habitat fragmentation, variable edge effects, and the landscape-divergence hypothesis. *PLoS One*, *2*(10), e1017.
- Levoy, L., Barrette, J., Ricard, J., Perron, M., & Giroud, G. (2021). *Qualité du bois du mélèze hybride (Larix marschlinsii Coaz.) non élagué dans*.
- Longuetaud, F., Mothe, F., Santenoise, P., Diop, N., Dlouha, J., Fournier, M., & Deleuze, C. (2017). Patterns of within-stem variations in wood specific gravity and water content for five temperate tree species. *Annals of Forest Science*, *74*(3), 1–19.
- Mäkinen, H., Saranpää, P., & Linder, S. (2002). Wood-density variation of Norway spruce in relation to nutrient optimization and fibre dimensions. *Canadian Journal of Forest Research*, *32*(2), 185–194.
- Martin-DeMoor, J., Lieffers, V. J., & Macdonald, S. E. (2010). Natural regeneration of white spruce in aspen-dominated boreal mixedwoods following harvesting. *Canadian Journal of Forest Research*, *40*(3), 585–594.
- Martin, A. R., & Thomas, S. C. (2011). A reassessment of carbon content in tropical trees. *PLoS One*, *6*(8), e23533.
- Maunu, S. L. (2002). NMR studies of wood and wood products. *Progress in Nuclear Magnetic Resonance Spectroscopy*, *40*(2), 151–174.
- McCulloh, K. A., Meinzer, F. C., Sperry, J. S., Lachenbruch, B., Voelker, S. L., Woodruff, D. R., & Domec, J.-C. (2011). Comparative hydraulic architecture of tropical tree species representing a range of successional stages and wood density. *Oecologia*, *167*, 27–37.
- Megraw, R. A. (1985). *Wood quality factors in loblolly pine: the influence of tree age, position in tree, and cultural practice on wood specific gravity, fiber length, and fibril angle*. Tappi Press.

- Moore, J. (2011). *Wood properties and uses of Sitka spruce in Britain*. (Issue 015). Forestry Commission.
- Moreau, G., Chagnon, C., Achim, A., Caspersen, J., D'Orangeville, L., Sánchez-Pinillos, M., & Thiffault, N. (2022). Opportunities and limitations of thinning to increase resistance and resilience of trees and forests to global change. *Forestry*, *95*(5), 595–615.
- Mörling, T. (2002). Evaluation of annual ring width and ring density development following fertilisation and thinning of Scots pine. *Annals of Forest Science*, *59*(1), 29–40.
- Mvolo, C. S., Stewart, J. D., Helmeste, C., & Koubaa, A. (2021). Variation of White Spruce Carbon Content with Age, Height, Social Classes and Silvicultural Management. *Energies*, *14*(23), 8015.
- Nienstaedt, H., & Zasada, J. C. (1990). *Picea glauca* (Moench) Voss white spruce. *Silvics of North America*, *1*, 204–226.
- O'Hara, K. L., & Ramage, B. S. (2013). Silviculture in an uncertain world: utilizing multi-aged management systems to integrate disturbance. *Forestry*, *86*(4), 401–410.
- Oliver, C. D., Larson, B. C., & Oliver, C. D. (1996). *Forest stand dynamics*. Wiley Publishing, New York.
- Olson, M. G., Meyer, S. R., Wagner, R. G., & Seymour, R. S. (2014). Commercial thinning stimulates natural regeneration in spruce-fir stands. *Canadian Journal of Forest Research*, *44*(3), 173–181. <https://doi.org/10.1139/cjfr-2013-0227>
- Omari, K., MacLean, D. A., Lavigne, M. B., Kershaw Jr, J. A., & Adams, G. W. (2016). Effect of local stand structure on leaf area, growth, and growth efficiency following thinning of white spruce. *Forest Ecology and Management*, *368*, 55–62.
- Ott, R. A. (2010). *Effects of Pre-Commercial Thinning on Stand Composition, Stand Structure, and White Spruce Diameter Growth in White Spruce Stands in Interior Alaska*. January, 16.
- Pan, Y., Birdsey, R. A., Fang, J., Houghton, R., Kauppi, P. E., Kurz, W. A., Phillips, O. L., Shvidenko, A., Lewis, S. L., & Canadell, J. G. (2011). A large and persistent carbon sink in the world's forests. *Science*, *333*(6045), 988–993.
- Pape, R. (1999). Effects of thinning regime on the wood properties and stem quality of *Picea abies*. *Scandinavian Journal of Forest Research*, *14*(1), 38–50.
- Paquette, A., & Messier, C. (2011). The effect of biodiversity on tree productivity: from temperate to

- boreal forests. *Global Ecology and Biogeography*, 20(1), 170–180.
- Park, Y.-S., Weng, Y., & Mansfield, S. D. (2012). Genetic effects on wood quality traits of plantation-grown white spruce (*Picea glauca*) and their relationships with growth. *Tree Genetics & Genomes*, 8(2), 303–311.
- Paul, B. H. (1958). Specific gravity changes in southern pines after release. *South. Lumberman*, 163, 122–124.
- Peltola, H., Gort, J., Pulkkinen, P., Zubizarreta Gerendiain, A., Karppinen, J., & Ikonen, V.-P. (2009). Differences in growth and wood density traits in Scots pine (*Pinus sylvestris* L.) genetic entries grown at different spacing and sites. *Silva Fennica*, 43(3).
- Peltola, H., Miina, J., Rouvinen, I., & Kellomäki, S. (2002). Effect of early thinning on the diameter growth distribution along the stem of Scots pine. *Silva Fennica*, 36(4).
- Perlin, L. P., do Valle, Â., & de Andrade Pinto, R. C. (2018). New method to locate the pith position in a wood cross-section based on ultrasonic measurements. *Construction and Building Materials*, 169, 733–739.
- Powers, M., Kolka, R., Palik, B., McDonald, R., & Jurgensen, M. (2011). Long-term management impacts on carbon storage in Lake States forests. *Forest Ecology and Management*, 262(3), 424–431.
- Pukkala, T., Miina, J., & Kellomäki, S. (1998). Response to different thinning intensities in young *Pinus sylvestris*. *Scandinavian Journal of Forest Research*, 13(1–4), 141–150.
- Rehfeldt, G. E., Tchebakova, N. M., Parfenova, Y. I., Wykoff, W. R., Kuzmina, N. A., & Milyutin, L. I. (2002). Intraspecific responses to climate in *Pinus sylvestris*. *Global Change Biology*, 8(9), 912–929.
- Rossi, S., Deslauriers, A., Anfodillo, T., Morin, H., Saracino, A., Motta, R., & Borghetti, M. (2006). Conifers in cold environments synchronize maximum growth rate of tree-ring formation with day length. *New Phytologist*, 170(2), 301–310.
- Schneider, R., Zhang, S. Y., Swift, D. E., Begin, J., & Lussier, J.-M. (2008). Predicting selected wood properties of jack pine following commercial thinning. *Canadian Journal of Forest Research*, 38(7), 2030–2043.
- Smith, D. M., & Hawley, R. C. (1993). *The practice of silviculture*. Wiley Publishing, New York.

- Tasissa, G., & Burkhart, H. E. (1997). Modeling thinning effects on ring width distribution in loblolly pine (*Pinus taeda*). *Canadian Journal of Forest Research*, 27(8), 1291–1301.
- Telewski, F. W. (1989). Structure and function of flexure wood in *Abies fraseri*. *Tree Physiology*, 5(1), 113–121.
- Vaganov, E. A., Hughes, M. K., & Shashkin, A. V. (2006). *Growth dynamics of conifer tree rings: images of past and future environments* (Vol. 183). Springer Science & Business Media.
- Van Gelder, H. A., Poorter, L., & Sterck, F. J. (2006). Wood mechanics, allometry, and life-history variation in a tropical rain forest tree community. *New Phytologist*, 171(2), 367–378.
- Varmola, M., & Salminen, H. (2004). Timing and intensity of precommercial thinning in *Pinus sylvestris* stands. *Scandinavian Journal of Forest Research*, 19(2), 142–151.
- Vaughan, D., Auty, D., Kolb, T., Dahlen, J., Sánchez Meador, A. J., & Mackes, K. H. (2021). Wood density variation in naturally regenerated stands of *Pinus ponderosa* in northern Arizona, USA. *Canadian Journal of Forest Research*, 51(4), 583–594.
- Wang, L., Payette, S., & Bégin, Y. (2002). Relationships between anatomical and densitometric characteristics of black spruce and summer temperature at tree line in northern Quebec. *Canadian Journal of Forest Research*, 32(3), 477–486.
- Wang, Q., Liu, X., Yang, S., Jiang, M., & Cao, J. (2019). Non-destructive detection of density and moisture content of heartwood and sapwood based on X-ray computed tomography (X-CT) technology. *European Journal of Wood and Wood Products*, 77(6), 1053–1062.
- Weber, J. C., Sotelo Montes, C., Abasse, T., Sanquetta, C. R., Silva, D. A., Mayer, S., Muniz, G. I. B., & Garcia, R. A. (2018). Variation in growth, wood density and carbon concentration in five tree and shrub species in Niger. *New Forests*, 49(1), 35–51.
- Wimmer, R. (2002). Wood anatomical features in tree-rings as indicators of environmental change. *Dendrochronologia*, 20(1–2), 21–36.
- Wimmer, R., & Downes, G. M. (2003). Temporal variation of the ring width–wood density relationship in Norway spruce grown under two levels of anthropogenic disturbance. *Iawa Journal*, 24(1), 53–61.
- Wimmer, R., & Grabner, M. (1997). Effects of climate on vertical resin duct density and radial growth of Norway spruce [*Picea abies* (L.) Karst.]. *Trees*, 11(5), 271–276.

- Worbes, M., Staschel, R., Roloff, A., & Junk, W. J. (2003). Tree ring analysis reveals age structure, dynamics and wood production of a natural forest stand in Cameroon. *Forest Ecology and Management*, 173(1–3), 105–123.
- Xiang, W., Leitch, M., Auty, D., Duchateau, E., & Achim, A. (2014). Radial trends in black spruce wood density can show an age-and growth-related decline. *Annals of Forest Science*, 71, 603–615.
- Zarnovican, R., & Laberge, C. (1996). *Effect of precommercial thinning on the production of young fir stands on the Upper North Shore*. (Issue LAU-X-118E). Canadian Forest Service-Quebec.
- Zhang, Q., Wang, C., Wang, X., & Quan, X. (2009). Carbon concentration variability of 10 Chinese temperate tree species. *Forest Ecology and Management*, 258(5), 722–727.
- Zhang, S. Y. (1995). Effect of growth rate on wood specific gravity and selected mechanical properties in individual species from distinct wood categories. *Wood Science and Technology*, 29(6), 451–465.
- Zhou, H., & Smith, I. (1991). Factors influencing bending properties of white spruce lumber. *Wood and Fiber Science*, 23(4), 483–500.
- Zobel, B. J., & Buijtenen, J. P. van. (1989). Wood variation and wood properties. In *Wood variation* (pp. 1–32). Springer.
- Zobel, B. J., & Van Buijtenen, J. P. (2012). *Wood variation: its causes and control*. Springer Science & Business Media.
- Zubizarreta Gerendiain, A., Peltola, H., Pulkkinen, P., Jaatinen, R., Pappinen, A., & Kellomäki, S. (2007). Differences in growth and wood property traits in cloned Norway spruce (*Picea abies*). *Canadian Journal of Forest Research*, 37(12), 2600–2611.